FACILE CONTROLLED PREPARATION OF MULTIFUNCTIONAL CORE-SHELL MAGNETIC NANOPARTICLES AND THEIR USE IN MICROFLUIDIC SEPARATION

XIA CHEN

A DISSERTATION SUBMITTED TO

THE FACULTY OF GRADUATE STUDIES

IN PARTIAL FULFILMENT OF THE REQUIREMENTS

FOR THE DEGREE OF

DOCTOR OF PHILOSOPHY

GRADUATE PROGRAM IN CHEMISTRY

YORK UNIVERSITY

TORONTO, CANADA

AUGUST, 2018

ABSTRACT

Continuous microfluidic technology has proven to be a potential competitor with established batch systems for facilitating chemical synthesis and purification, and more amenable to miniaturization, integration, and automation. Nevertheless, combining synthesis, purification and analysis remains a challenge due to the lack of development in efficient continuous flow purification techniques. An emerging continuous-flow purification technique is magnetophoresis, which utilizes surface-functionalized magnetic particles to selectively capture target molecules through specific binding, followed by manipulating the migration of particles through external magnetic force.

This dissertation explores the synthesis of monodisperse core-shell functionalized magnetic nanoparticles composed of a single-core structure, and their application in magnetic manipulation for capture and isolation of targets in the continuous flow. First, single-cored magnetic nanoparticles with surface functionalities were prepared by coating functional triethoxysilanes onto iron oxide nanoparticles. The morphology, size, and colloidal stability of the resulting functionalized magnetic nanoparticles can be predicted and controlled. Second, a microfluidic device was fabricated from poly(dimethylsiloxane)(PDMS), consisting of two major components, a mixer and a separator (a diagram shown below). In the mixer, target molecules were captured by functionalized magnetic nanoparticles in a T-shape microchannel. Then the magnetic bead-target complex is directed into the separator, where the captured target molecules are magnetically steered out of the matrix while passing through a laminar co-flow profile. For proof of concept, we used a mixture of toluidine blue O (TBO) and sodium fluorescein as a model target and nontarget, respectively, and carboxyl functionalized magnetic beads as a receptor, leading to the selective complexation of TBO and magnetic beads via electrostatic binding. The device

allowed for complete separation of the target from the nontarget molecules with high separation selectivity and efficiency as well as excellent reliability and flexibility.

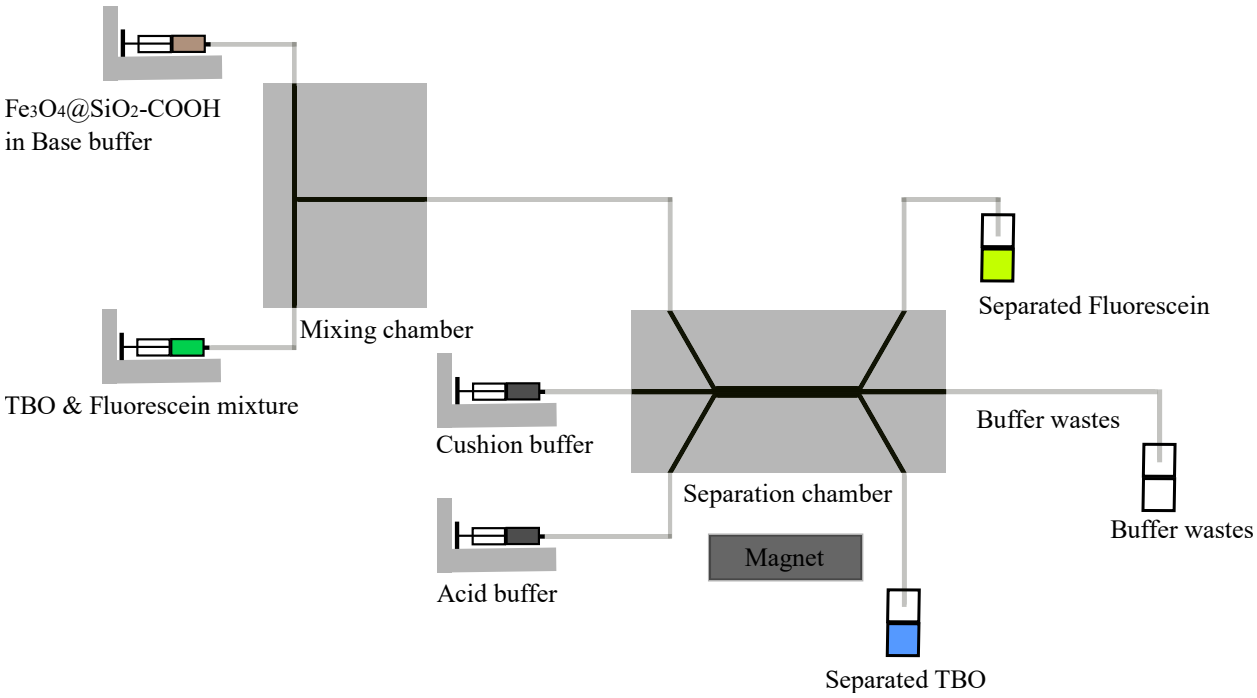

Diagram of a continuous microfluidic magnetic separation system.

DEDICATIONS

To my parents, who gave me life and raised me with unconditional love and support.

ACKNOWLEDGEMENTS

This thesis would not have been possible without the help and support of many people. First and foremost, I would like to thank my supervisors, Professor Michael Organ for kindly offering me the opportunity to pursue my Ph.D. study abroad; and Professor William Pietro for the continuous encouragement, advice, patience, and support throughout my graduate studies. I would also like to extend thanks to my research committee advisor, Prof. Jennifer Chen for giving me a lot of great advice on designing experiments. In addition, I would like to thank my internal and external examiners, Prof. Mark Gordon and Prof. Timothy Bender, respectively, for agreeing to examine this thesis.

Next, I would like to thank all current and former members of the Organ group: Mallik Debasis, Sepideh Sharif, Abir Khadra, Chris Schruder, Jee Kwak, Jennifer Farmer, Kristina Somerville, Guanlong Li… who offered me great help and encouragement during my Ph.D. study. Each one of you made my experience at York University enjoyable and unforgettable both in and outside of the laboratory.

Finally, I would like to thank my friends and family for all their love and support throughout the years. Thank you-mom, dad, and sister, for all your encouragement and support oversea. Thanks to my husband Dr. Hai Zhang, for all the good moments we have come through over the past 10 years. A special thanks to my little son, Alan Junxi Zhang, who made us a family in Canada.

TABLE OF CONTENTS

LIST OF TABLES

LIST OF FIGURES

LIST OF SCHEMES

LIST OF ABBREVIATIONS

Ac: Acetate

APIs: active pharmaceutical ingredients

APTES: 3-aminopropyltriethoxysilane

CMMS continuous microfluidic magnetic separators

CuAAC: copper-catalyzed alkyne azide cycloaddition

CTAB: cetyltrimethyl ammonium bromide

3D: 3 dimensional

2D: 2 dimensional

DMF: dimethylformamide

DCM: dichloromethane

DMPA: 2,2-Dimethoxy-2-phenylacetophenone

DMSO: dimethyl sulfoxide

DSL: dynamic light scattering

EDX: energy dispersive X-ray spectroscopy

EE: ethyl ether

Ems: electromagnets

EtOH: ethanol

Fe_3O_4@C: carbon coated iron oxide nanoparticles

Fe3O4@SiO_2: silica coated iron oxide nanoparticles

Fe_3O_4@SiO_2-COOH: silica coated iron oxide nanoparticles with surface carboxylic groups.

Fe_3O_4@SiO_2-NH_2: silica coated iron oxide nanoparticles with surface primary amine groups.

Fe_3O_4@SiO_2–COOEt: silica coated iron oxide nanoparticles with surface primary ester groups.

Fmoc-Cl: 9-Fluorenylmethoxycarbonyl chloride

FFE: free-flow electrophoresis

FFF: Field Flow Fractionation

Igepal CO-520: polyoxyethylene (5) nonylphenylether

IONPs: iron oxide nanoparticles

IPTEOS: 3-(triethoxysilyl)propyl isocyanate

LLE: liquid-liquid extraction

LOC: lab-on-a-chip

MPQ: magnetic particle quantification

MRI: magnetic resonance imaging

M $(acac)_n$: metal acetylacetonates

NaOAc: sodium acetate

NH_4OH: ammonium hydroxide

PAA: poly(acrylic acid)

PACA: poly(alkylcyanoacrylates)

PANI: poly (aniline)

PBS: phosphate buffer

PC: polycarbonate

PCL: poly(ε-caprolactone)

PEAA: poly(ethylacrylic acid)

Pd: palladium

PDMS: poly(dimethylsiloxane)

PEG: poly (ethylene glycol)

PEI: poly(ethylenimine)

PI: polyimide

PINPAAm: poly (N-isopropylacrylamide)

PLA: poly (lactic acids)

PMMA: poly(methyl methacrylate)

PMs: permanent magnets

PPAA: poly(propylacrylic acid)

PPy: poly(pyrrole)

PS: polystyrene

PVA: poly(vinyl alcohol)

PVC: polyvinyl chloride

PVP: poly(vinylpyrrolidone)

PXRD: powder X-ray diffraction

R: the radius of particle

SFC: sodium fluorescein

TBO: toluidine blue o

TEA: trimethylamine

TEM: transmission electron microscopy

TEOS: Tetraethoxysilane (TEOS)

VTEOS: vinyltriethoxysilane

$\vec{F}_{mag}$ magnetic force

$\vec{F}_{drag}$ hydrodynamic drag force

$\vec{v}_p$ velocity of magnetic nanoparticles

$\vec{v}_{flow}$ hydrodynamic flow velocity

$\vec{v}_{mag}$ magnetically induced flow velocity

$\vec{H}$ external magnetic field

$\nabla\vec{H}$ gradient of magnetic field

V_p particle volume

χ_m magnetic susceptibility

μ_0 permeability of free space

η fluid viscosity

$\vec{m}_s$. magnetic saturation moment of the particle

CHAPTER 1. INTRODUCTION

1.1 Continuous Flow Synthesis

Organic synthesis in both laboratory and industrial scale is traditionally performed in batch process, which combines all reagents in round-bottled flasks, test tubes, or closed vessels. Over the past decade, a growing interest has been focused on improving efficiency and safety, reducing cost, and developing automated operation units for organic synthesis.[1] This is particularly important in the fine chemical and pharmaceutical industry, where the drug substances and active pharmaceutical ingredients (APIs) are highly valuable and the synthesis processes of them are considerably more complex than raw chemicals because it requires multiple steps of reactions and purifications. Continuous-flow manufacturing, which performs chemical reactions in a flowing stream of carrier, has become an increasingly attractive alternative to batch process as it affords a more flexible approach to pharmaceutical manufacturing.[2] The advantages of continuous-flow synthesis over conventional lab-scale techniques have been widely recognized both in academia and industry.[3,4] First, many parameters can be realized in small-scale continuous-flow synthesis over batch processes, such as enhanced heat and mass transfer, precise mixing and residence times, and safer synthesis of dangerous compounds.[5] Continuous-flow reaction is a particularly useful option when it comes to some harsh reaction conditions requiring sharp reaction times (e.g. in 5 seconds), hazardous material handling, and/or very high temperature/pressure.[1] In addition, scaling can be achieved in continuous-flow synthesis without significant modification to conditions by simply running optimized conditions for a longer period of time or numbering up reactors in parallel. This is attractive for the pharmaceutical industry where production at the hundreds of grams to kilograms scale is necessary during preclinical and clinical trials.[6] Perhaps one of the most compelling aspects of continuous manufacturing is the possibility of performing multiple

reaction steps in a streamlined and information enriched sequence. That means traditional discontinuous chemical transformation, separations and purifications, analysis, and even crystallizations, drying, and formulation are all linked together to generate one single, fully automated continuous process without offline holding. Such integrated process is of profound significance for pharmaceutical industry in terms of green production process, safety, and economic savings. More importantly, the implementation of in-line purification and analysis allows for real-time monitoring and optimization, which could maximize the reaction efficiency and minimize the reagent wastes.

A few integrated continuous-flow systems have been built for continuous multistep synthesis of APIs, including ibuprofen,[7,8] rufinamide,[9] aliskiren,[6,10] diphenhydramine, lidocaine, diazepam and fluoxetine[11] (Shown in Figure 1.1). A great work has been done by the Novartis MIT Center for Continuous Manufacturing for API, where aliskiren hemifumarate is produced from a chemical intermediate to a finished tablet using a bench-scale, fully integrated, continuous pharmaceutical plant.[6,10] This plant produces 0.8 tons of aliskiren/year using a continuous reactor of volume 0.7 L. The throughput of aliskiren is nominally 45 g/h, corresponding to 2.7×10^6 tablets per year. The flow process requires 48 h of processing time and 13 unit operations, which is much more efficient than the batch process requiring 300 h processing time and 21 unit operations of the batch process. If our target scale is 188 tons of API/year, the batch reactor volume required would be 1500 L, which is 10 times larger in size than using continuous-flow technique requiring only 136 L of reactor volume. The plant layout at Novartis is very compact with a 2.4×7.3 m^2 footprint. Another continuous-flow and formulation of API system uses an even smaller refrigerator-sized platform (1.0 m (W) x 0.7 m (L) x 1.8 m (H)) and successfully produces liquid doses of four well-known pharmaceutical drugs.[11] All those figures demonstrate that pharmaceutical manufacturing

will benefit from integrated and precisely controlled continuous-flow manufacturing systems with enhanced safety, shorter processing times, improved product quality, and reduced footprint and production costs.

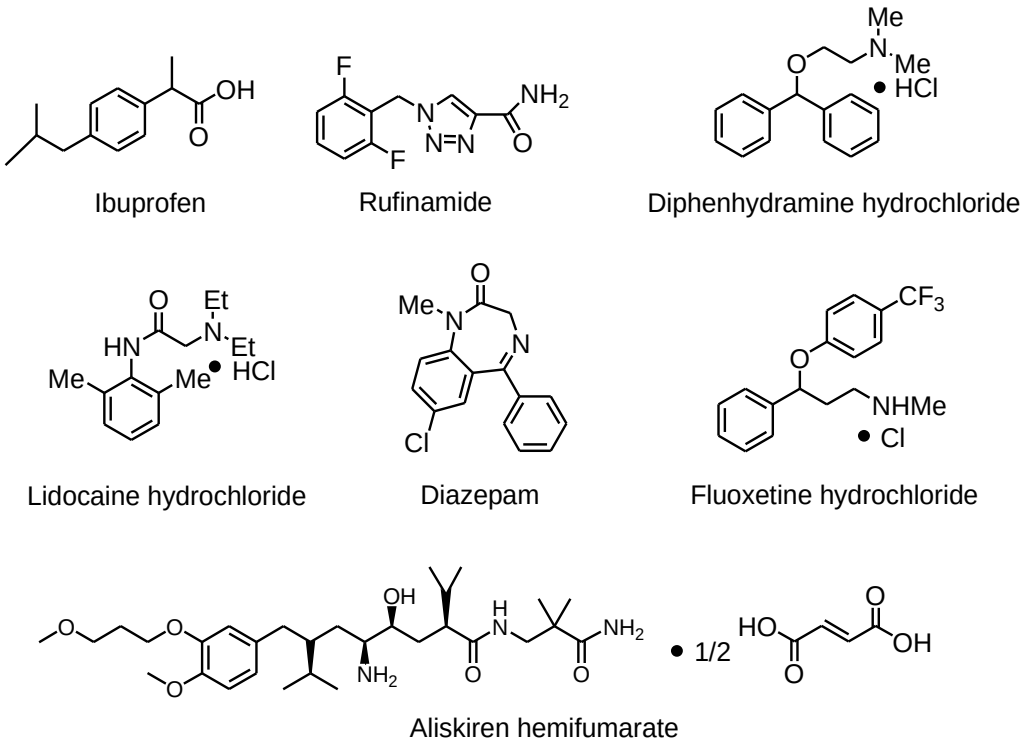

Figure 1.1. Examples of APIs synthesized by integrated continuous-flow systems.

1.2 Continuous-Flow Separations for Continuous-Flow Synthesis

In spite of several examples found in literature showing the potential of integrated continuous-flow manufacturing APIs, building a fully integrated continuous-flow system for manufacturing a broader scope of APIs remains challenging, due to the limited number of available separation techniques that can be applied in continuous-flow synthesis. Thus, continuous synthesis is usually followed by "discontinuous" purification in most cases. With the development of advanced continuous-flow synthesis techniques, the development of continuous-flow separation and purification techniques has become highly demanding for designing the next generation of

fully integrated continuous-flow system for a broader scope of pharmaceutical manufacturing. There are several criteria needed to be considered when developing continuous-flow separation techniques:[12] 1) the purification device should be able to selectively "pick" target molecules from reaction mixtures containing impurities, by-products, and unreacted reagents with minimum contamination; 2) the purification device must be compatible with the solvents used in the flow reactor; 3) the entire continuous flow system should operate in steady-state after integrating continuous-flow synthesis and purification. Until recently, the continuous-flow purification techniques satisfying these criteria are limited. Below we will briefly discuss the existing purification techniques that are potentially viable for integrated continuous flow chemistry system, including liquid-liquid extraction (LLE), simulated moving-bed chromatography (SMBC), electrophoresis, and magnetophoresis.

1.2.1 Liquid-liquid extraction

Liquid-liquid extraction is a purification technique based on the separation of two liquid phases with differences in the density. Extraction efficiency is determined by the polarity of each liquid phase and the solubility of the target solutes in each phase.[12] At the micro-scale, complete phase separation using difference in the density is more difficult to achieve compared to batch LLE process because gravitational forces are small compared with surface forces.[13] Thus, alternative driving forces for continuous phase separation in microfluidic device must be considered. Membrane-based LLE using surface tension effects seems to be a good candidate for continuous-flow separation at the micro-scale. Jensen group[13] developed a membrane LLE separator based on hydrodynamic pressure drop and capillary pressure forces. The micro-separator was fabricated with a thin, porous, hydrophobic Teflon membrane sandwiched between microchannels, allowing only organic phase to pass through it. To achieve high-throughput

separation, it is crucial to have a smaller pore size of the membrane to allow higher capillary pressure than the hydrodynamic pressure for the organic phase to transfer. Later on, they implemented the same separation technique to an above mentioned fully integrated continuous-flow pharmaceutical plant for the preparation of aliskiren.[10] The same group also developed a second generation of membrane-based LLE separator by adding a secondary hydrophilic glass microfiber membrane parallel to the hydrophobic Teflon membrane.[14] The dual membrane separator system was used for continuous separation of complex mixture of APIs with enhanced phase separation efficiency. However, the main problem with the membrane-based LLE is the clogging of, or damage to, the membrane over time. Also, LLE is very useful for carrying out single step extraction, but it is still challenging when separating multiple targets with different solubilities. One solution is to optimize the extraction of each solute by using multiple LLE units in series, but such systems are plagued with inefficient control of pressure drops and flow rates.[5]

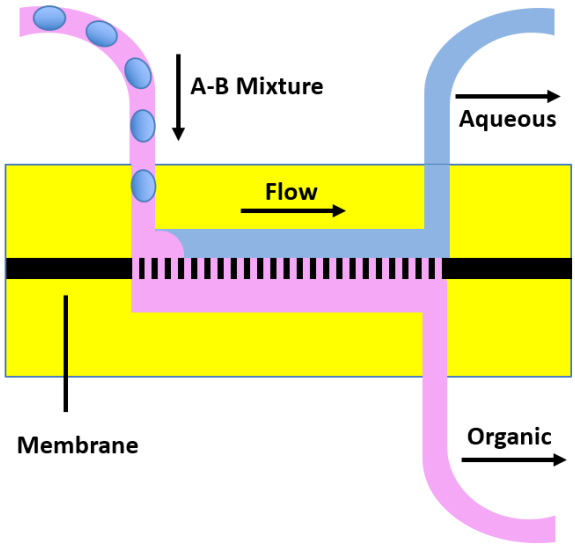

Figure 1.2. Continuous liquid-liquid extraction. A segmented flow of an aqueous solution(A) dispersed in an organic phase (B). The organic phase wets the hydrophobic membrane and is driven through the membrane pores by the imposed pressure difference leaving the aqueous solution behind in the top portion of the device. Reprinted with permission from **Ref. 13**. Copyright 2007 Royal Society of Chemistry.

1.2.2 Simulated moving-bed chromatography (SMBC)

SMBC is a continuous multi-column chromatographic process performing adsorption/desorption of a sample between mobile and stationary phase. It was invented in the early 1960s in the petrochemical and sugar industries, and later widely adapted for separation of enantiomers of chiral drugs in pharmaceutical industry. Traditional chromatography achieves separation by injecting the solute mixture into a stream of mobile phase flowing through a column packed with stationary phase.[15] The solutes are separated based on their different affinity to the stationary phase, meaning the less retained solute will move faster in the column and exit the column earlier than a more retained one. However, single column chromatography can only carry one sample at a time because the separation of the first sample must be completed before the next injection starts in order to avoid overlapping. SMBC improves the productivity by using multiple smaller columns connected in series with valves placed between each column and exploiting a continuous countercurrent movement between mobile and stationary phases. In a SMBC setup, the columns are stationary still, but the inlet and outlet ports can be rotated periodically in the direction of fluid flow so as to simulate the continuous countercurrent movement of the columns containing the solid adsorbent (beds). The component that is strongly adsorbed to the resin called the raffinate and the component that remains in the mobile phase is called the extract. Both the raffinate and the extract are transported by the eluent, as shown in Figure 1.3. A sample is injected and extracted by automatically switching valves at appropriate points between columns, which could count as continuous-flow separation when operating at a steady state.

SMBC has already been combined with flow reactor for the synthesis of APIs.[16,17] A recent study for the synthesis of artemisinin using an integrated continuous-flow system implemented with SMBC afforded the product mixture with 92% purity, and 99.9% purity after crystallization

from the concentrated mixture.[18] However, the design of SMBC is technically complex and costly because it requires highly precise control over the separation process using mathematical model and expensive solid adsorbents. Moreover, SMBC is ideal for the separation of binary mixture. For a more complex sample containing multiple components, such as APIs from multistep reactions, additional crystallization process may be required to achieve approved purity. Finally, the saturation capacity of the column must be considered for productivity reason.

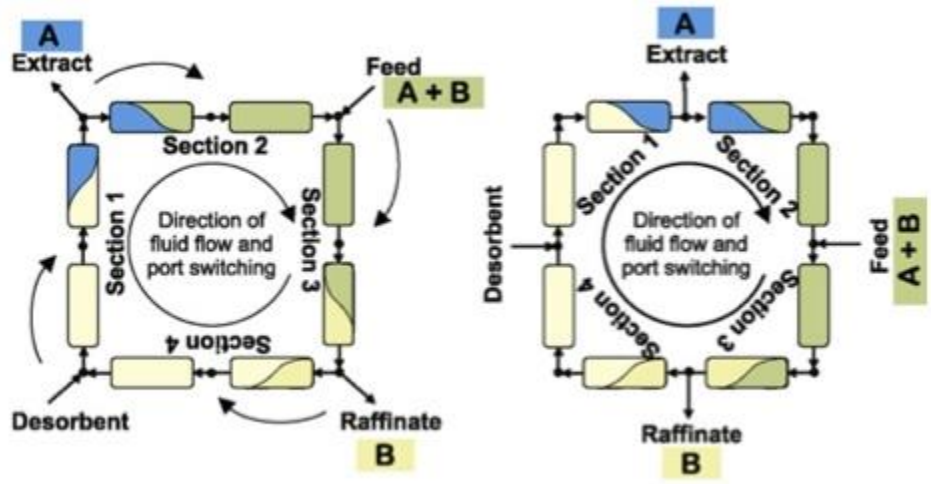

Figure 1.3. Schematic of simulated moving bed (SMB) units separating a binary mixture (A and B). The dashed arrows in the SMB scheme represent the port switch. Reprinted with permission from **Ref. 15**. Copyright 2009 Elsevier.

1.2.3 Electrophoresis

Another common technique for separations in continuous microflow is electrophoresis. It is performed in a shallow chamber, and it continuously separates target compounds from a sample solution by applying a homogeneous electric field perpendicular to the direction of flow. Charged molecules are separated because of two flow vectors: the hydrodynamic flow along the y-direction and the electrophoretically induced flow along the x-direction (Figure 1.4). The deflected direction of the molecules depends on the charges, and the extent of deflection depends on the charge to size

ratio of molecules, the strength of the electric field, and the hydrodynamic flow rate. Electrophoresis was originally applied for the continuous purification of complex biological samples. Recently, several research groups have demonstrated its potential in the integration of synthesis, separation, and analysis into lab-on-a-chip systems. Benz and co-worker[19] presented an approach for coupling free-flow electrophoresis (FFE) through the attachment of capillaries to mass spectrometry. After successfully demonstrated the concept by detecting the separation process for fluorescent molecules, they applied this system to a [3+2]-cycloannulation reaction using anthranilic acid, benzaldehyde, and bis(silyl)dienediolate to form a product pyrrolobenzoxazinone. The reaction mixture was continuously separated by electrophoresis and directed across the mass spectrometric outlet for product identification. Regardless of the manner of electrophoresis, contamination could be difficult to avoid due to the high dependence of separation upon ionic strength and pH. Also, the generation of Joule heating and bubbles by electrolysis could be problematic for efficient separation.[20]

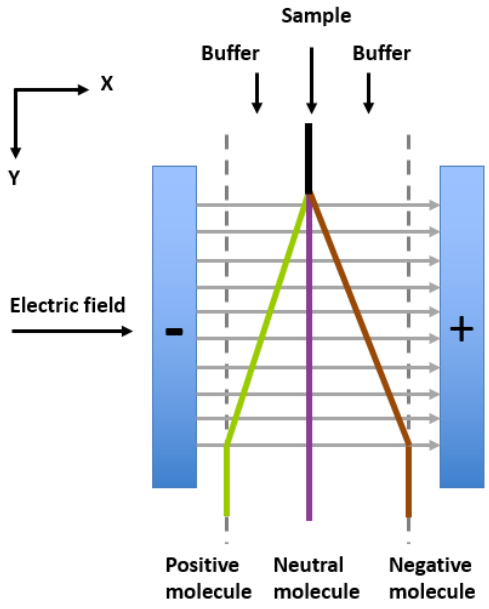

Figure 1.4. Two-dimensional electrophoretic purification system. Sample is injected in the y-direction in a narrow band in the middle of the plate. An electric field is applied in the x-direction across the plate, thus separting the molecules on the basis of their charge to size ratio.

1.2.4 Magnetophoresis

Purification using solid support scavengers is a common technique in batch process. Particularly, functionalized magnetic particles, also referred as “magnetic beads”, is a popular scavenger for the removal of impurities. Magnetic scavengers are most commonly seen in the form of iron oxide nano- or micro-particles coated with a polymer or silica layer for colloidal stability and functionality. Separation using an external magnetic force requires very simple handling steps, and no need for expensive equipment such as chromatography systems, centrifuges, or filters. A magnet with decent magnetic strength is enough to separate the target of interest directly from crude samples in a very short period. Moreover, magnetic carriers are usually in the form of magnetic particles that are prepared from various synthetic routes and tailored with surface functionalities, allowing for very high selectivity and affinity towards targets. Another unique feature of magnetic separation is that magnetic carriers can be recovered for multiple cycles of separation. It is worth mention that magnetic nanoparticles become superparamagnetic when their size is below a certain critical diameter (e.g., 50 nm for Fe_3O_4), unlike bulk Fe_3O_4, which is ferromagnetic. So they exhibit a very strong response to an external magnetic field, but have zero magnetic moment and no attraction to each other in the absence of the field. This property offers excellent colloidal stability without aggregation. Those advantages make nanoparticles good candidate for application in continuous-flow separation.

In analogy to free-flow electrophoresis, which is based on electric manipulation of sample deflection, magnetophoresis is a method based on magnetic manipulation of the migration of magnetic particles using either a permanent magnet or an electromagnet. Magnetophoresis was first reported by a Russian group in 1977,[21] but it was not until the year 2000 that the number of publications related to this subject started growing exponentially (Figure 1.5). Such fast-growing

attention is attributed to the many unique properties of magnetophoresis. First, magnetic gradients can penetrate a closed vessel or micro-channels, allowing for no physical contact between the magnet and liquid to reduce contamination. In addition, unlike electrically induced forces, magnetic forces do not generate heat, and they are not influenced by ionic strength, pH or surface charges, which could be a benefit for the separation of soft particles such as cells and other biological molecules. Finally, the continuous flowing process would not interrupt the flow, resulting in the reduce of non-specific entrapment of sample impurities in the capturing regions.

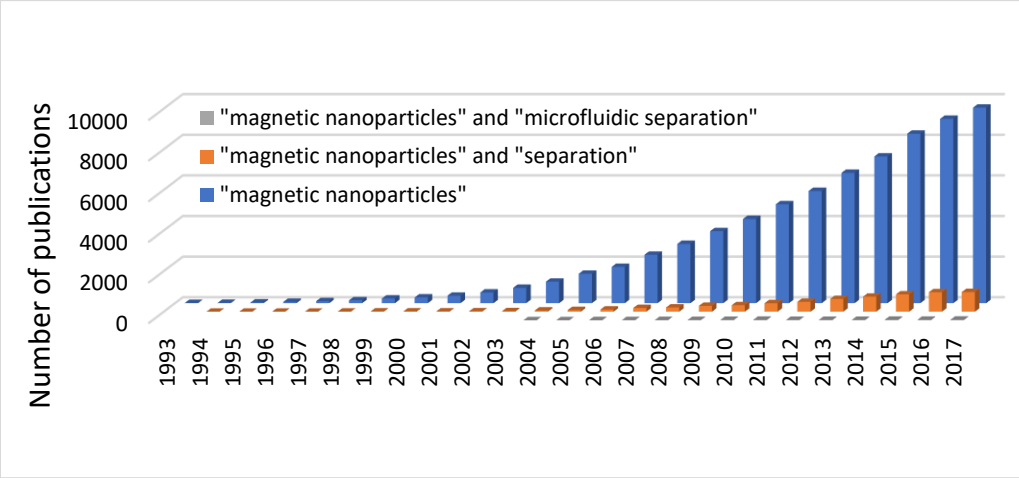

Figure 1.5. Number of publications in the last 24 years related to the separation using magnetic nanoparticles.

Multiple outlets and fluid streams can be introduced onto continuous microfluidic devices, allowing for trajectory deflection of magnetic particles from the original stream to a buffer stream in the presence of magnetic field (Figure 1.6). Moreover, such multi-fluid streams inside the microchannel would generate a laminar co-flowing profile, meaning no apparent turbulent mixing would occur between neighboring miscible fluids. This technique is ideal for the application of purifying an original input stream in a continuous mode where the input fluid solutions containing particles can be incorporated with washing streams in the same device.[22] Based on this concept, a variety of applications have been recognized by continuously flowing magnetic particles within a

microfluidic separation system. For example, continuous microfluidic magnetic separators (CMMS) have been successfully demonstrated for the separation of magnetic beads and biological samples at small scale with high efficiency and selectivity.[23]

Aside from the distinct advantages over other continuous-flow separation methods, magnetophoresis also has its limitations. First, individual nanoparticles can not be manipulated because the magnetic force on a single nanoparticle is too small, unless the nanoparticles form agglomerates after they "pick up" the targets. It is known that magnetic force is proportional to the cube of the particle radius. But individual magnetic nanoparticles would lose the on/off magnetic response and become permanent magnetic nanoparticles if their size is above a certain range. Second, the applied flow rates tend to be slow (hundreds of μm s^{-1} or at most a few mm s^{-1}), [20]because enough time is needed for the magnetic nanoparticles to deflect before they come out from the desired outlet. Finally, only very few materials, like red blood cells and magnetotactic bacteria, can be manipulated naturally by magnetophoresis, all other materials exhibiting no intrinsic magnetism have to be labelled with magnetic micro/nanoparticles. Fortunately, the magnetic labelling can be easily achieved through various surface functionalization strategies.

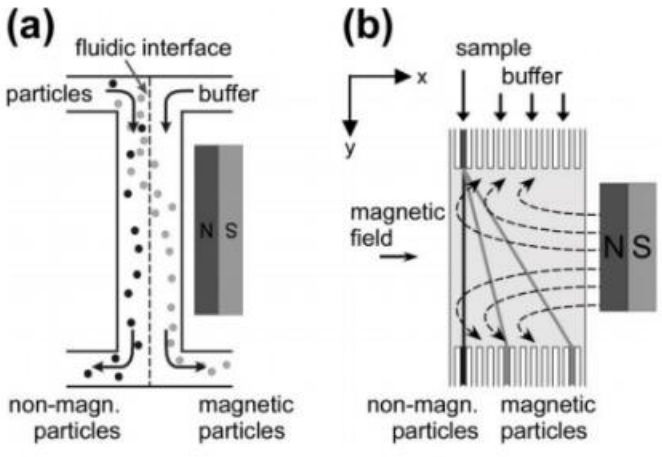

Figure 1.6. *Continuous flow magnetic separations carried out via (a) two outlets, (b)multiple outlets.* Reprinted with permission from **Ref. 20**. Copyright 2007 Royal Society of Chemistry.

1.3 Fundamentals of Magnetophoresis in Microfluidic Environment

1.3.1 Laminar flow

One way to assess the flow inside a microfluidic channel is through Reynolds number (R_e), as defined by equation (1.1).[24]

$$R_e = \frac{\rho d v}{\eta} \tag{1.1}$$

Where ρ is the fluid's density (e.g. H_2O, 1000 kg/m^3), d is the height of the separation channel, v is hydrodynamic velocity, and η is viscosity. When the Reynolds number is much less than 1, the viscous forces are greater than the inertial forces, meaning that the flow inside the channel is laminar. For example, the Reynolds number is 0.28 for aqueous samples flowing through a microchannel (3cm (L) x 300 μm (W) x 100 μm (D)), considering ρ is 1000 kg/m^3, d is 100 μm, v is 2.78 x 10 $^{-3}$ m/s (20 μL/min), η is 1.002 x 10^{-3} kg m^{-1} s^{-1}. Therefore, the flow inside the channel is laminar not turbulent.

1.3.2 Basic physics of magnetic separation

When a particle flows through the microfluidic channel, forces exerted on this magnetic particle to drive the migration must be considered. Those forces include (a) external force (here is magnetic force), (b) viscous drag force, (c) particle/fluid interactions (perturbations to the flow field), (d) gravity, (e) thermal kinetics (Brownian motion), (f) interparticle interactions including (i) magnetic dipole-dipole interactions, (ii) electric double-layer interactions, and (iii) van der Walls attraction force.[25] Many of these forces could be ignored for microfluidic separation, depending on the size of the particle and the magnetic field strength. Particle/fluid interactions can be taken into account by solving for the flow field and particle trajectories numerically, applying appropriate fluidic boundary conditions of the surface of the particles during each time step.

Similarly, interparticle (e.g., dipole-dipole) interactions can be included in the equations of motion and calculated during each time step. But for dilute particle suspensions (typical concentrations are of the order of 1 $g \cdot L^{-1}$), the particle-particle and particle-fluid interactions are neglected to simplify the analysis.[25,26] Brownian forces, referring to random movement of suspended particles caused by the random collisions with molecules of the fluid, can also be neglected because the magnetic force dominates. In a relatively high magnetic field, as produced by a permanent magnet, gravitational forces can be ignored as well. Based on most common conditions used for magnetic separation, the most dominant forces acting on a magnetic nanoparticle are the hydrodynamic viscous drag force and magnetic force. So the particle trajectory inside a microchannel relies on the balance of these two vectors. Meanwhile, to simplify the analysis, several other assumptions need to be considered.[27] First, we assume the magnetic nanoparticle to be perfectly spherical. Second, the ferrofluid is assumed magnetically saturated. We further assume the z components of the magnetic field gradient and ferrofluid flow velocity are much smaller than those in the x and y direction. Therefore, the 3D system analysis can be reduced to a 2D cross section plane (x, y analysis),[27-29] and the particle motion equation can be defined by Newton's second law as below:[28,30-33]

$$\vec{F} = m_p \frac{d\vec{v}_p}{dt} \tag{1.2}$$

When a particle is flowing through the microchannel with existence of an external magnetic field, the particle will acquire the velocity $\vec{v}_p$ from the hydrodynamic flow velocity $\vec{v}_{flow}$ and the magnetically induced flow velocity $\vec{v}_{mag}$.

$$\vec{v}_p = \vec{v}_{flow} + \vec{v}_{mag} \tag{1.3}$$

The magnetic force, equation (1.4), is proportional to a product of the external magnetic field $\vec{H}$, its gradient $\nabla\vec{H}$, and also is proportional with particle volume V_p and magnetic

susceptibility χ_m. However, if the magnetic field is strong enough to saturate the particle, the equation (1.4) turns in equation (1.5), because $V_p\chi_m\vec{H}$ represents the magnetic saturation moment of the particle $\vec{m}_s$.

$$\vec{F}_{mag} = \mu_0 V_p \chi_m \vec{H} \cdot \nabla \vec{H} \tag{1.4}$$

$$\vec{F}_{mag} = \mu_0 \vec{m}_s \cdot \nabla \vec{H} \tag{1.5}$$

For very low Reynolds number, the drag force is defined by equation (1.6), which came from the Stokes drag law. In this equation, R is the radius of particle:

$$\vec{F}_{drag} = 6\pi\eta R\vec{v}_p = 6\pi\eta R(\vec{v}_{flow} + \vec{v}_{mag}) \tag{1.6}$$

So, what is needed for tracking the particle position as a function of time will be the following equation:

$$m_p \frac{d\vec{v}_p}{dt} = \mu_0 \vec{m}_s \cdot \nabla \vec{H} + 6\pi\eta R(\vec{v}_{flow} + \vec{v}_{mag}) \tag{1.7}$$

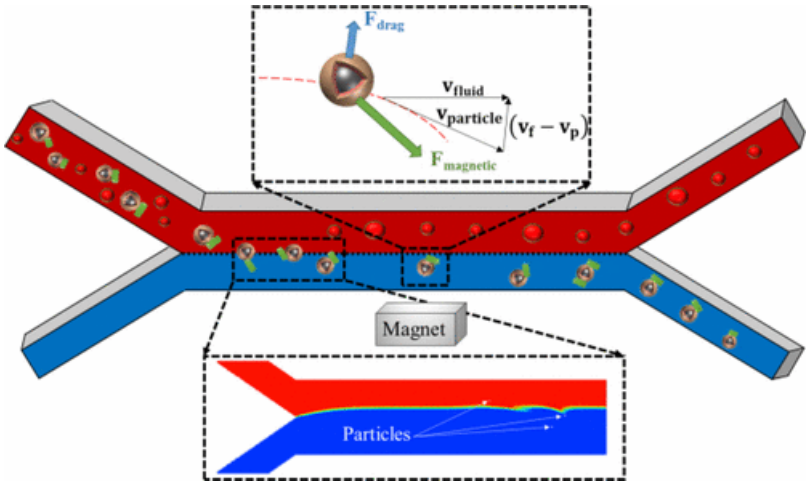

Figure 1.7. Schematic diagram of the continuous-flow magnetic separation. Reprinted with permission from **Ref. 34**. Copyright 2017 Ameican Chemical Society.

1.3.3 Magnetic source

Continuous flow separation of magnetically susceptible sample components is usually achieved by applying an external magnetic field perpendicular to the flow direction. The degree of magnetic particles deflecting from the main direction of flow depends on the magnetic strength and the magnetization of the particle. For nano-and micro-sized magnetic particles, the observed trajectory is the sum of two flow vectors: the hydrodynamic velocity and the magnetically induced velocity. [25,27] Hydrodynamic velocity is determined by the flow rate of the liquid (usually aqueous solution) pumping through the microchannel. Therefore, the magnetic force of the applied magnetic field plays a key role for particle deflection. The magnetic force could be determined by the choice of magnetic sources. There are two main types of magnetic sources, permanent magnets (PMs) and electromagnets (EMs). Considering the application of micro-scale flow devices, the use of permanent magnets is more efficient and straightforward than that of electromagnets, due to the complexity and bulkiness of design and fabrication of an electromagnet. An electromagnet can give maximum gradients ($\sim 10^4$ Tm^{-1} by using high current densities),[35] but it usually comes with very large size and the magnetic inductions offered by electromagnets is about 100 times lower than that of a permanent magnet.[22] Furthermore, current generated by electromagnets can induce inevitable Joule heating, evaporation, which is undesirable for some samples, especially biological samples.[32] Recently, hybrid magnets combining a larger external magnet and a small microfabricated magnet are also powerful tool for continuous flow separation. The hybrid magnet is reported to have a three times higher magnetic gradient than applying an external magnet alone.[36,37]

1.4 Fabrication of Microfluidic Devices

Early in the field, silicon and glass materials were used to fabricate microfluidic devices. By the late 1990s, polymer materials became great substitutes because of their simplicity, low cost, and disposal advantages over silicon and glass.[38] The polymer microfabrication process involves the identification of the microfluidic chip application and requirements, the design of microchannel/chamber layouts, selection of proper polymer materials, and determination of the fabrication strategy. The two major polymer materials used in microfluidics are polydimethylsiloxane (PDMS) elastomer and thermoplastics such as poly(methyl methacrylate) (PMMA), polycarbonate (PC), polystyrene (PS), polyvinyl chloride (PVC), polyimide (PI), and the family of cyclic-olefin polymers.[39] Also, various fabrication technologies have been developed based on polymers to meet different requirements for creating polymer microfluidic devices. Figure 1.8 summarizes the polymer microfluidic fabrication procedures and selection strategies, associated with different polymer materials.[39]

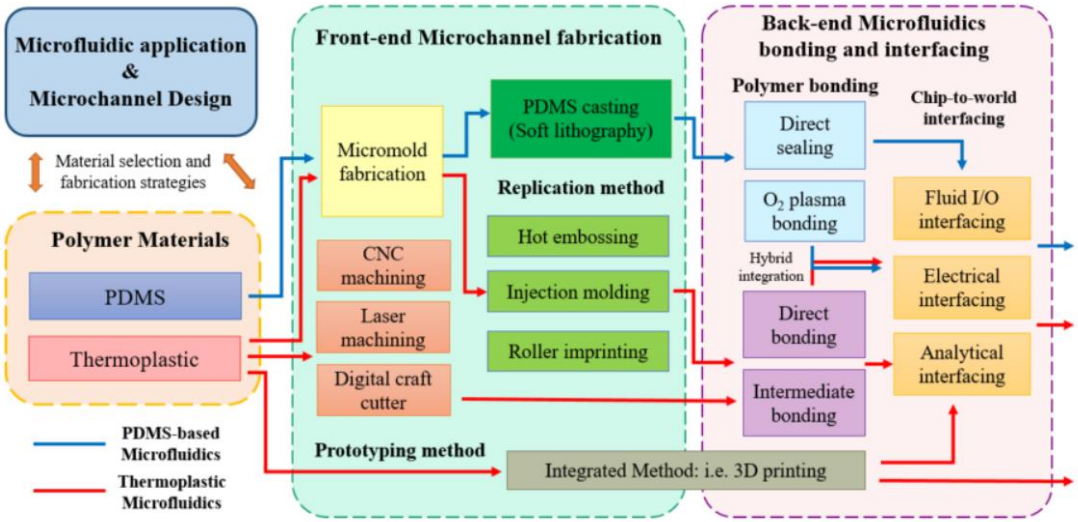

Figure 1.8. Polymer microfluidics fabrication process chart. The blue line indicates the PDMS-based microfluidics fabrication procedure, and the red line indicates the thermoplastic microfluidics fabrication procedure. Reproduced from **Ref. 39** with permission from Molecular Diversity Preservation International.

The flow regions of microfluidic devices are in the order of micrometers, enabling a noticeable reduction of surface-to-volume ratios, and thus decreased samples/reagents consumption. However, corresponding to small Reynolds number values, flows in such miniaturized regimes are predominantly laminar and not turbulent. With appropriate design and controlled flow rate, it is possible to force the target of interest into specific flow streamlines and realize high-throughput separation. For example, separators can feature either two outlets or multiple outlets. Multiple outlets allow for the separation of different magnetic particles from each other, as well as from non-magnetic material. By controlling magnetic field gradients using a small permanent magnet or integrated electromagnet on the chip, magnetic nanoparticles can be collected at the desired outlet.

1.5 Synthesis, Surface Functionalization, and Characterization of Magnetic Nanoparticles

Nanoparticles are a class of materials with the size range from 1 to 100 nm, presenting unique optical, thermal, magnetic and electrical properties, which are highly related to their size and morphologies. Among a broad range of nanoscale materials, magnetic nanoparticles, such as iron, cobalt and nickel oxides, are undergoing accelerated development for applications in biomedicine, separation, catalysis, and water treatment. In particular, iron oxide nanoparticles (IONPs) are ideal support because of their advantages over other magnetic materials, including low cost, ease of preparation, low toxicity (FDA approved material) and chemical stability.[40-42] Iron atom has very strong magnetic moment because of the unpaired electrons in 3d shell (4 unpaired electrons on Fe^{2+} and 5 unpaired electrons on Fe^{3+}). Therefore, crystals are magnetic when they are formed from iron ions. Magnetite (Fe_3O_4) has an inverse spinel structure with oxygen forming a face-centered cubic crystal system. The unit cell of Fe_3O_4 contains 32 O^{2-} ions which are regular cubic close packed along the [110] direction. Generally, the crystal structure of

Fe_3O_4 contains two sites: tetrahedral sites occupied by Fe^{3+} and octahedral sites occupied by both Fe^{3+} and Fe^{2+} along the [111] direction. In most applications, the performance of IONPs greatly depends on their size and morphologies. Typically, IONPs present the unique physical property of superparamagnetism at sizes below 50 nm, meaning that each nanoparticle bears a large magnetic moment (as high as 90 emu g^{-1}) in the presence of a magnetic field, yet does not permanently magnetize once the field is removed. [43-45] In addition, the large surface-to-volume ratios can be exploited for facile heterogeneous reactions at surface functionalities.

1.5.1 Synthesis of iron oxide nanoparticles

In the last decades, the synthesis of magnetic nanoparticles has been devoted to making size-/shape- tunable, highly stable, and monodisperse magnetic nanoparticles. With the progress in understanding the thermodynamic and kinetic mechanism of metal oxide nanocrystal growth, advanced technologies for the synthesis of precise size-and shape-controlled IONPs have been developed. Several research groups have reported different synthetic routes to prepare high-quality magnetic nanoparticles. The most popular methods include co-precipitation,[46] thermal decomposition,[47,48] microemulsion,[49] and hydrothermal synthesis,[50] with yields, shapes, and size distributions varying between these various methods.

Co-precipitation is the most common and simplest method in which iron oxides (Fe_3O_4) are formed by mixing ferrous (Fe^{2+}) and ferric (Fe^{3+}) salts into a basic aqueous medium at a pH range 8~14 under non-oxygen environment. The reaction can be described as the following equation (Equation a).

$$Fe^{2+} + 2Fe^{3+} + 8OH^- \rightarrow Fe_3O_4 \downarrow + 4H_2O \quad \text{(a)}$$

The quality of the magnetic nanoparticles (size, shape, and composition) is highly dependent on the type of salts used (e.g., chlorides, sulfates, nitrates), the Fe^{2+} /Fe^{3+} ratio, temperature, pH value and ionic strength of the media.[43] Fe_3O_4 nanoparticles obtained by this method usually with very small size (10-20 nm), exhibiting superparamagnetic property. Superparamagnetism explains the state that nanoparticles at nanometer size become a single magnetic domain so that the total magnetic moment of the nanoparticle can be consider as one giant magnetic moment. Individual nanoparticles at this state behave as huge paramagnetic atom with a fast response to an external magnetic field with negligible remanence (residual magnetism) and coercivity (the field required to bring the magnetization to zero), leading to the reduction of agglomerating of nanoparticles at room temperature.[43]

Theoretically, the magnetic nanoparticles are reproducible by chemical coprecipitation technique once the synthetic conditions are fixed. However, despite the advantages that it is a facile and convenient way to obtain IONPs in large scale, the drawbacks of coprecipitation are also obvious. For instance, it is very hard to control the particle size distribution because the growth of the crystal is only controlled by kinetic factors. In addition, severe aggregation of nanoparticles from this method has been found to be a hindrance to their performance and applications.[51] Therefore, monodisperse iron oxide nanoparticles are pursued.

The mechanism for the formation of IONPs can be divided into two steps, nucleation and crystal growth.[52] In particular, there is a short burst of nucleation when the solution is highly supersaturated, followed by a rapid size focusing growth process on the surface of the nuclei. The complete separation of nucleation and growth is critical to obtain monodisperse iron oxide nanoparticles. In addition, a very narrow size distribution of monodisperse nanoparticles can be obtained if all nuclei form at the same time, as it is the end of nucleation during the reactively short

period rather than the particle growth that determines the final particle number.[53] Fortunately, a variety of methods have been used to control the nucleation and crystal growth process by precisely controlling the reaction temperature, choosing solvents with different boiling points, and adding stabilizing or reducing agents such as oleic acid, polyvinlyalcohol.[54 55]

Thermal decomposition is a promising method for making high-quality magnetic nanoparticles, in which organometallic precursors (eg. metal acetylacetonates [$M(acac)_n$]) are decomposed to metal oxides in high-boiling organic solvents in the presence of stabilizing surfactants. In such methods, the size, shape, magnetic characteristics, and surface properties of iron oxide nanoparticles can be controlled by varying experimental conditions during synthesis, including pH, ionic strength, temperature, nature of salts and so forth. For example, Hyeon and co-workers[56] developed a very facile thermal decomposition method to produce monodisperse iron oxide nanospheres (5~22 nm) on an ultra-large-scale of 40 g in a single reaction without a further size-sorting procedure. In their method, iron oleate precursors were made first using inexpensive iron (III) chloride and sodium oleate, followed by a decomposition process of the precursors in high boiling point solvents, in the presence of fatty acids as capping agents. The reaction was carried under an inert atmosphere at a steady temperature ramp of 3.3 °C/min up to 320 °C, allowing for a separated nucleation and crystal growth process to form monodisperse nanocrystals. The size and shape of the nanocrystals could be tuned by decomposition temperature and aging period, which are corresponding to the reactivity. In Hyeon's work, solvents with different boiling points were used to control the reactivity, including long-chain alkene (1-hexadecene, 1-octadecene, e-eicosene), amine (trioctylamine), or ether (octyl ether). Similar work has been reported that the reaction could be faster with shorter chain length and a higher concentration of fatty acid. Thermal decomposition methods not only give very good control for size and shape of

the nanoparticles in a scalable manner, but also allows for the synthesis of both hydrophobic and hydrophilic nanocrystals. Gao group developed several synthetic routes for water-soluble IONPs by adding water-miscible solvents and capping agents. [57,58]

Hydrothermal reduction of nanocrystals is based on a phase transfer and separation mechanism occurring at the liquid-solid-solution interfaces. As an example, Li group developed a hydrothermal reduction method to synthesize monodisperse and hydrophilic magnetic beads with controlled size in the range of 200-800 nm.[50] Typically, the reaction was carried in a sealed Teflon-lined stainless-steel autoclave containing a mixture of $FeCl_3$, ethylene glycol, sodium acetate, and polyethylene, and kept at 200 °C for 8-72 h. In this reaction, ethylene glycol worked as a reducing agent, sodium acetate and polyethylene worked as the stabilizer to prevent particle agglomeration. It is worth mentioning that this multicomponent reaction mixture worked excellently to lead the formation of desired materials. In addition, this process can be extended to the synthesis of a series of ferrite MFe_2O_4 (M=Fe, Mn, Co, Zn) with controllable particle size by adjusting the reaction time.

Microemulsions are dispersions of oil and water stabilized by surfactant molecules. They are made of droplets surrounded by a surfactant monolayer and dispersed in a continuous phase.[59] There are two types of microemulsions: water-in-oil (W/O) and oil-in-water (O/W). A W/O microemulsion is composed of water droplets surrounded by surfactant molecules in a nonpolar organic phase. Vice versa, an O/W microemulsion system is formed by a stable suspension of oil drops in an aqueous phase. By taking advantage of the highly ordered and stable feature, a microemulsion can be used as nanoreactor to generate various types of nanoparticles. For example, a mixture of two identical water-in-oil microemulsions, each containing the desired reactants, will continuously collide, coalesce, and break again, resulting in the formation of magnetic

nanoparticles in the micelles.[43] The size of the reverse micelle is determined by the molar ratio of water and surfactant, which finally determines the size of the resulting nanoparticles. Ganguli and coworkers[60] prepared cuboidal Fe_3O_4 nanoparticles with size of 60~70 nm by the reverse microemulsion method in the presence of cationic surfactant cetyltrimethyl ammonium bromide (CTAB). Although microemulsion techniques afford very good control on the size and shape of resulting nanoparticles, scaling-up is rather difficult due to the requirement of large amount of solvents. Some other commonly used methods are also summarized in Table 1.1.

Table 1.1 Summary comparison of synthetic methods for producing magnetic IONPs.

Method	Reaction and conditions	Reaction temp. [°C]	Reaction period	Size distribution	Shape control	Yield
Co-precipitation	Very simple, ambient	20-150	Minutes	Relatively narrow	poor	High/ scalable
Thermal decomposition	Complicated, inert atmosphere	100-350	Hours-days	Very narrow	Very good	High/ scalable
Hydrothermal synthesis	Simple, high pressure	150-220	Hours-days	Very narrow	Very good	High/ scalable
Microemulsion	Complicated, ambient	20-80	Hours	Narrow	Good	Low

1.5.2 Surface functionalization

IONPs are usually considered inert, which make them ideal for imaging and separation.[61] However, the application of magnetic core alone is limited due to the instability and lack of surface functionality for adsorption and immobilization. First, bare IONPs are not physically and chemically stable, because magnetic cores have large surface-to-volume ratio and therefore tend to agglomerate to reduce the surface energies. They are also chemically active and can be easily

oxidized in air, resulting in loss of magnetism and dispersibility. So proper surface modification of magnetic core is necessary to improve IONP behavior in solution, including colloidal stability, pH response, toxicity, and further application. Second, surface-functionalized monodisperse IONPs promise great advancement in a wide range of applications, including drug delivery,[62] magnetic resonance imaging (MRI),[63,64] bioseparation of proteins, DNA and cells,[65-67] catalysis,[68,69] ferrofluids,[70] data storage,[71] and adsorption,[72]. Fortunately, the surface of IONPs can be easily hybridized or coated with one or more materials, including organic materials (small molecules, surfactants, polymers, biomolecules) and inorganic materials (silica, carbon, noble metals (Ag, Au, Pt), metal oxide and sulfides), depending on the purpose of applications.[51,73] Such surface modification process provides not only the magnetic core a shield from surrounding environment, but also allows for further conjugation of the magnetic particle with various targets.

Small molecules and surfactants. High-quality IONPs generated from thermal decomposition method are hydrophobic due to the nonpolar groups at the end of long-chain capping reagents such as oleic acid and oleylamine. Ligand exchange strategies using small molecules or surfactants have been used to transfer IONPs from organic phase to aqueous phase, including using small molecules or surfactants.[74] It is usually a one-step process that provides good dispersibility of resulting nanoparticles in aqueous solution with only a slight decrease in magnetization. However, the drawbacks of such strategy are also obvious, that is, IONPs modified by such a thin layer of small molecules or surfactants are generally not chemically stable towards surrounding environments.

Polymer coating. Surface coating with polymers is a very useful strategy regarding the stability of IONPs and the diversity of functionalities at the surface of IONPs. Particularly, the hydrophobic nature of the magnetic core is not a problem because the polymer coating does not

involve the replacement of surface ligands on nanoparticles for solubility purposes. In general, polymers can be chemically anchored or physically adsorbed on IONPs to stabilize the nanoparticles in suspension through electrostatic repulsion or steric repulsion. Polymers used to coat the magnetic cores usually contain desired functional groups for target conjugation, such as carboxylic acids, amines, phosphates, and sulfates. Widely used polymers for coating include poly (lactic acids) (PLA), poly(propylacrylic acid) (PPAA), poly(ethylenimine) (PEI), poly (ethylene glycol)(PEG), poly(vinyl alcohol)(PVA), poly(ε-caprolactone) (PCL), poly(alkylcyanoacrylates) (PACA), poly(methyl methacrylate)(PMMA), poly (aniline) (PANI), poly(pyrrole) (PPy), poly(vinylpyrrolidone) (PVP), and their copolymers.[75-77] Interestingly, polymer coating enables the formation of a variety of "smart" IONPs, which are highly responsive to the surrounding conditions such as pH, temperature, and light, depending on how the polymer chains are functionalized. For example, poly (N-isopropylacrylamide) (PINPAAm) is a well-known thermal-responsive polymer because of the –NH-CO-group. Polymers containing carbonyl groups (PMMA, PAA, PEAA) or amine groups (PEI, chitosan) are good candidates to make pH-sensitive IONPs for adsorption and separation applications.

Metal coating. Magnetic nanoparticles coated with noble metals (e.g., Au, Ag, Cu, Pd, Co, Pt) are highly stable and exhibit unique physicochemical properties such as localized surface plasmon resonance and surface-enhanced Raman scatting.[78] The combination of metallic NPs and magnetic IONPs possess great potential for applications in catalysis, contrast imaging, medicine, and sensing.[51] The formation of IONP/metal structures involves molecular or charged links between IONPs and metal, or electron transfer at the interface of IONPs and metal for dumbbell IONP/metal structure. They can be realized through various synthetic routes, including redox

transmetalation, microemulsion, self-assembly, iterative hydroxylamine seeding, or other methods.[43]

Carbon coating. Carbon-protected IONPs are also attractive surface modification strategy because of their high chemical and thermal stability, intrinsic high electrical conductivity, as well as good biocompatibility. Carbon coated IONPs can be generated by the process of polymerization on magnetic seeds followed by subsequent carbonization. Such approach has been used to successfully make large-scale monodispersed Fe_3O_4@C core-shell structures with different morphologies such as spheres, chains, and rings.[79] Fe_3O_4/graphene hybrids are another popular routes to make multifunctional IONPs because of many readily available functional groups on graphene including carboxyl, hydroxyl, and epoxide groups. Fe_3O_4/graphene hybrids have shown some unique properties such as high conductivity, large surface-to-volume ratio, and high magnetism, which make them good candidates for a broad range of applications including lithium-ion batteries, sensors, catalysts, etc.

Silica coating. Silica coating has been one of the most popular surface modification strategies. Because a silica shell does not only protect magnetic cores from oxidation and acid erosion, but also provides –OH groups for further introduction of functionalities. There are two main approaches to make silica coated magnetic nanoparticles. One prevailing method is the well-established Stöber sol-gel process, in which silica is grown on the surface of nanoparticles through hydrolysis and condensation in the mixture of alcohol, ammonia, and water. Silanes including tetraethoxysilane (TEOS), vinyltriethoxysilane (VTEOS), and octadecyltrimethoxysilane are most commonly used silane source. The thickness of silica shell can be controlled by varying the concentration of ammonia and the ratio of TEOS to water. After silica coating, the surface of nanoparticles is full of –OH groups that are readily modified with other functional groups. Also,

the silica coated IONPs present excellent dispersibility owing to the negative surface charge on the silica shells.

The second method is microemulsion synthesis, which is also a sol-gel process. It utilizes micelles or inverse micelles in a microemulsion system to precisely confine the growth of silica on magnetic cores. The synthesis of core-shell structures with single IONP cores loaded into silica shell is challenging, because the surface energy of sub-50-nm IONPs is so high that the aggregation can be easily triggered either by pre-treatment of IONPs or by a vital change of the microemulsion composition. During the formation of core-shell nanoparticles, core-free silica beads and multi-core loading are the two main obstacles to obtain uniform single-cored structures. The energy barrier for heterogeneous nucleation is lower than the homogeneous nucleation, but heterogeneous and homogeneous nucleations are competing with each other throughout the reaction. Multi-loading phenomena may also be caused by the aggregation of IONPs before being injected into the reverse microemulsion system, or by the break of microemulsion stability during the reaction due to the evaporation of organic solvent and ammonia. [80]

It is noteworthy that core-shell nanoparticles with a single core and tunable silica shell thickness have been realized by the reverse microemulsion method.[81] This phenomenon may be explained by La Mer theory, in which the concentration of hydrolyzed TEOS monomer (C) must fall in the range between its solubility concentration (C_s) and homogeneous nucleation concentration (C_{homo}) throughout the reaction process (Figure 1.9). Based on this theory, Ding [81] found that the number of magnetic cores must match the number of reverse micelles by careful adjustment of the proportions among the concentration of TEOS, ammonia, surfactant, and IONP cores. Ding *et al.* have also demonstrated an equivalently fractionated drop method by adding fresh TEOS sequentially after the previous TEOS was consumed. Also, Chen[82] demonstrated that it is

hard to guarantee the reproducibility of single-loaded nanoparticles from batch to batch by adding TEOS manually, but adding TEOS using a syringe pump help better control of the final products.

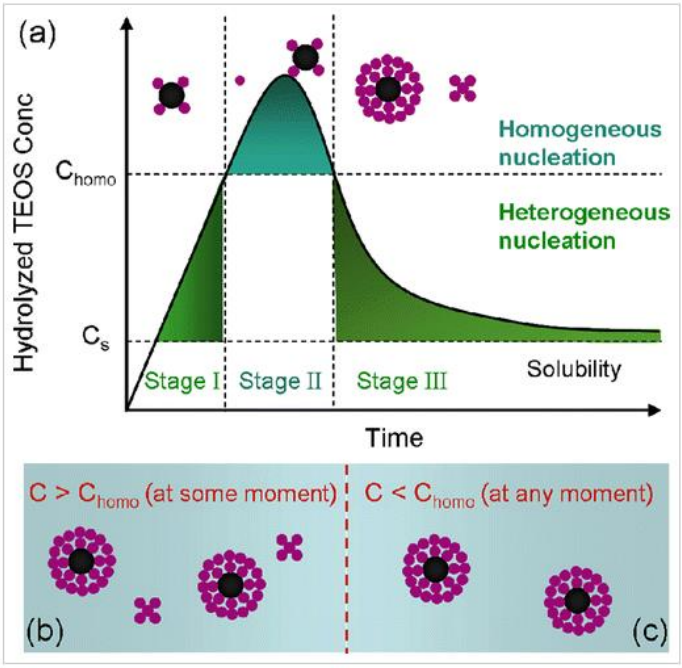

Figure 1.9. (a) La Mer-like diagram: hydrolyzed TEOS (monomers) concentration against time on homogeneous nucleation and heterogeneous nucleation, (b) the existence of Fe_3O_4@SiO_2 core/shell NPs and SiO_2 NPs when $C > C_{homo}$ at some moment. (c) the existence of only Fe_3O_4@SiO_2 core/shell NPs when $C < C_{homo}$ at some moment. Reprinted with permission from **Ref. 81**. Copyright 2012 Ameican Chemical Society.

1.5.3 Reverse microemulsion system strategies.

Reverse microemulsions are usually described as small water droplets surrounded by a monolayer of surfactant in a nonpolar solvent. It is a phenomenon caused by the self-assembly of surfactant with its polar head groups packed towards the aqueous core. In a reverse microemulsion system, water-in-oil reverse micelles are of great interest in the synthesis of inorganic nanoparticles. Silica coating of inorganic nanoparticles in a water/polyoxyethylene(5) nonylphenylether (Igepal CO-520)/cyclohexane reverse microemulsion has been proven very effective for the synthesis of nanoparticles. These reverse micelles provide confined space of nanometers for silica shells to grow on nanoparticles, resulting in functionalized nanoparticles with

exceptionally sharp size distributions. More interestingly, the reverse microemulsion technique allows for the formation of uniform silica shell on single hydrophobic nanoparticles, such as oleate-modified hydrophobic IONPs. A surfactant-exchange mechanism has been suggested by several research groups for the silica shell formation,[83,84] in which the capping agent of oleic acid on the particle surface is exchanged with a nonionic surfactant.[81] To further uncover the mechanism of the formation of single-core type nanoparticles, Katagiri and Ritcey research groups studied the surfactant-exchange and shell growth of silica coated IONPs using dynamic light scattering (DSL).[85,86] They calculated the concentration of free surfactant according to DSL data and found that the concentration of free surfactant and volume occupied by the surfactant within the polar core are not negligible. Particularly, they found that the amount of free surfactant in a fixed amount (15 mL) of cyclohexane exceeded 50%. After taking into consideration the free surfactant concentration, the volume taken up by the polar head of the surfactant within the micelles, and effective length of hydrophobic part of the surfactant, Lemyre and co-workers developed a model to predict the hydrodynamic radius of reverse micelles, with the assumption that the shape of reverse micelles is spherical: [86]

$$r_{DLS} = \sqrt[3]{\frac{3N}{4\pi}\left(\frac{V_{H_2O,total}}{n_{surf,\ in\ micelles}} + V_{surf,\ hphile}\right)} + l_{hphobe} \quad (1.8)$$

Where r_{DLS} is the hydrodynamic radius of the reverse micelle; N is the aggregation number, meaning the number of surfactant molecules per reverse micelle; $V_{H_2O,total}$ is the total volume of water in the system; $n_{surf,\ in\ micelles}$ is the number of surfactant molecules in all reverse micelles; $V_{surf,\ hphile}$ is the volume of the hydrophilic part of the surfactant (Igepal CO-520, 0.35 nm^3); l_{hphobe} is the effective length of the hydrophobic tail of the surfactant (Igepal CO-520, 1.35 nm).

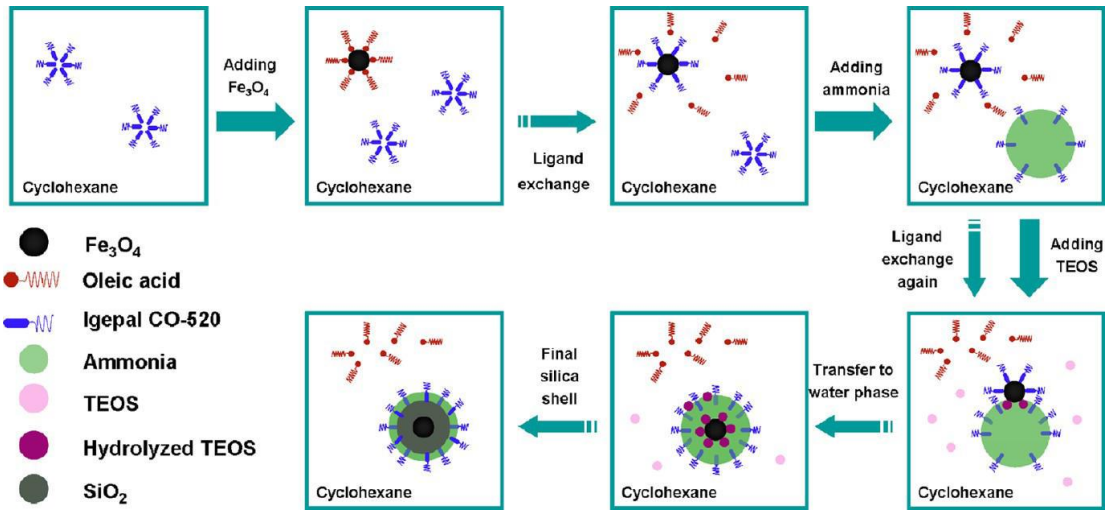

Figure 1.10. A ligand-exchange mechanism of silica coating in a water/Igepal CO-520/cyclohexane reverse microemulsion system. Reprinted with permission from **Ref. 81**. Copyright 2012 Ameican Chemical Society.

1.6 Plan of study

Given the fact that a lot of APIs and biomolecules (proteins and nuclei acids) contain amines and carboxylic acids, it is of significance to develop a continuous-flow purification platform to selectively separate such molecules. One attractive solution is to realize selective attachment of desired product to the surface charged magnetic nanoparticles via electrostatic binding, accompanied by continuous detachment of products. The association and dissociation between product and magnetic nanoparticles are achieved by changing pH (Figure 1.11). The magnetic force assisted microfluidic separation does not require the consideration of the nature of products because the magnetic forces that drive the separation is free of contact with targets. Magnetic separation in a continuously flowing mode also avoids sharp loss of targets from multiple washing cycles and reduces trapping of impurities in magnetic aggregates. While most currently used magnetic materials are microbeads or nanoclusters, which have shown high magnetization by sacrificing the size and morphology control, core-shell magnetic nanoparticles with a single core and controlled silica shell thickness and abundantly available surface functionalities as

binding sites would be ideal for effective separation. Controlled silica shell thickness could provide enough protection for the magnetic core without significantly losing the magnetization. In addition, with only a thin layer of functionalities attached on the surface, the separation efficiency is largely increased. Moreover, single-core structures can maintain magnetization for a longer period because unencapsulated magnetic nanoparticles tend to aggregate over time to reduce energy, which could result in magnetization loss. Therefore, the first objective of this project was to synthesize single-cored magnetic nanoparticles with surface amines and carboxylic acids. Once the magnetic nanoparticles were prepared, the second objective of the project was to utilize the functionalized nanoparticles for affinity-based separation in a microfluidic device. The microfluidic device is fabricated with PDMS through a general micromold casting procedure. It is composed of a mixing chip and a separation chip connecting with capillary tubing. As a proof of principle, dye mixture of toluidine blue O (TBO) and fluorescein, resembling drug molecules, were separated by carboxyl functionalized IONPs Fe_3O_4@SiO_2-COOH in the micro-channel, where Fe_3O_4@SiO_2-COOH can selectively capture TBO via electrostatic binding.

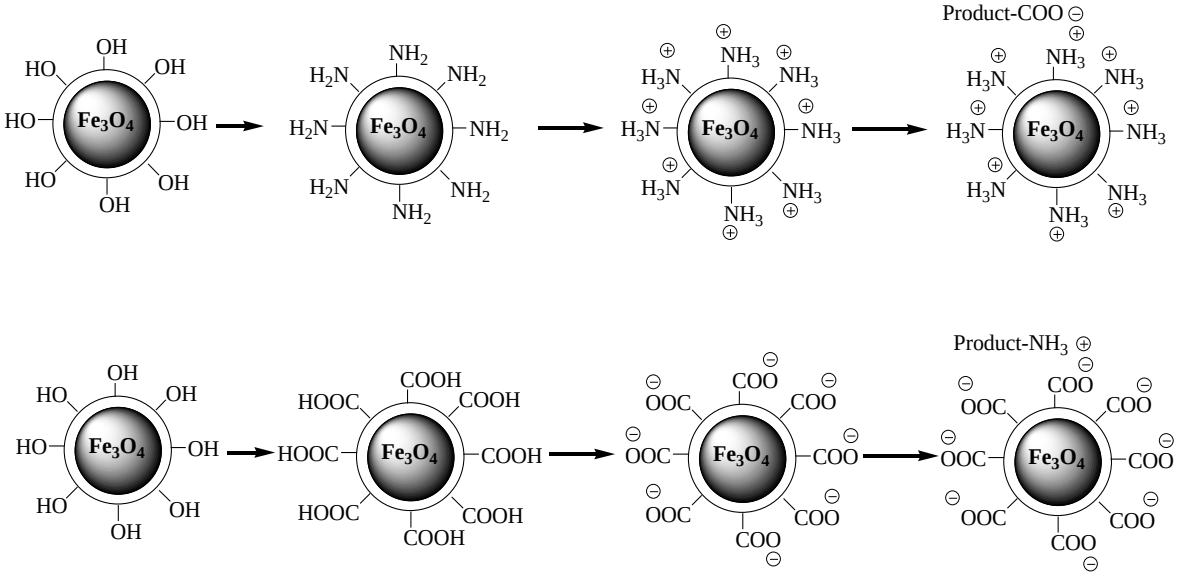

Figure 1.11. Reversible complexation of charged iron oxide magnetic nanoparticles with amine/carboxyl-based products.

CHAPTER 2. ONE-POT SYNTHESIS OF SIZE CONTROLLABLE AMINE-FUNCTIONALIZED CORE-SHELL MAGNETIC NANOPARTICLES

2.1 Introduction

Surface modified IONPs with controlled morphologies, fast magnetic responsiveness, high colloidal stability, and high density of surface functionalities are ideal for selective separation in a microfluidic device. In particular, iron oxide magnetic nanoparticles have gained popularity because of their low cost and ease of preparation. Among various methods of making IONPs, thermal decomposition has proven superior to other methods such as coprecipitation and solvothermal reduction, for obtaining monodisperse, size controllable, as well as superparamagnetic nanoparticles. In a thermal decomposition process, an iron oleate precursor is mixed with a surface capping agent (e.g., oleic acid), and decomposed in a high-boiling nonpolar solvent at temperatures above 300 °C, resulting in iron oxide nanocrystals with very high scalability, narrow size distributions, tunable sizes and low crystalline defects.[43,87] However, IONPs prepared using this method are hydrophobic. Subsequent application of those IONPs for aqueous microfluidic separations requires the replacement of the long hydrophobic alkyl surfactants on their surfaces with hydrophilic or amphiphilic ligands. Ligand exchange using small molecules seems a very simple and straight forward strategy. For example, Liu and co-workers[88] recently demonstrated a direct conversion method from hydrophobic to hydrophilic IONPs using 3,4-dihydroxyhydrocinnamic acid without any complicated organic synthesis. Despite the convenience of ligand-exchange strategy, the modified surface with such a thin layer of small molecules could not provide enough protection, meaning the IONPs will aggregate and even lose magnetization after being used several times. Therefore, a more efficient generalizable surface modification strategy is an important step towards the application of IONPs in separation.

An attractive method is coating the nanoparticles with silica shells. Because silica shells can not only protect the nanoparticles from being oxidized, but can also easily be further modified with various functionalities for a large range of desired applications. Another advantage of a silica coating lies in its nontoxicity, which enables the application of IONPs in a broader range of applications, especially in the biomedical field. Moreover, hydrophobic IONPs made from non-polar solvents can be made hydrophilic with the coating of a silica shell due to the surface hydroxyl groups present. Ding and coworkers[81] reported an easy way to prepare size tunable Fe_3O_4@SiO_2 core/shell nanoparticles with a single magnetic core by a reverse microemulsion method. They discovered that the ratio of IONPs, Igepal CO-520 and ammonium in the silica coating reaction is very important to obtain high quality of core-shell structures with a single magnetic core in the center of a silica shell. Also, the shell thickness can be controlled by the amount of TEOS added.

The formation of core-shell IONPs comprising a silica layer coating onto a single magnetic core seems attractive towards realizing our goal of continuous separation in microfluidic devices. Simple microemulsion methods have been reported for the facile encapsulation of a variety of nanoparticulate cores with silica shells.[81,83,84,89,90] Unfortunately, subsequent shell functionalization typically involves complicated multi-step procedures and polymerizations, which are time-consuming and labor-intensive.[91] Therefore, less complicated synthetic routes towards functionalized magnetic nanoparticles are desirable. In this work, we demonstrated a simple one-pot synthesis of amine functionalized core-shell magnetic nanoparticles with a tunable shell thickness using a reverse microemulsion method, and its potential applicability in microfluidic separations.

2. 2. Experimental

2. 2. 1 Materials and methods

Ferric chloride hexahydrate ($FeCl_3$•$6H_2O$) was purchased from Fisher, sodium oleate was obtained from TCI America. Tetraethyl orthosilicate (TEOS), (3-aminopropyl)triethoxysilane (APTES), cyclohexane, 1-butanol, and IGEPAL®CO-520 (average Mn 441), Fmoc chloride, piperidine, dimethylformamide (DMF), and sodium fluorescein were purchased from Sigma-Aldrich. Sodium acetate (NaOAc), Triton-X100 were bought from BDH chemicals; ammonium hydroxide (NH_4OH, 28%~30%) was obtained from Caledon. All solvents were dried over 4A molecular sieves and filtered prior to use.

UV-Vis spectroscopy was performed on a NanoDrop 2000c/2000 UV-Vis spectrophotometer. High-speed centrifugation was performed using a Baxter Biofuge 17R centrifuge. Sonication was performed using a Branson 450 Digital Sonifier. High temperature reactions were carried out in either a Welmet FT3034 or Carbolite STF 16/180 tube furnace. A sintered $Nd_2Fe_{14}B$ permanent supermagnet was used for magnetically-assisted precipitation of nanoparticles. Morphologies and particles sizes were examined on a transmission electronic microscopy (TEM, Philips 2000). Powder X-ray diffraction (PXRD) spectra were run on a Siemens D5000 Diffractometer System operating at 50Kv/35 mA. The surface functionalities were determined by a Fourier transform infrared spectroscopy (FTIR, Thermo Fisher).

2. 2. 2 Synthesis of monodisperse hydrophobic Fe_3O_4 nanoparticles

Monodisperse hydrophobic IONPs were obtained using a modified thermal decomposition method by Hyeon.[48] Iron oleate was first prepared by refluxing a mixture of $FeCl_3$•$6H_2O$ (8 mmol, 2.16g) and sodium oleate (24 mmol, 7.31g) in a solvent mixture of H_2O, EtOH, C_6H_6 (12 mL, 16

mL, 28 mL) at 70°C for 4 h. The expected $Fe(oleate)_3$ complex was extracted from the organic layer using a separatory funnel, washed with distilled water 3 times, and dried *in vacuo*. 4.24g (4.72 mmol) $Fe(oleate)_3$ was transferred into an 80 mL tube containing 1-octadecene (29.9 mL), oleic acid (2.36 mmol, 0.75 mL), and made homogeneous with a votex mixer. The tube was transferred to a tube furnace and flushed with argon (Figure 2.1). The reaction mixture was heated to 320 °C and refluxed at this temperature for 30 min under a static pressure head of argon. The resulting black solution was cooled to room temperature and precipitated by excess ethanol. The precipitate was collected by centrifugation, then redispersed in hexane and precipitated with ethanol several times to purify the resulting Fe_3O_4 nanoparticles. The purified IONPs were dried *in vacuo* and stored as a suspension in cyclohexane (25 mg/mL) under Ar.

Figure 2.1. A modified reaction setup for the synthesis of hydrophobic Fe_3O_4 nanoparticles using a thermal decomposition method.

2. 2. 3 Synthesis of amine modified Fe_3O_4 core-shell nanoparticles with controllable shell thickness

A modified reverse microemulsion method by Ding[81] was used to obtain amine functionalized core-shell IONPs, herein symbolized as Fe_3O_4@SiO_2-NH_2 (as shown in Scheme 2.1). Typically, 0.25 mL of Igepal CO-520 surfactant was dissolved in 10 mL cyclohexane, and subjected to sonication for 15 min. Then 100 μL NH_4OH was added followed by 2.5 mg Fe_3O_4 (2.5 mg/mL in cyclohexane). After 30 min of continuous magnetic stirring, 50 μL TEOS was added to the mixture via an equivalently fractionated dropping method at a rate of 35 μL every 16 h. A certain molar ratio of APTES to TEOS was subsequently added 24 h after the TEOS was added. When the reaction finished, 2 mL of methanol was added to break the microemulsion. The hydrophilic product was purified by alternatively washing with EtOH and distilled water. The resulting Fe_3O_4@SiO_2–NH_2 IONPs were collected magnetically and dried *in vacuo*.

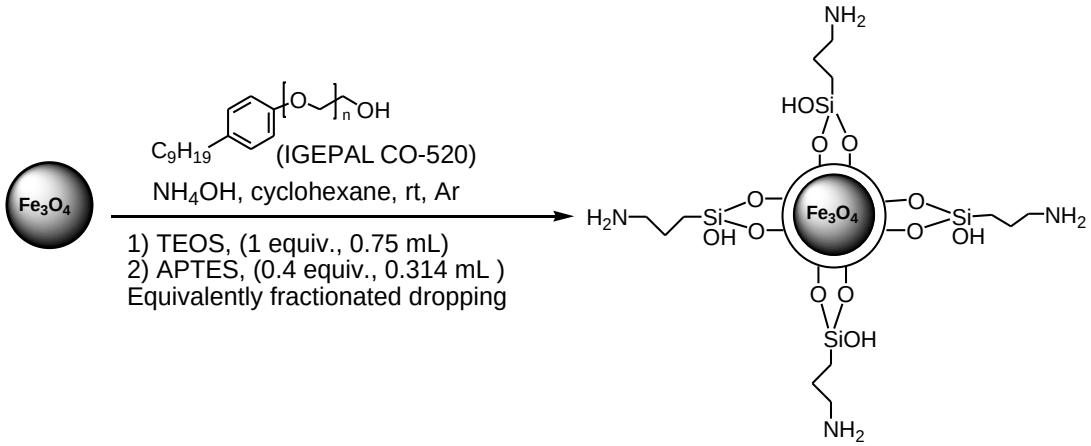

Scheme 2.1. One-pot synthesis of amine-functionalized Fe_3O_4@SiO_2-NH_2 magnetic nanoparticles.

2. 2. 4 Determination of active amine groups on Fe_3O_4@SiO_2–NH_2 IONPs

Because there are unavoidable embedded amine groups by the top layer and unreacted APTES, the number of active functional groups on the surface of magnetic nanoparticles was

examined using a reported Fmoc method.[92] The experimental procedure was as follows: 20 mg Fe_3O_4@SiO_2–NH_2 were dispersed in 2 mL dry DMF. An excess amount of Fmoc-Cl (1.07 mmol, 277 mg) was added and the mixture was sonicated for 40 min under argon. The nanoparticles were isolated by high-speed centrifugation, washed with MeOH 5 times to remove unattached Fmoc-Cl residues, and dried *in vacuo*. The attached Fmoc molecules were then cleaved by the action of piperidine (200 μL) in DMF (800 μL) under sonication for 20 min. The nanoparticles were removed by high-speed centrifugation, and the number of Fmoc-Cl molecules covalently bound to the NH_2 groups was determined spectrophotometrically at 226 nm and the NH_2 groups was calculated from a calibration curve of optical density vs. known Fmoc-Cl concentration, assuming that each group binds a single Fmoc-Cl molecule.

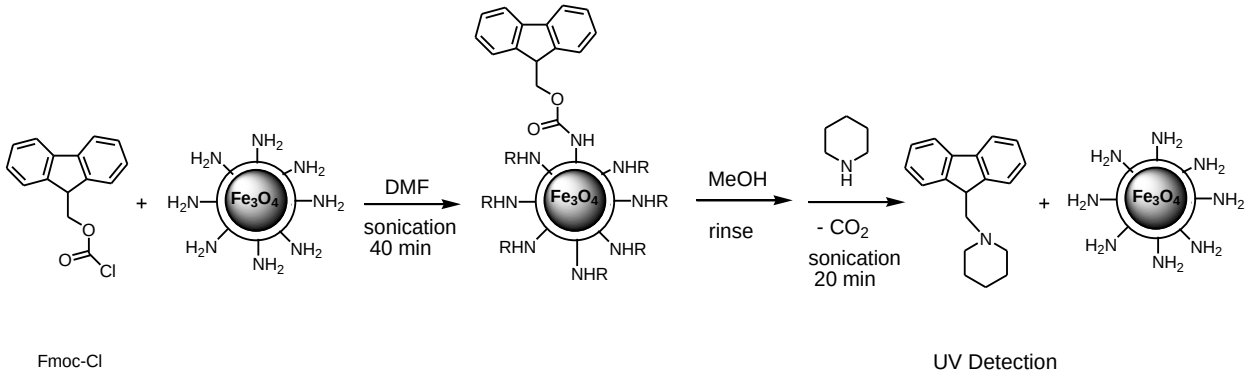

Scheme 2.2. Assay of active amine groups on Fe_3O_4@SiO_2-NH_2 nanoparticles.

2. 2. 5 Surface binding capacity of Fe_3O_4@SiO_2-NH_2 IONPs

The active amine groups were detected by reacting with Fmoc-Cl through covalent binding. But to realize fast capture and release in a microfluidic device, electrostatic binding is preferred. The binding efficiency may vary due to different binding forces. So the binding capacity of resulting Fe_3O_4@SiO_2-NH_2 IONPs was studied by a colorimetric method using fluorescein as target molecules. Briefly, 20 mg Fe_3O_4@SiO_2-NH_2 IONPs were homogenously dispersed and

incubated in HCl solution (pH 5), allowing for the protonation at the particle surface. Then sodium fluorescein (0.54 mL, 0.01 M) was added as a model target resembling carboxylate drug molecule. The mixture was kept at pH 5 and stirred for 1 h, then rinsed with ethanol/water by repeated sonication/magnetic isolation cycles, in order to remove unbound fluorescein molecules from the surface of IONPs. The precipitated IONPs were dried *in vacuo*, then sonicated into 1000 μL NaOH to release fluorescein molecules from the IONPs. The amount of bound fluorescein was determined using a UV-vis spectrophotometer at 490 nm. Prior to this, a calibration curve of optical density vs. known fluorescein concentrations was obtained. And the calculation of binding capacity was based on the assumption of 1:1 ratio between the fluorescein and the NH_2 groups.

2. 3 Results and Discussion

2. 3. 1 Monodisperse Fe_3O_4@SiO_2 core-shell nanoparticles

Hydrophobically-capped iron oxide cores obtained by the thermal decomposition method are highly reproducible, monodisperse, and size controllable. Transmission electron microscopy (TEM) in Figure 2.2 (a) indicates the material exists as highly monodisperse spherical nanoparticles having average diameter of 20 nm. Powder X-ray diffraction (PXRD) studies (Figure 2.2 (b)) confirm that these particles are magnetite (Fe_3O_4). Application of the Scherrer equation (equation 2.1) to the broadening of the (311) reflection signal corroborate an average diameter of 20 nm.

$$D = \frac{k\lambda}{\beta cos\theta} \qquad (2.1)$$

Where D is the mean size of the crystallites (nm), k is crystallite shape factor approximate to 0.9, λ is the x-ray wavelength, β is the line broadening at half the maximum intensity of the peak, and θ is the diffraction angle.

In our experiment, the reactions were carried out in a tube furnace, obtaining the same spherical monodisperse IONPs nanocrystals as reported in the literature, in which the reaction was carried in a round flask placed in a temperature-controlled heating mantle, with the exception that the size of our IONPs are larger. The size of IONPs could be result of a co-effect of solvents and capping agents. Heyon[56] reported in their work that the size of IONPs can be increased by increasing the boiling point of solvents. Also, the capping agents can modify the surface energy at the solid-liquid interface and therefore have a significant effect on the size and shape of resulting IONPs. Willis and coworkers[54] proved that oleic acid acts like reducing reagent by losing the double bond on the backbone, which is necessary for the synthesis of stable monodisperse iron oxide nanocrystals. Thus, it is the coexistence of oleic acid and 1-octadecene in a proper proportion that determined morphology and size distribution of IONPs.

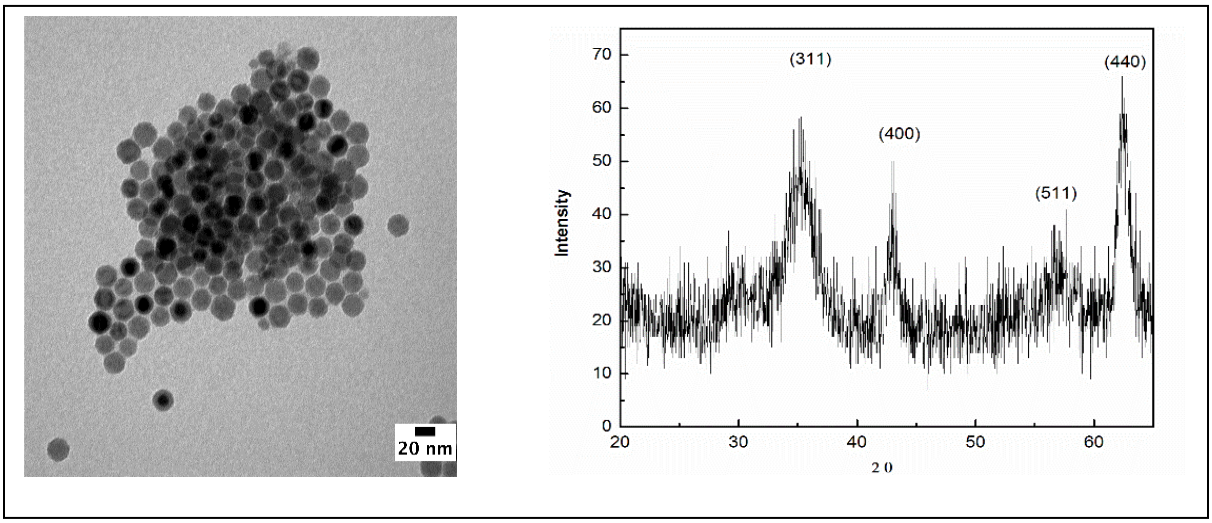

Figure 2.2. (a) TEM image and (b) PXRD pattern of Fe_3O_4 cores.

Fe_3O_4@SiO_2 core-shell nanoparticles were obtained by silica coating of the Fe_3O_4 cores through a water-in-oil (w/o) microemulsion process,[90] in which base-catalyzed hydrolysis of tetraethyoxysilane (TEOS) occurs in the interior of reverse micelles that are surrounded by a

monolayer of Igepal CO-520 surfactant in cyclohexane. The silica coating process actually undergoes a ligand exchange mechanism in the reverse microemulsion system, where the long-chain oleic acid on the IONP surface was replaced by the surfactant and the surfactant was replaced by silanol again. After two ligand exchange steps, the IONPs enter the ammonia aqueous domain, in which each iron oxide magnetic core behaves like a nucleation site for TEOS to grow on the particle surface to form core-shell structures. Figure 2.3 showed the TEM images of resulting silica-coated nanoparticles Fe_3O_4@SiO_2. The coating conditions were summarized in Table 2.1. In Figure 2.3, images 1, 2, and 8 indicate that decreasing the amount of ammonia resulted in obtaining no core-shell structures. According to image 1, 6, 7, and 10, no core-shell structures could be obtained at either low or high concentration of surfactant CO 520. Image 1 and 5 show that addition of cosurfactant 1-butanol is not necessary. Images 4 (T-N) and 9 (N-T) represent adding TEOS (T) and NH_4OH (N) in different order, and the result show that reversing the sequence of adding TEOS and ammonia did not affect the formation of single-cored structures. So after figuring out the proportion of the surfactant and ammonia hydroxide to form core-shell structures, the core-free silica beads were minimized by increasing the amount of iron oxide magnetic cores. According to image 10 and 12, with more Fe_3O_4 cores added, no core-free structures were found. Image 11 and 12 indicate that the addition of TEOS only affect the shell thickness but not the formation of core-shell structures. Comparing the entries in table 2.1, it was found that the amount of surfactant added and NH_4OH played a more significant role on the obtaining core-shell nanostructure than that of TEOS and co-surfactant 1-butanol. Therefore, to obtain core-shell nanostructures with a single magnetic core, and without core-free SiO_2 nanoparticles, it is crucial to match the number of magnetic cores with the number of inverse micelles. It is known that the size and number of inverse micelles in a base-catalyzed silica

microemulsion is governed by a complex interplay between the concentrations of base, organosilane, and surfactant.[81] The competition between homogenous and heterogenous nucleation is highly determined by the concentration of hydrolyzed TEOS in the microemulsion system. If the concentration of the hydrolyzed TEOS passes a threshold for homogenous nucleation, core-free silica beads would be found in the products. Also, at low core to micelle ratios, core-free silica nanoparticles form; at high core to micelle ratios, multicore structures are present. We found the optimum conditions in our experiments for producing the highest yield of single-core structures with little or no core-free silica has a core: NH_4OH : CO-520 mass ratio of 2.5 : 0.1 : 0.25. Moreover, under these optimum conditions, the thickness of the shell can be controlled by the gross amount of TEOS in the reaction mixture. For example, the addition of 50 μL and 75 μL TEOS to 2.5 mg of Fe_3O_4 cores in 10.0 mL cyclohexane gave silica shell wall thicknesses of 15 nm and 20 nm, respectively.

Table 2.1. A summary of condition optimization for silica coating.

Entry	Fe_3O_4 (mg)	TEOS (μL)	NH_4OH (μL)	CO-520 (g)	1-butanol (μL)	Core-shell formed
1	1.25	75	100	0.50	0	no
2	1.25	75	50	0.50	0	no
3	1.25	50	100	0.50	0	no
4 (T-N)	1.25	75	100	0.25	0	yes
5	1.25	75	100	0.50	100	no
6	2.50	75	100	0.50	0	no
7	1.25	75	100	0.20	0	no
8	1.25	75	75	0.25	0	no
9 (N-T)	1.25	75	100	0.25	0	yes
10	1.25	75	100	0.25	0	yes
11	2.50	50	100	0.25	0	yes (no core free)
12	2.50	75	100	0.25	0	yes (no core free)

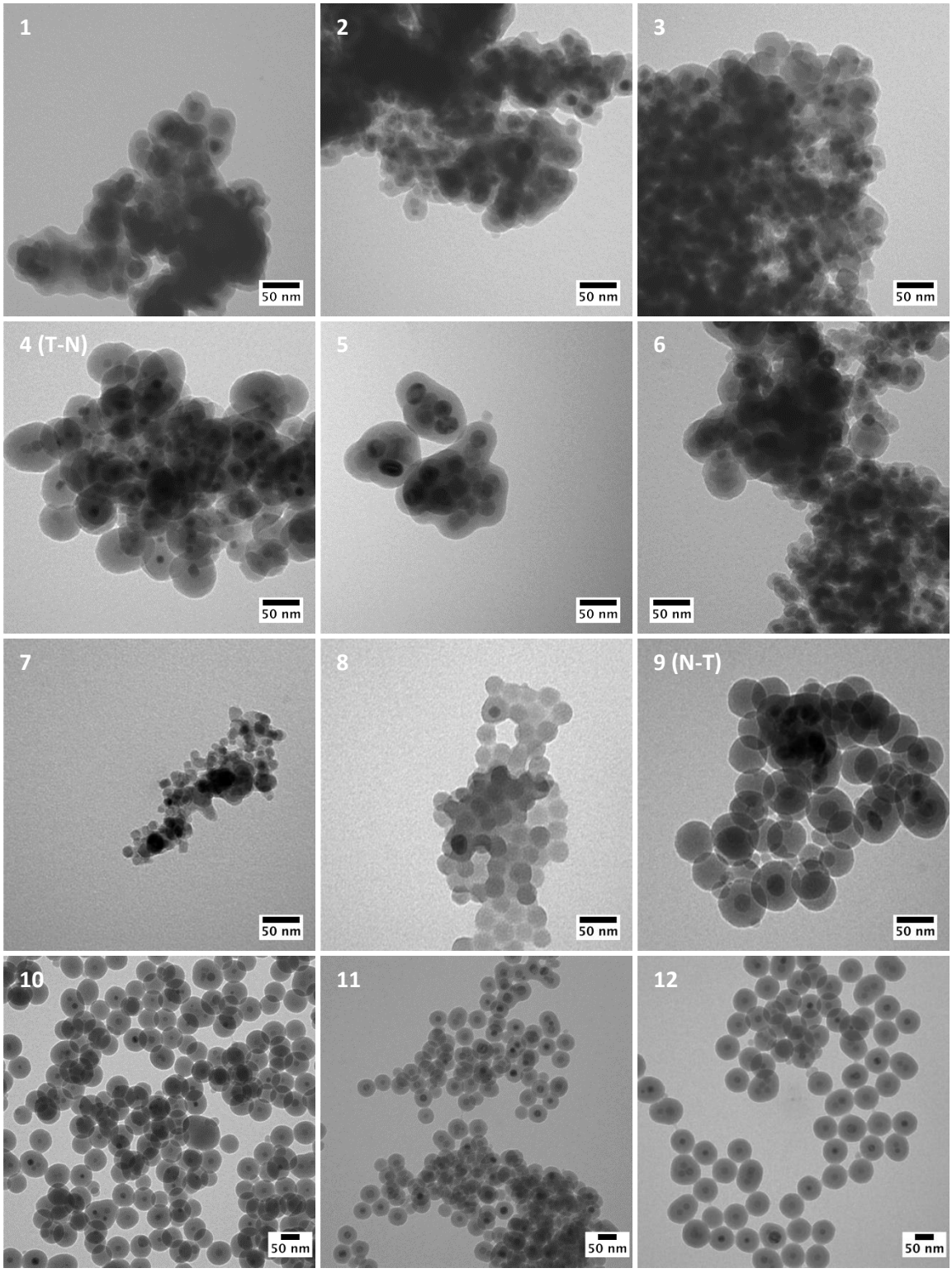

Figure 2.3. TEM images of optimization of silica coating conditions with various ratios of Fe_3O_4, TEOS, NH_4OH, CO-520.

2. 3. 2 Size-tunable amine-functionalized Fe_3O_4@SiO_2-NH_2 IONPs

A series of amine terminated core-shell nanoparticles were obtained by adding various mole fractions of APTES. The IONPs after surface modification are single-cored structures with the magnetic cores in the center of the nanostructure. With the increment of the APTES added, the shell thickness increased accordingly, as shown in Figure 2.4. Compared to the surface of unfunctionalized core-shell nanoparticles, the surface of nanoparticles after amine functionalization appears to be rough. This may be because of the large amount of free -OH groups existing on the surface, enabling the growing of multiple layers of amine functional groups. The roughness could also because of the nucleation of small independent particles due to the hydrolysis of APTES.

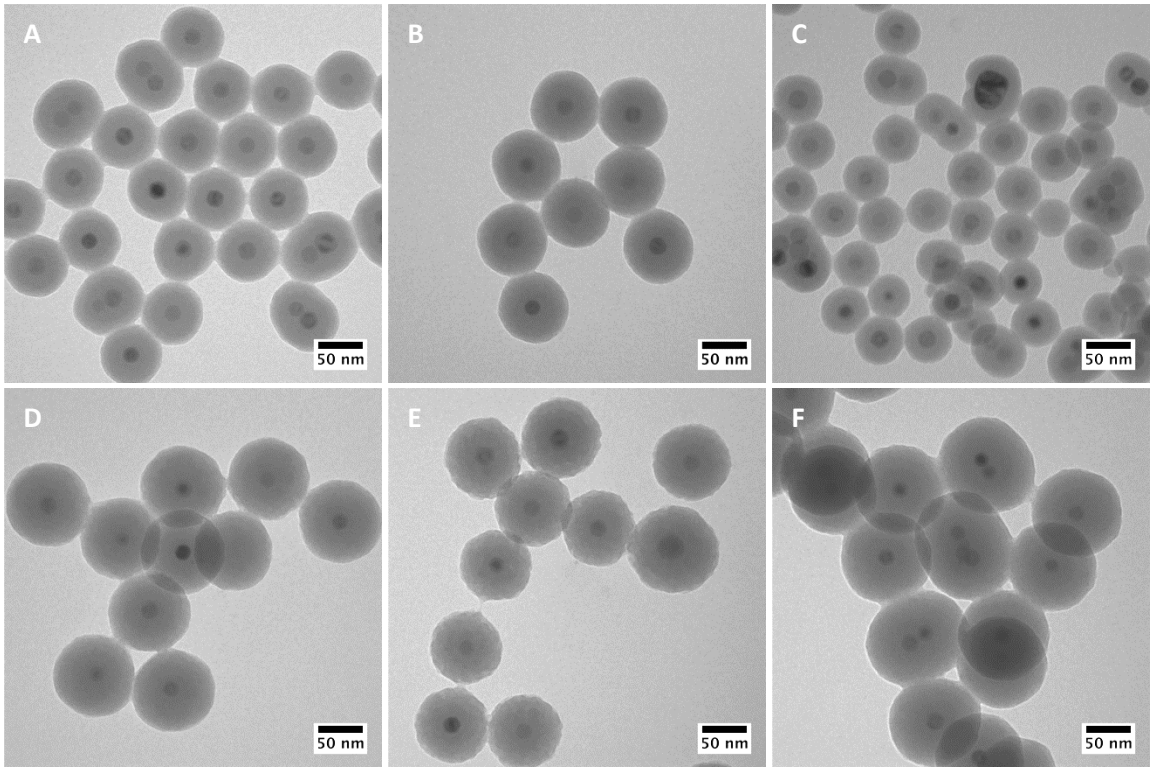

Figure 2.4. TEM images of size controllable Fe_3O_4@SiO_2-NH_2 IONPs with different mole ratios of APTES: A, 0% APTES (55nm); B, 10% APTES (76 nm); C, 20% APTES (67 nm); D, 30% APTES (92 nm); E, 40% APTES (86 nm); F, 50% APTES (100 nm).

Figure 2.5 shows that the thickness of the amine layer is controlled by the percent mole ratio of APTES (mole ratio of APTES to TEOS). The shell thickness increased from 15 to 40 nm with the increment of APTES added (0–50 %mol). The resulting Fe_3O_4@SiO_2-NH_2 nanoparticles exhibited high magnetization and were very responsive to a magnet. As shown in Figure 2.6, the resulting IONPs showed very fast response to a magnet.

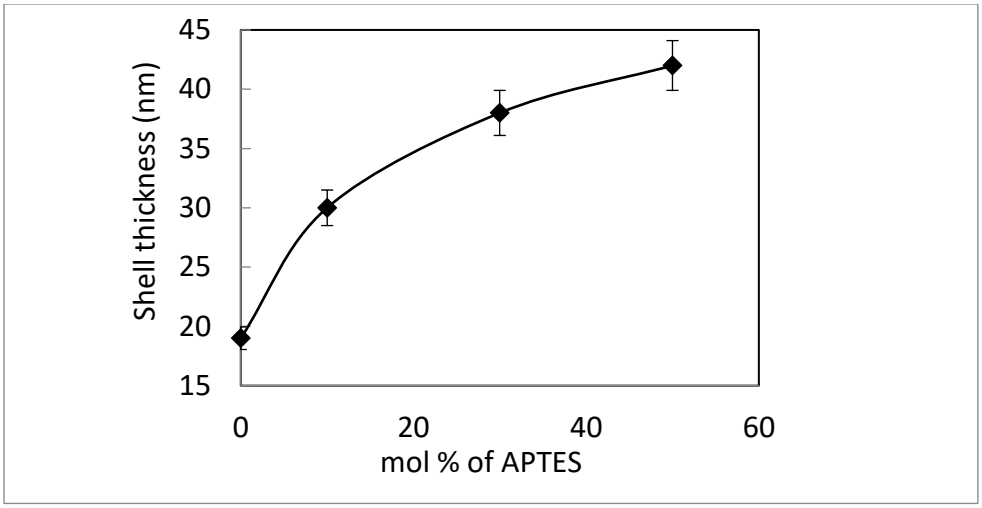

Figure 2.5. Average SiO_2 shell thickness dependence on APTES concentration.

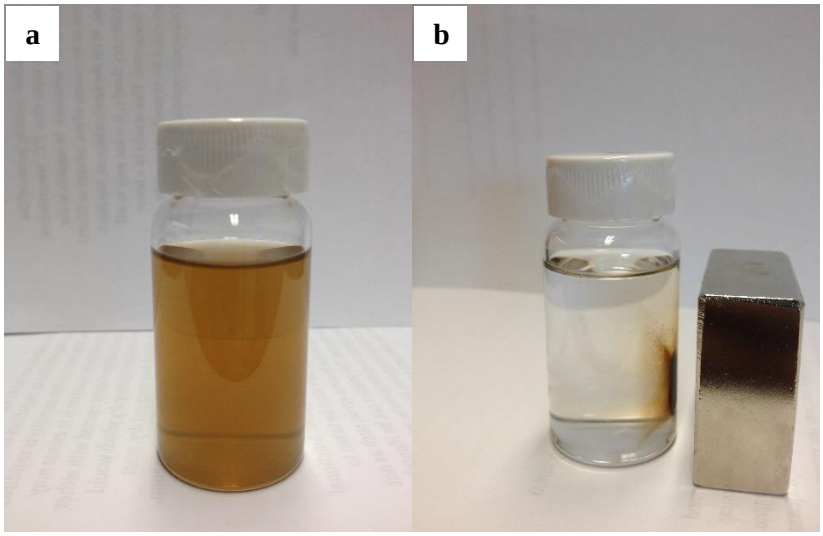

Figure 2.6. Separation of resulting Fe_3O_4@SiO_2-NH_2 nanoparticles using a magnet, a) particle suspension before separation; b) particles collected by a magnet (within 5 min).

The presence of surface amine groups was confirmed by IR spectroscopy. Figure 2.7 presents the IR spectra of (a) oleate capped Fe_3O_4 nanoparticles, (b) Fe_3O_4@SiO_2 core-shell nanoparticles, and (c) Fe_3O_4@SiO_2-NH_2 amine-functionalized core-shell structures (10% APTES). In spectrum (a), the absorptions at 2923 cm^{-1} and 1624 cm^{-1} are attributed to aliphatic C-H and carboxylate C=O, respectively, and indicate the existence of oleic acid capping groups. The absorptions near 1099, 947, 800, and 471 cm^{-1} appear in spectra b and c, and are assigned to vibrational modes of SiO_2. The broad peak centered at 3408 cm^{-1} arises from the stretching vibration of surface Si-O-H bonds. In spectrum c, the broad peak occurred near 3400 cm^{-1} indicates the presence of Si-O-H on the particle surface due to hydrolysis. But the two distinct bands observed at 3392 and 3257 cm^{-1} can be assigned to the stretching vibrations of primary amines - NH_2. The band observed at 1506 cm^{-1} is assigned to the $–NH_2$ bending mode.

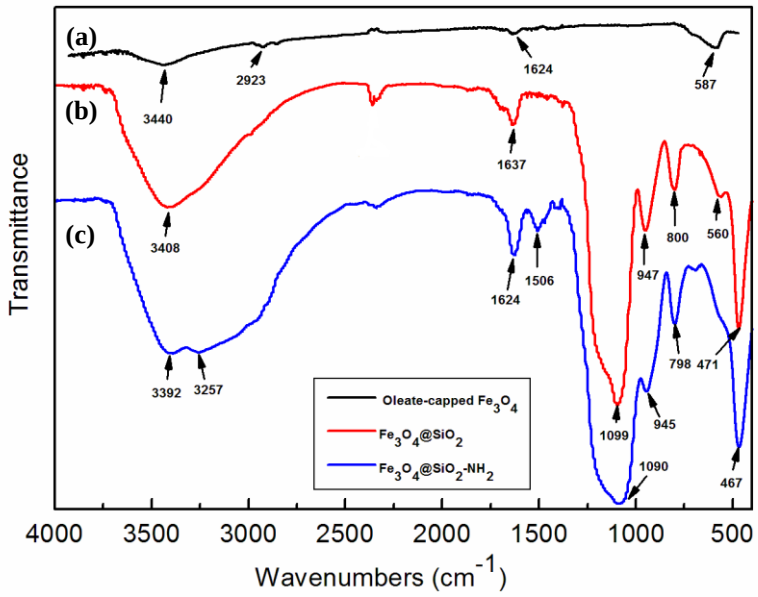

Figure 2.7. IR spectra of (a) oleate-capped Fe_3O_4 cores, (b) Fe_3O_4@SiO_2 core-shell nanoparticles, and (c) Fe_3O_4@SiO_2-NH_2 10% functionalized core-shell nanoparticles.

Assay of the active surface amine moieties was accomplished by a standard Fmoc quantification protocol.[93] Fmoc chloride undergoes quantitative covalent binding to primary amine residues via an amide linkage. Thus, the Fe_3O_4@SiO_2-NH_2 nanoparticles were incubated with excess Fmoc chloride, then isolated and washed extensively to remove any unbound Fmoc. The Fmoc tagged nanoparticles were then suspended in clean DMF, and the amide linkage was cleaved by the action of piperidine. The concentration of released Fmoc in solution was determined spectrophotometrically, using the predominant absorption bands of Fmoc at 226 nm. As shown in table 2.2, assuming each amine group binds a single Fmoc-Cl molecule, we determined that for the Fe_3O_4@SiO_2-NH_2 IONPs prepared with 20 mol% APTES resulting in 67 nm size, the number of amine groups per nanoparticle was $1.6 \pm 0.046 \times 10^4$, representing 1.2 ligands/nm^2 amine moieties per nanoparticle. A control sample of unfunctionalized Fe_3O_4@SiO_2 resulted in no detectable UV absorption.

Table 2.2. Assay of NH_2 groups on a single IONPs by Fmoc-Cl quantification.

Name	**NH_2 / IONPs** (ligands/nm^2)	**% error**
Fe_3O_4@SiO_2-NH_2	1.2	3.6%
Fe_3O_4@SiO_2	0.0	0.0%

2. 3. 3 Magnetic separation of anionic organic targets by Fe_3O_4@SiO_2-NH_2 nanoparticles

We demonstrate the potential of our surface-functionalized core-shell magnetic nanoparticles for use in a microfluidic separation device, by electrostatically binding fluorescein carboxylate as a model target, magnetically separating the target-nanoparticle complex from the target solution, and releasing the target into fresh solvent by pH induced desorption from the nanoparticle, as illustrated in Scheme 2.3. Fluorescein is a convenient model target, as its intense

visible fluorescence can be readily detected by the naked eye under UV illumination, and accurately assayed fluorometrically.

The Fe_3O_4@SiO_2-NH_2 suspension was first brought to pH 5. At low pH, the amine groups on the surface of IONPs were protonated. This suspension is then added to an aqueous solution of sodium fluorescein, in which the anionic fluorescein electrostatically adsorbs to the cationic surface of nanoparticles. The formed fluorescein-attached IONPs were symbolized as Fe_3O_4@SiO_2-NH_3^+ FL^- (FL means fluorescein). The fluorescein-bound nanoparticles are then isolated from the target solution by magnetic separation and, after several washings with ethanol to remove any unbound fluorescein, ultrasonically suspended in a clean aqueous solution. This suspension shows no visible fluorescence, indicating that the fluorescein is likely bound through its (non-fluorescent) open-ring carboxylate form. By adding NaOH to raise pH, the ammonium groups on the nanoparticle surface were deprotonated, causing the fluorescein molecules to be released in the solution in their fluorescent conformation (Figure 2.8 (a)). The unbound nanoparticles were then completely removed from the supernatant by high-speed centrifugation. Fluorescence of the solution was observed, indicating the successful adsorption and desorption of model molecules from IONPs by adjusting the pH of environment.

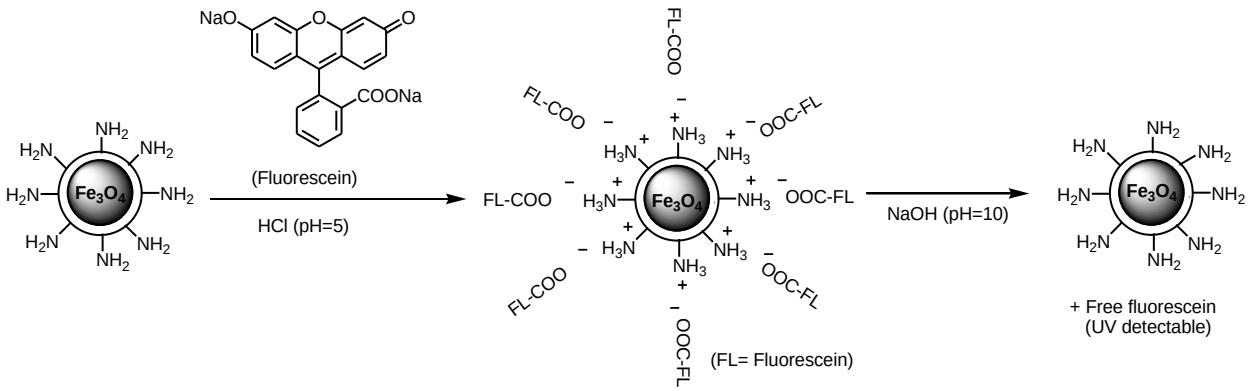

Scheme 2.3. Adsorption/desorption of an anionic target on Fe_3O_4@SiO_2-NH_2 nanoparticles.

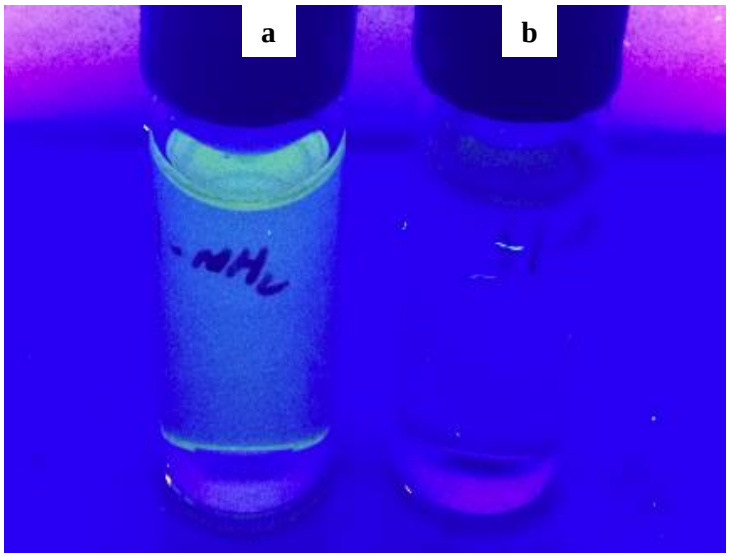

Figure 2.8. Fluorescence of released fluorescein molecules under UV light, a) $Fe_3O_4@SiO_2$-NH_2, fluorescence observed after release of free fluorescein; b) $Fe_3O_4@SiO_2$ (control group), no fluorescence.

At high pH, fluorescein exists in its highly fluorescent lactone-phenolate form, causing the solution of released target to glow visibly under long-wave UV light. Fluorometric analysis of fluorescein concentration in the supernatant indicated an average of 2.8×10^3 adsorbed target molecules per nanoparticle, nearly six times lower than the number of active amine moieties, as determined by Fmoc quantification. This discrepancy is likely due to the difference in binding mechanism – the target is electrostatically bound, whereas the binding of Fmoc is covalent.

2. 4 Conclusion

Core-shell structures of amine functionalized magnetic nanoparticles with tunable shell thickness have been successfully fabricated using a one-pot reverse microemulsion method. The nanoparticles prepared by this method are predominantly single-core and highly monodisperse. The silica shell can be readily functionalized with a wide variety of target-specific moieties, while the superparamagnetic core enables bound targets to be magnetically "fished-out" of a reaction

mixture. Fluorescein was used as a model carboxylate molecule to demonstrate the potential separation ability of Fe_3O_4@SiO_2-NH_2 nanoparticles towards cationic targets. This system shows great promise for use in a microfluidic separation device.

CHAPTER 3. PREPARATION OF MULTIFUNCTIONAL CORE-SHELL MAGNETIC NANOPARTICLES USING FUNCTIONALIZED TRIETHOXYSILANES PRECURSORS BY THIOL-ENE CLICK REACTION

3. 1 Introduction

Primary functional groups are tailored onto the surface of IONPs through various chemical approaches to prevent nanoparticle agglomeration and provide binding sites for further association with targets of interest. For example, amines and carboxylic acids are high-affinity functional groups and present remarkable adsorption properties.[94] Nanoparticles with charged carboxylic acids and amines are excellent candidates for the purification and adsorption of molecules and noble metals such as gold and silver.[95] Unfortunately, there are few commercially available anchor molecules containing amine and carboxylic acids. Thus, very intense research activities have been devoted to make amine and carboxyl functionalized ligands. One simple and direct route is to use hydrolyzable organosilanes that are derivatized with functional organic fragments. Such organosilanes could be covalently bond to IONPs surface via hydrolysis reaction, with functional groups stretching out for further conjugation. In our previous work, we have demonstrated a facile one-pot method of making size controllable amine functionalized core-shell magnetic nanoparticles using amine terminated APTES. This approach showed potential of making surface modified magnetic nanoparticles by directly using functionalized triethoxysilanes, which can be added as a second silanol source to form uniform core-shell magnetic nanoparticles without sacrificing their morphology and other properties. Therefore, it is promising to simplify the surface modification process by making trialkoxysilane precursors with a variety of functional groups on the end. Under such circumstance, the functionalized trialkoxysilanes enables the terminal silanes to be attached onto the surface of magnetic nanoparticles via hydrolysis; and the other end with a

variety of functional groups to be utilized for a specific purpose including adsorption, detecting, purification, etc. However, the synthetic routes are limited due to the moisture sensitive feature of organotrialkoxysilanes,

In the past decade, click chemistry has emerged as a powerful tool to tailor a variety of functionalities on material surfaces. The use of click chemistry in material chemistry has proven to be unique and superior due to its versatile mechanisms, mild reaction conditions, rapid reaction rates, clean products, high yields, excellent selectivity, and good biocompatibility. A highly effective and most widely used click chemistry is the Cu(I)-catalyzed alkyne−azide cycloaddition (CuAAC).[96-98] Functional organotralkoxysilanes have been reported by using the CuAAC reaction under anhydrous conditions. By applying microwave activation, organotriethoxysilanes can be synthesized with high yield and easy purification steps. [99] But using copper as the catalyst can be disadvantageous for some materials. For example, due to the strong coordination between copper and silica, complete removal of the copper species from the silica surface is difficult even under harsh conditions including highly acidic/basic solutions, which may be undesirable for many applications such as catalyst loading and biomolecule binding.[100] Some groups reported catalyst-free click reactions such as strain-promoted cycloaddition by using cyclooctyne and derivatives.[101] The catalyst-free click reaction works well for biological applications, but it resulted in low reaction selectivity and functionalities loading due to the stereo hindered effect.[102] The radical-mediated thiol-ene reaction as one type of click reaction has become increasingly attractive to material scientists. It contains all the desirable features of a click reaction as mentioned above, in addition to the advantages of metal-free and easy accessibility to numerous starting marterials.[103,104] Examples of surface modification via thiol-ene click reactions found in the literature mostly involve a two-batch reactions: the synthesis of surface modified nanomaterials

with terminated alkene (or thiol), followed by the reaction of the nanoparticles with functionalized thiol (or alkene) under UV light in the presence of the photoinitiator. Nevertheless, such two-batch procedures cannot guarantee high surface coverage, and again it requires multiple steps for obtaining the final products. Very recently, several groups have been focusing on the thiol-ene synthesis of functional water-sensitive organotrialkoxysilanes precursors for surface coating.[99,105] The thiol-ene reaction is tolerant of a broad range of functional groups using fewer organic synthesis steps, and it is of significance to provide access to a diversity of commercially-unavailable-functionalized-trialkoxysilanes with quantitative yields and high purity even on large scale.[95] However, they were more likely to focus on the organic synthesis and less on the surface coating. More detailed study of making well-defined nanoparticles using these trialkoxysilanes is necessary for future applications.

Herein, we used a facile one-pot method for making single-loaded core-shell magnetic nanoparticles terminated with a variety of functionalities using thiol-ene clicked triethoxysilanes. These triethoxysilanes contain functional groups including amine, carboxylic acid, and ester. None of them are commercially available but easy to synthesize using inexpensive and easily accessible materials such as triethoxyvinylsilane, cysteamine, 3-mercaptopropionic acid, and ethyl mercaptoacetate. The products are very clean, high yielded, and ready to use for surface coating without any post-synthesis work-up steps. The significance of this strategy are that we provided a less tedious but more efficient one-pot synthetic route using the commercially unavailable organotriethoxysilanes; and the nanoparticles are size- and morphology-controllable with terminated amine and carboxyl groups, but not limited to the functional groups we discussed in this chapter. Such well-prepared functionalized nanoparticles show the potential of fulfilling a

broad range of highly demanded applications, like microfluidic separations, biomolecule adsorption, drug targeting, and catalyst loading.

3. 2 Experimental

3.2.1 Chemicals

Ferric chloride hexahydrate ($FeCl_3$•$6H_2O$) was purchased from Fisher, ammonium hydroxide (NH_4OH, 28%~30%) was obtained from Caledon. Tetraethyl orthosilicate (TEOS), sodium azide, (3-chloropropyl) triethoxysilane (95%), triethoxyvinylsilane (98%), trimethylamine (TEA, 99%), 3-(triethoxysilyl)propyl isocyanate (IPTEOS, 95%), cysteamine (95%), 3-mercaptopropionic acid (99%), ethyl mercaptoacetate (97%), 2,2-Dimethoxy-2-phenylacetophenone (DMPA, 99%), IGEPAL®CO-520 (average Mn 441), propargyl alcohol, cyclohexane, dimethyl sulfoxide (DMSO), dichloromethane (DCM) and all other solvents were purchased from Sigma-Aldrich.

3. 2. 2 Characterization techniques.

High temperature reactions were carried out in a Welmet FT3034 or Carbolite STF 16/180 tube furnace. High-speed centrifugation was performed using a Baxter Biofuge 17R centrifuge. Sonication was performed using a Branson 450 Digital Sonifier. Morphologies and particles sizes were investigated by a transmission electronic microscopy (TEM, FEI Tecnai 20). The samples were prepared by depositing a drop of a diluted colloidal solution on carbon-film-coated copper grid (200 mesh). The surface functionalities were determined by a Fourier transform infrared spectroscopy (FTIR, Bruker StepScan). The samples were prepared by making pellets with dried KBr powder. Nuclear magnetic resonance (NMR) spectra for all synthesized triethoxysilanes were recorded on Bruker AV 400 MHz spectrometer. Energy-dispersive X-ray spectroscopy (EDX) was run on a Thermo Fisher Scientific Quanta 3D equipment operating at 2.0 kV. The magnetization

of resulting IONPs was measured using a Quantum Design MPMS SQUID magnetometer. UV-Vis spectroscopy was performed on a NanoDrop 2000c/2000 UV-Vis spectrophotometer. A sintered $Nd_2Fe_{14}B$ permanent supermagnet was used for magnetically-assisted precipitation of nanoparticles.

3.2.3 Synthesis of functional triethoxysilanes

A variety of triethoxysilanes with different terminal functionalities were synthesized. The surface modification of the IONPs can be done through two routes. One method is forming azido/ alkyne functionalized IONPs in reverse microemulsion, followed by an in situ CuAAC reaction, in which Cu (I) was formed by adding $CuSO_4$ and sodium ascorbate to catalyze the 1,3-dipolar azide-alkyne cycloaddition. Another method is using thiol-ene reaction to directly synthesize triethoxysilanes precursors with various functional groups, then adding them into reverse microemulsion for coating a thin outer layer of functionality on particle surface. Both those two methods were carried in our work for comparison.

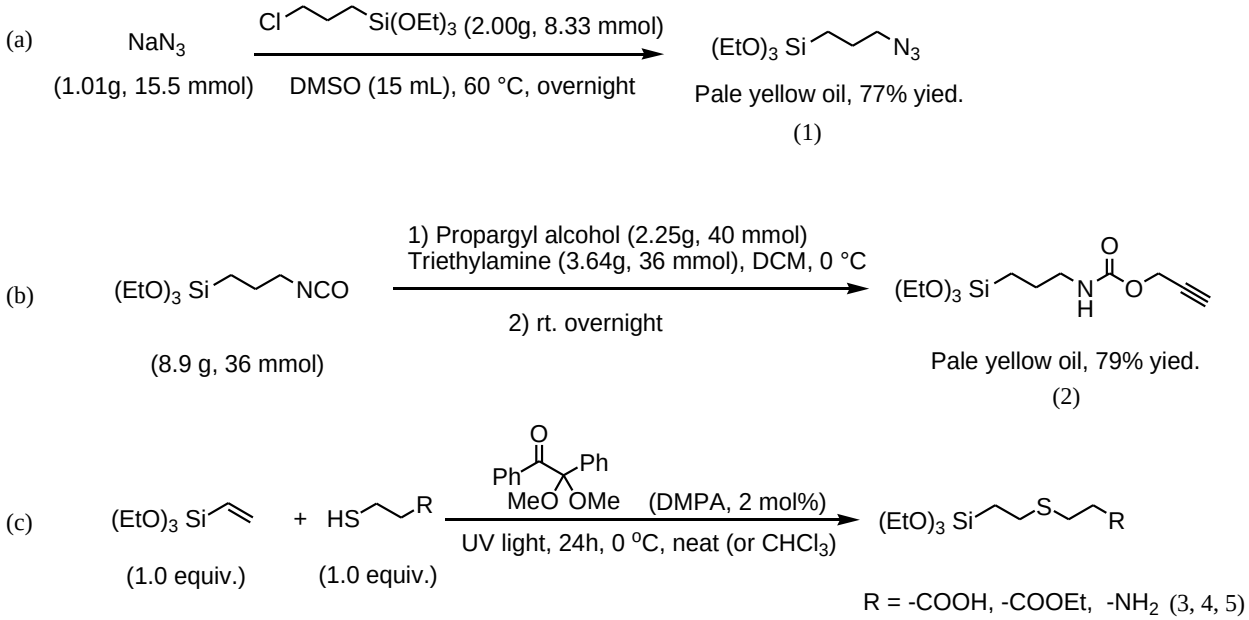

Scheme 3.1. Synthesis of functional triethoxysilanes using various synthetic strategies.

3. 2.3.1 Synthesis of (3-azidopropyl)triethoxysilane (Compound 1)

(3-azidopropyl)triethoxysilane was synthesized according to Jian's method:[106] sodium azide (1.01 g, 15.5 mmol) and dimethyl sulfoxide (DMSO, 15 mL) was added into a flame dried and Ar filled 100 mL-round flask. The mixture was heated with an oil bath up to 60 ˚C until sodium azide was dissolved. Then (3-chloropropyl) triethoxysilane was added into above preheated mixture and stirred overnight. After the reaction finished, water (10 mL) was added and the aqueous phase was quickly extracted with diethyl ether one time, the organic layer was transferred to an Erlenmeyer flask and dried over anhydrous Na_2SO_4. Clear yellow oil was obtained after filtration and removal of the solvent.

(3-azidopropyl)triethoxysilane (Compound 1): (77% yield) The spectra for the product is: ^{1}H-NMR (400 MHz, $CDCl_3$) δ 3.78 (m, *J* = 6.8 Hz, 6H), 3.22 (t, *J* = 6.8 Hz, 2H), 1.65 (m, *J* = 7.2 Hz, 2H), 1.58 (t, *J* = 7.2 Hz, 9H), 0.62 (t, *J* = 8.4 Hz, 2H). All the peaks assigned are consistent with the literature reported.

3.2.3.2 Synthesis of [(2-Propynylcarbamate)propyl] Triethoxysilane (PPTEOS) (Compound 2).

PPTEOS was synthesized using Lu's method:[107] propargyl alcohol (2.25g, 40 mmol) and trimethylamine (TEA, 3.64g, 36 mmol) were added into a 50 mL round flask and dissolved in dichloromethane (DCM, 20 mL). The mixture was cooled in an ice bath. 3-(triethoxysilyl)propyl isocyanate (IPTEOS, 8.9 g, 36 mmol) dissolved in 10 mL of DCM was added drop wise under argon. The ice bath was removed after finishing dropping and the reaction mixture was stirred at room temperature overnight. DCM and excess propargyl alcohol were removed under vacuum, resulting in the product as colorless oil.

[(2-Propynylcarbamate)propyl] Triethoxysilane (PPTEOS)(Compound 2): (79% yield) The spectra for the product is: ^{1}H-NMR (400 MHz, $CDCl_3$) δ 5.05 (s, 1H), 4.65 (s, 2H), 3.82 (m, *J* = 7.2 Hz, 6H), 3.20 (m, *J* = 6.4 Hz, 2H), 2.45 (S, 1H), 1.62 (m, *J* = 8.0 Hz, 2H), 1.25 (t, *J* = 7.2 Hz, 9H), 0.62 (t, *J* = 8.4 Hz, 2H). All the peaks assigned are consistent with the literature reported.

3. 2. 3.3 Thiol-ene synthesis of 3-(2-(triethoxysilyl)ethylthio)propanoic acid. (Compound 3)

Compound **3** was synthesized via a modified radical mediated photochemical click reaction by Tucker-Schwartz,[105] Typically, triethoxyvinylsilane (5.22 mL, 25 mmol) and 3-mercaptopropionic acid (2.18 mL, 25 mmol) were added into a flame dried pyrex tube flask, and mixed with photoinitiator DMPA (128.15 mg, 2mol%). The flask was sealed with a plastic septa and the mixture was vacuumed and purged with argon for 3 times. After that, the mixture was stirred till all solid starting materials dissolved. A thiol-ene reactor was equipped with a steel cabinet, inside an ACE photochemical UV medium pressure quartz mercury lamp (CN, PC451050, 450 watt) was placed in a water-reflux-quartz-well. The flask was attached onto the water-reflux-quartz-well using elastic bands. The reaction mixture was irradiated at 0 ˚C by turning on the UV lamp from an adaptor outside the steel cabinet and refluxed with tap water for 24h. The reaction was run neat in the absence of any solvent. Afterwards, the product obtained was light yellow oil with quantitative yield. No further work-up or purification steps are required for the next step of surface modification.

3-(2-(triethoxysilyl)ethylthio)propanoic acid (Compound 3): (>95% yield). The spectra for the product are: ^{1}H-NMR (400 MHz, CD_3OD) δ 3.85 (q, *J* = 6.8 Hz, 6H), 2.80 (t, *J* = 7.2 Hz, 2H), 2.68-2.60 (m, 4H), 1.22 (t, *J* = 7.2 Hz, 9H), 0.95 (t, *J* = 8.4 Hz, 2H). ^{13}C-NMR (100 MHz, CD_3OD): 174.20, 58.10, 34.08, 26.08, 25.46, 17.16, 11.19.

3. 2. 3. 4 Thiol-ene synthesis of 2-(2-(triethoxysilyl)ethylthio) ethanamine. (Compound 4)

Compound **4** was synthesized via the photoinitiated click reaction mentioned above. Typically, cysteamine (192.88 mg, 2.5 mmol) and DMPA (12.82 mg, 2 mol %) were added into a flame dried pyrex tube flask. The flask was sealed with a plastic septa and the mixture was vacuumed and purged with argon for 3 times. After that, triethoxyvinylsilane (0.522 mL, 2.5 mmol) and anhydrous chloroform (5 mL) were added into the mixture with an argon-purged-syringe. The mixture was stirred till all starting materials dissolved. The tube flask was placed in the thiol-ene reactor by attaching it onto the water-reflux-quartz-well. The reaction mixture was irradiated 0 ˚C for 24h. The product obtained was clear oil with quantitative yield. The product was kept in a glass vial filled with argon and ready to use for the surface modification.

2-(2-(triethoxysilyl)ethylthio) ethanamine (Compound 4): (>95%) The spectra for the product is: 1H-NMR (400 MHz, $CDCl_3$) δ 3.80 (q, J = 6.4 Hz, 6H), 2.85 (t, J = 6.4 Hz, 2H), 2.62 (m, 4H), 1.35 (bs, 2H), 1.20 (t, J = 7.2 Hz, 9H), 0.92 (t, J = 8.4 Hz, 2H). 13C-NMR (100 MHz, CDCl3): δ 58.34, 40.93, 35.97, 25.87, 18.11, 11.83.

3. 2. 3. 5 Thiol-ene synthesis of ethyl 2-(2-(triethoxysilyl)ethylthio)acetate. (Compound 5)

The synthesis procedure of compound **5** was similar to what described above. The reaction was set up by mixing equimolar amount of triethoxyvinylsilane and ethyl mercaptoacetate in the presence of 2 mol % of DMPA and running under neat condition at 0 ˚C for 24h. After the reaction finished, clear oil product was obtained with quantitative yield. The product was kept in a glass vial filled with argon and was ready to use for the surface modification.

Ethyl 2-(2-(triethoxysilyl)ethylthio)acetate (Compound 5): (>95%) The spectra for the product are: 1H-NMR (400 MHz, CDCl3) δ 4.16 (q, J = 6.8 Hz, 2H), 3.80 (q, J = 6.8 Hz, 6H), 3.21

(s, 2H), 2.73 (t, J = 8.8 Hz, 2H), 1.26 (t, J = 7.2 Hz, 3H), 1.20 (t, J = 6.8 Hz, 9H), 0.97 (t, J = 8.4 Hz, 2H). 13C-NMR (100 MHz, CDCl3): 170.40, 61.08, 58.38, 33.39, 27.00, 18.11, 14.01, 11.14.

3. 2. 4 Synthesis of monodisperse hydrophobic Fe_3O_4 nanoparticles.

Monodisperse hydrophobic Fe_3O_4 IONPs were prepared according to literature with a little modification.[108,109] $FeCl_3$•$6H_2O$ was recrystallized from distilled water before use. Then $FeCl_3$•$6H_2O$ (20 mmol, 5.41 g) was dissolved in the solvent mixture of distilled water, ethanol and hexane (60 mL, 80 mL, 140 mL). After that, oleic acid (60 mmol, 19 mL) was added and the mixture was stirred at room temperature for 30 min. Then 2.4 g NaOH was added to the above solution. The reaction mixture was heated up to 70 °C and stirred under refluxing for 4 h. The product $Fe(oleate)_3$ complex was obtained by extracting the organic layer from the aqueous layer using a separatory funnel, washing with distilled water for 3 times, and removing the organic solvent with a rotary evaporator. After the precursor $Fe(oleate)_3$ was made, 4.5 g (5 mmol) $Fe(oleate)_3$ was transferred into a 80 mL tube flask containing 1-octadecene (32 mL), oleic acid (2.5 mmol, 0.79 mL), and magnetically stirred to homogeneous. The tube flask was then placed in a tube furnace, flew with argon, and heated to 320°C and refluxed at this temperature for 30 min. The resulting black solution was cooled to room temperature and precipitated by adding excess ethanol. The precipitates were collected by centrifugation, then redispersed in hexane and precipitated with ethanol for several times in order to purify the resulting Fe_3O_4 nanoparticles. The purified Fe_3O_4 nanoparticles were stored as a suspension in cyclohexane (25 mg/mL) filled with Ar, with an adding of several drops of oleic acid to stabilize the colloid.

3. 2. 5 Synthesis of surface functionalized core-shell magnetic nanoparticles by a CuAAC strategy and by directly adding thiol-ene synthesized triethoxysilanes.

The multi-functional magnetic nanoparticles were prepared based on our previous work described in Chapter 2. Here, two click reaction strategies were carried out for comparison. As a proof of principle, carboxyl functionalized IONPs Fe_3O_4@SiO_2–COOH was made by the CuAAC click reaction in one-pot. Briefly, 0.25 mL surfactant Igepal CO-520 was dissolved in 10 mL cyclohexane and subjected to sonication for 15 min, and then 100 μL NH_4OH was added followed by adding 2.5 mg Fe_3O_4 (2.5 mg/mL in cyclohexane). After 30 min of continuous magnetic stirring, 50 μL TEOS was added into the mixture via an equivalently fractionated dropping method (adding 35 μL per 16 h). After 24 hours of TEOS being added, (3-azidopropyl)triethoxysilane (2, 22.5 μL, 9.0 x 10^{-5} mol) was added into the microemulsion system for another 24 h. Grounded CuSO4•$5H_2O$ (1.1 mg, 4.5 x 10^{-6} mol), sodium ascorbate (1.1 mg, 5.4 x 10^{-6} mol), heptynoic acid (11.4 μL, 9.0 x 10^{-5} mol) were added to allow for the azide-alkyne cycloaddition reaction to start. 48 hours later, 2 mL of methanol was added to break the microemulsion. Products precipitated in the layer of methanol and were obtained by washing with EtOH and distilled water alternatively. The resulting Fe_3O_4@SiO_2–COOH IONPs were collected and dried under vacuum.

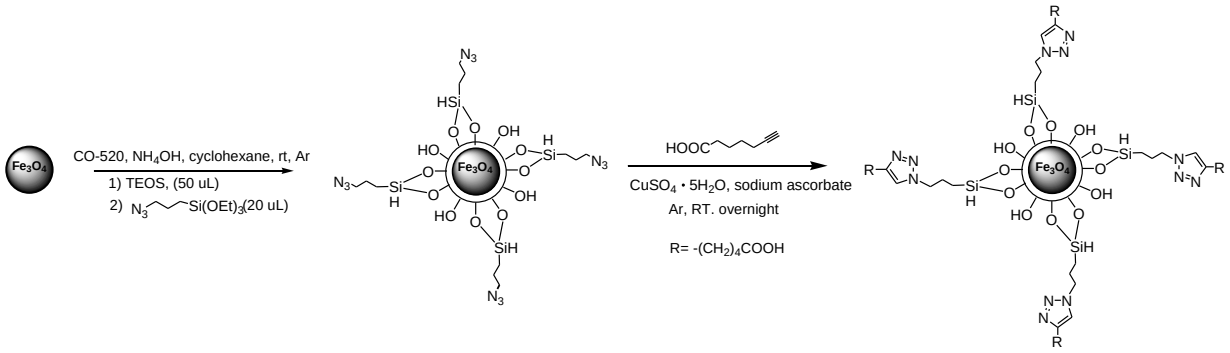

Scheme 3.2. Synthetic procedure of one-pot CuAAC-catalyzed carboxyl functionalized IONPs in reverse microemulsion.

The second surface modification strategy was carried out using the thiol-ene synthesized functional triethoxysilanes. By using this method, IONPs with a broad range of surface functionality were prepared in a reverse microemulsion system described in our previous work. As shown in scheme 3.3, the surface modification process involves a two-steps reaction in one-pot. First, 0.25 mL surfactant Igepal CO-520 was dissolved in 10 mL cyclohexane and subjected to sonication for 15 min, and then 100 μL NH_4OH was added followed by adding 3.0 mg Fe_3O_4 (2.5 mg/mL in cyclohexane). After 30 min of continuous magnetic stirring, 50 μL TEOS was added into the mixture using a syringe pump at rate 2.5 mL/h. Afterwards, 20 mol% thiol-ene synthesized triethoxysilanes to TEOS was added 24 h after TEOS being added. When the reaction finished, 2 mL of ethanol was added to break the reverse microemulsion. The products precipitated in the layer of ethanol and were obtained by washing with EtOH and distilled water alternatively. The resulting products were named as Fe_3O_4@SiO_2–COOH, Fe_3O_4@SiO_2–NH_2, and Fe_3O_4@SiO_2–COOEt, respectively.

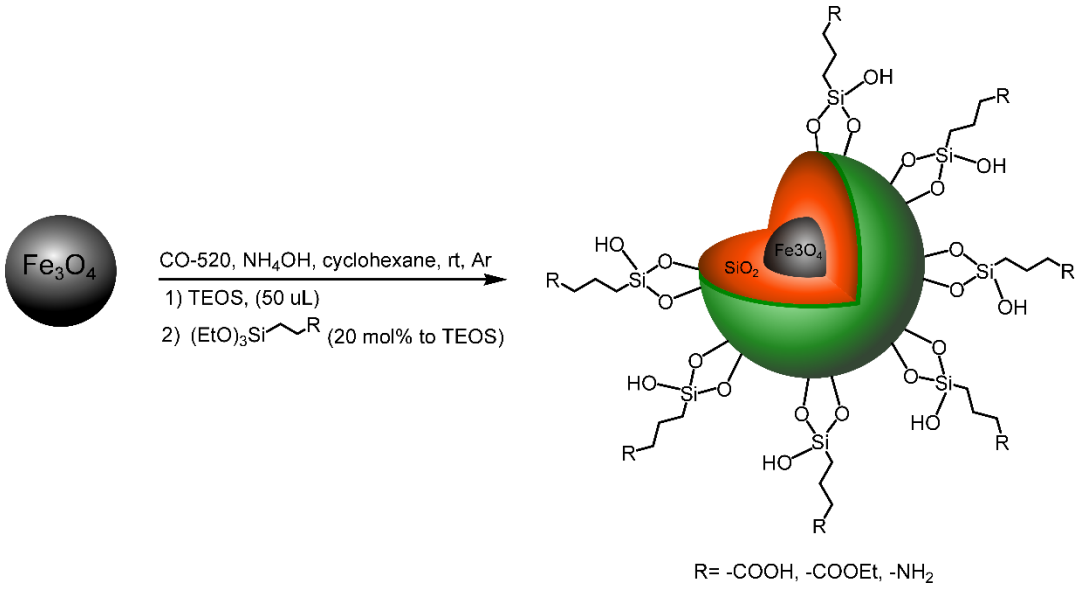

Scheme 3.3. Synthesis of functionalized IONPs in reverse microemulsion.

3. 2. 6 Characterization of surface functionalities.

The ionic dye molecules have shown to be excellent candidates to test the potential adsorption ability of the resulting amine functionalized IONPs Fe_3O_4@SiO_2-NH_2 in our previous work. Here, a toluidine blue o (TBO) staining method was used to determine the capture and recovery efficiency of carboxyl functionalized Fe_3O_4@SiO_2-COOH nanoparticles.[110] First, 10 mg of Fe_3O_4@SiO_2-COOH nanoparticles were homogenously dispersed in a plastic vial with 10 mL PBS solution buffer (pH=8) containing TBO (0.2 mM). The mixture was incubated for 1h to allow for the formation of ionic complex between the surface –COOH groups and cationic dye molecules. After that, the amount of TBO loaded onto IONPs was determined by measuring the UV absorbance of residual concentration. To be specific, after adsorption, the concentration of the residual coloring in the solution was measured using UV-vis spectrophotometer at 590 nm. Prior to this, a calibration curve of known TBO concentration was obtained. So the amount of bound TBO molecules was calculated by subtracting the residual concentration of TBO in the solution from the initial concentration.

To determine the recovery efficiency of functionalized nanoparticles, the IONP-TBO complex was rinsed with acetone and then PBS buffer to remove unbound TBO. After dried in air, the bound dye moieties were released from the material surface by adding into 5 mL of acetic acid solution (50% v/v), and the mixture was subjected to sonication for 15 min. The release procedure was repeated 3 runs for each sample. Then the amount of TBO released from the IONPs was determined at wavelength 590 nm^{-1}. The percentage of recovered TBO was calculated according to a calibration curve of optical density vs. known TBO concentrations, with the assumption that each -COOH group binds a single TBO molecule.

3. 3 Results and Discussion

3. 3. 1 Synthesis of core-shell magnetic nanoparticles using Cu-catalyzed azide-alkyne cycloaddition click reaction.

In our previous work, the one-pot synthesis has highlighted the potential of functional trialkoxysilanes for surface modifications of magnetic nanoparticles in a reverse microemulsion reaction system. With such a one-pot, two step procedures, meaning the pre-functionlization of magnetic core with an inner silica shell, followed by an outer layer grafting with functional triethoxysilanes, we hope to prepare well controlled functionalized core-shell IONPs.

The CuAAC click strategy allows for introducing click reactive sites on the surface for further surface modification. In this work, both azide and alkyne triethoxysilanes were made to graft azide and alkyne terminated IONPs and click desired functional groups via the cycloaddition reaction. As shown in Figure 3.1, both azide and alkyne functionalized IONPs resulted clear core-shell structures. However, the nanoparticles were cross-linked to each other after CuAAC reaction. This might be attributed to the unreacted azide ligands remaining in the one-pot reaction system, causing the cycloaddition to occur in the microemulsion other than on the particle surface. This is consistent with the IR spectra (Figure 3.2 (c)), showing incomplete azide-alkyne cycloaddition.

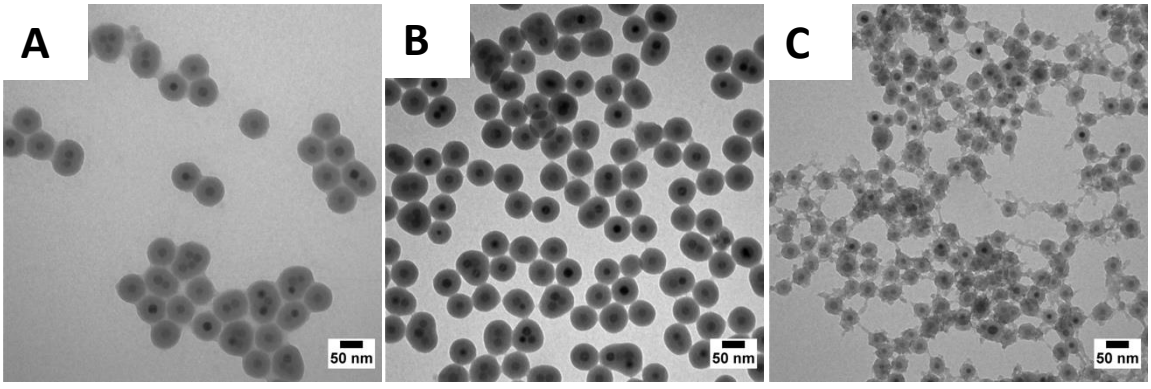

Figure 3.1. TEM images of Fe_3O_4 (A), Fe_3O_4@SiO_2-N_3, (B) Fe_3O_4@SiO_2-C≡C-H, (C) Fe_3O_4@SiO_2-COOH via CuAAC reaction.

The IR spectra (Figure 3.2) proved the successful surface modification with azide and alkyne groups. Because the absorbance at 2180 cm^{-1} refers to the stretching vibration of azide was found from curve (a). Aslo, on curve (b) peaks at 3296, 1703, and 1539 cm^{-1} are corresponding to the vibration modes of alkynyl (C≡C-H), carbonyl (C=O), and amino (N-H), respectively, indicating the successful alkynyl-functionalization of magnetic nanoparticles with PPTEOS. According to Figure 3.2 (c), the peak at 2104 cm^{-1} representing azide is not fully disappeared; while a very weak absorbance at 1680 cm^{-1} was observed, indicating the low yield of CuAAC cycloaddtion on the surfaces of magnetic nanoparticles.

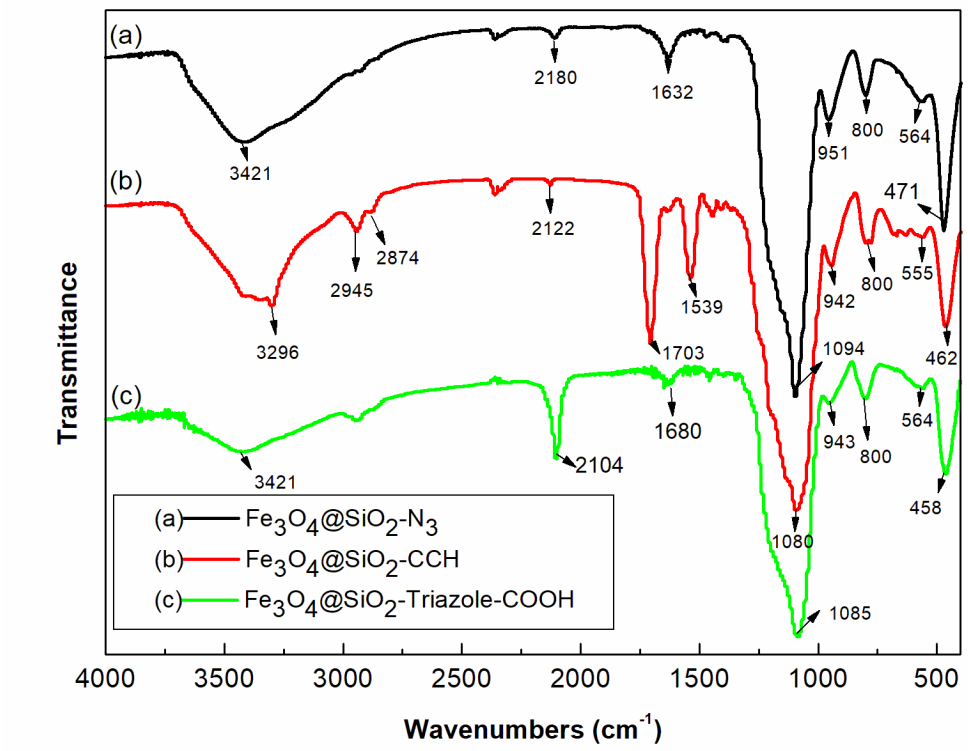

Figure 3.2. IR spectra of core-shell magnetic nanoparticles with terminal functional groups.

3. 3. 2 Synthesis of core-shell magnetic nanoparticles using thiol-ene clicked precursors.

As summarized in Table 3.1, the catalyst-free thiol-ene click reaction can give all functional triethoxysilane very high yield and purity. Efficient mixing is very important to obtain high yield of products. Also, Ar atmosphere and well-sealed flask is crucial to make the radicals active for reaction completion. The reactions require 1:1 molar ratio of starting materials, with very tiny amount of photoinitiator, as well as nearly free of solvent, which make this method very cost effective. More importantly, the resulting products are readily for use in surface functionalization. This greatly reduced the time for post-synthesis work-up process and enhanced the efficiency for surface functionalization.

Table 3.1. Summary of the thio-ene click synthesis of functional triethoxysilanes.

Entry	R	Molar ratio	Time (h)	DMPA (mol%)	Solvent	Temperature (°C)	Yield (%)
1	-COOH	1:1	24	2	neat	0	>95
2	-COOH	1:1	24	2	$CHCl_3$	0	>95
3	-COOEt	1:1	24	2	neat	0	>95
4	$-NH_2$	1:1	24	2	$CHCl_3$	0	>95

We found that the reproducibility of monodisperse single-loaded core-shell IONPs is crucially dependent on the addition rate of triethoxysilanes. The morphology of functionalized IONPs varies from batch to batch by adding triethoxysilanes manually. However, reproducible functionalized magnetic nanoparticles were obtained from each batch by adding triethoxysilanes using a syringe pump (New Era Pump Systems, Inc., NE-300) at controlled rate. As shown in Figure 3.3, in the preparation of Fe_3O_4@SiO_2–COOH, a low pumping rate 0.5 mL/h and 1 mL/h, homogeneous nucleation dominate, and a large amount of core-free structures were observed. At rate 2.5 mL/h, reproduceable core-shell IONPs were obtained, with single-loaded core . One might

assume that the concentration of hydrolyzed silanes is higher at higher adding rate of TEOS, which could cause homogeneous nucleation to form core-free silica nanoparticles. However, we obtained core-free silica beads at lower addition rates and core-shell IONPs at higher adding rate. This result seems contradictory to the La Mer theory that heterogeneous nucleation is favored at lower hydrolyzed TEOS concentration. The reverse microemulsion is not highly stable system due to the volatile organic phase. Also, at very low addition rate, the IONPs might not overcome the gravity force and tend to precipitate before silica start growing on the particle surface. While at very high addition rate, the local concentration of TEOS might be overly high so as to favor homogeneous nucleation. Therefore, the lower adding rate of silanes may not necessary to form single-cored structures due to the complexity of reverse microemulsion system.

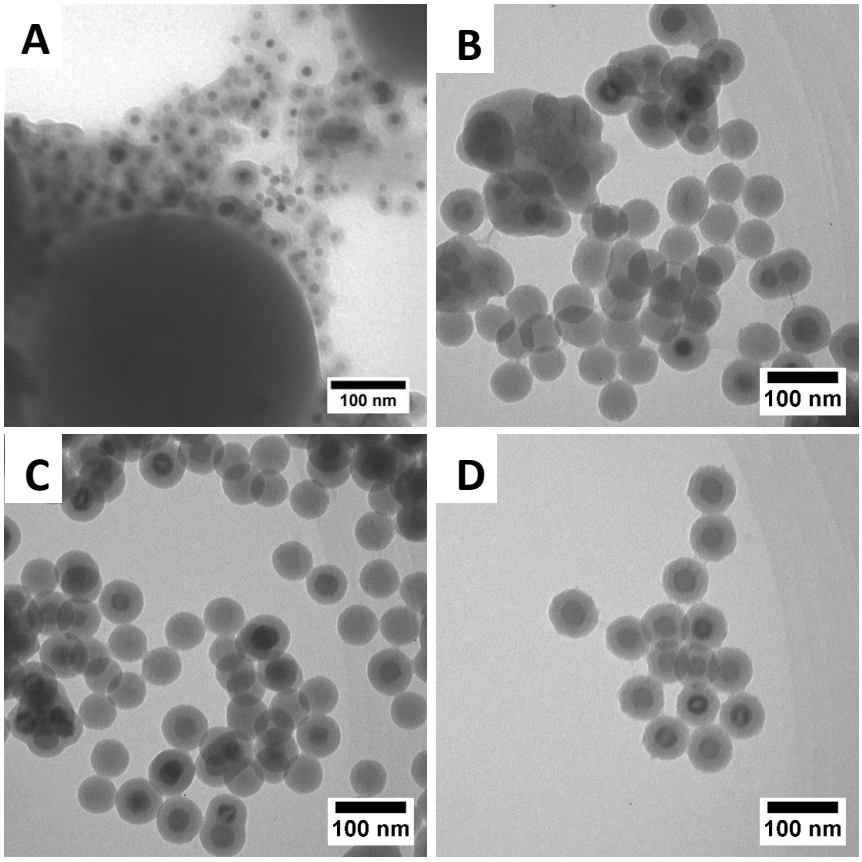

Figure 3.3. TEM images of Fe_3O_4@SiO_2-COOH by adding silanes by hand (A), and by syringe pumping at different rate: 0.5 mL/h (B),1 mL/h (C), 2.5 mL/h (D).

The amount of thiol-ene clicked triethoxysilanes used for surface modification was studied in order to gain the desired density of surface functional groups without sacrificing the morphology. The result shows that, at low mole ratio of 3-(2-(triethoxysilyl)ethylthio)propanoic acid (Compound **3**), core-shell structures were kept. But when the mole ratio was raised up to 30 mol%, Compound **3** started to polymerize between core-shell nanoparticles and a big block of polymer encapsulating the nanoparticles was formed (Figure 3.4 (C)). Therefore, economically and morphologically, the amount of thiol-ene clicked triethoxysilanes needs to be considered.

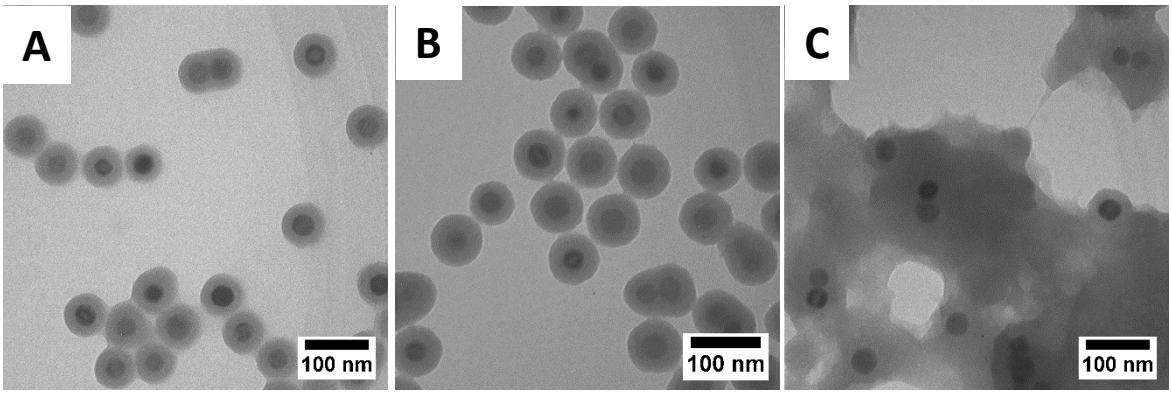

Figure 3.4. TEM images of Fe_3O_4@SiO_2-COOH with different mole ratio of compound 3 to TEOS: 5 mol % (A), 20 mol % (B), 30 mol % (C).

The TEM images in Figure 3.5 show that, after condition optimization, the iron oxide magnetic cores after surface modification using the thiol-ene clicked triethoxysilane precursors were single loaded monodisperse core-shell structures. The average size measured by ImageJ with 50 counts were 30 ± 2 nm, 75 ± 3 nm, 79 ± 5 nm and 94 ± 5 nm for Fe_3O_4, Fe_3O_4@SiO_2–COOH, Fe_3O_4@SiO_2–COOEt, and Fe_3O_4@SiO_2–NH_2, respectively. The result indicates that the one-pot method of making single-loaded core-shell magnetic nanoparticles terminated with various functionalities using thiol-ene clicked triethoxysilanes was successful. More importantly, by synthesizing the commercially unavailable organotrialkoxysilanes, well size- and -morphology

controlled nanoparticles with a broad range of functional groups, not limited to the functional groups we presented in this work, are readily prepared.

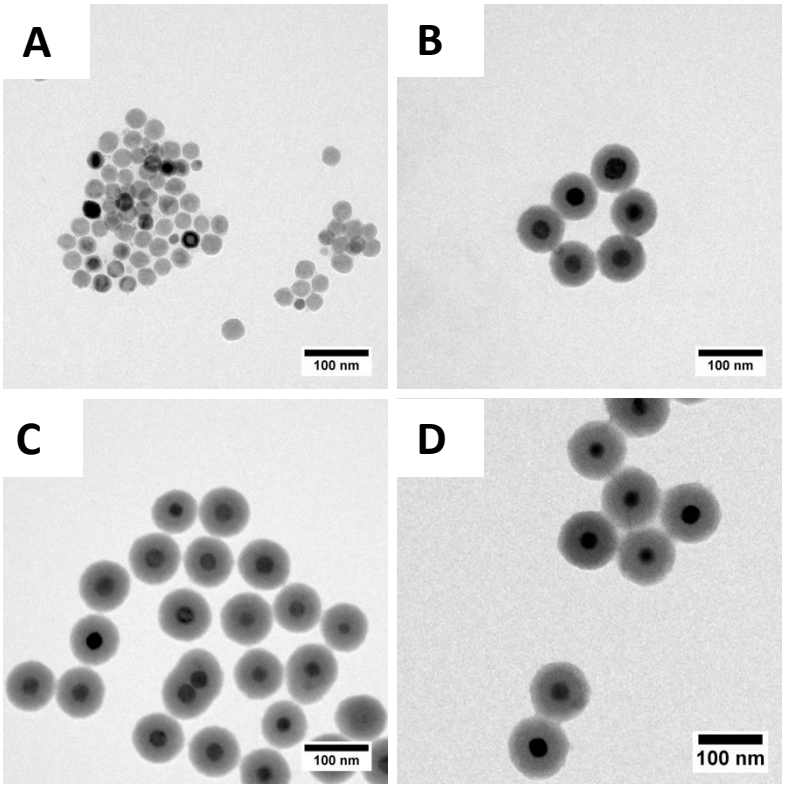

Figure 3.1. TEM images of Fe_3O_4 (A), Fe_3O_4@SiO_2-COOH (B), Fe_3O_4@SiO_2-COOEt (C), Fe_3O_4@SiO_2-NH_2 (D).

The magnetic properties of iron oxide cores and functionalized IONPs after surface coating were investigated. According to Figure 3.6 (a), the saturation magnetization of Fe_3O_4 core and –COOH, –COOEt, and –NH_2 functionalized IONPs were 36.0, 10.8, 6.9, and 6.1 emu·g^{-1}, respectively. The amount of decrease in the saturation magnetization after surface coating is in accordance with the increase of the shell thickness. However, the decrease in magnetization of IONPs is not because of the silica coating but the decrease in mass of magnetic cores for measurements. For example, the magnetization of 10 mg iron oxide magnetic cores would be much higher than that of 10 mg IONPs after silica coating because the silica shell contributes more than half of the total mass used for measurements. Therefore, after normalizing the magnetization curve

by the mass of Fe_3O_4, as shown in Figure 3.6 (b), the magnetization did not change after silica coating. Also, they are all superparamagnetic at 300K, as no hysteresis loop was observed. The resulting functionalized IONPs show fast on/off response to an external magnetic field.

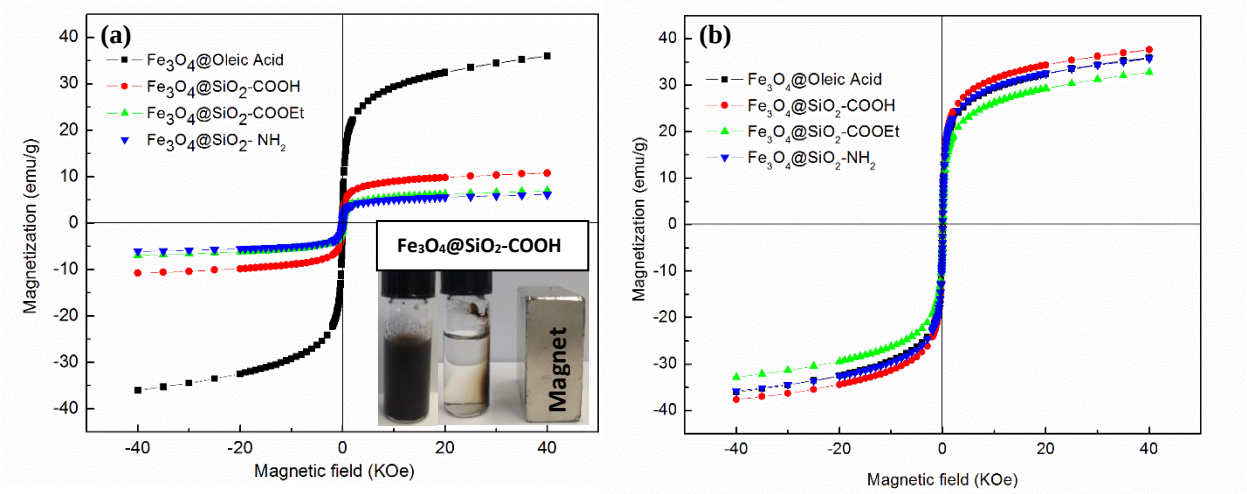

Figure 3.2. Field-dependent magnetization curve at 300K: (a) core-shell IONPs, (b) core-shell IOPNs after normalizing by the mass of Fe_3O_4. (For measurement, the Fe_3O_4 magnetic cores were dispersed in hexane, and the core-shell particles were dispersed in water.)

By using the thiol-ene synthesized triethoxysilane precursors, all functional groups were successfully introduced onto the surface of IONPs. The surface functional groups of magnetic nanoparticles were demonstrated by FTIR spectra (Figure 3.7). For all the curves, there are absorption peaks near 579 cm^{-1}, representing the stretch vibration mode of Fe-O bonds. And peaks near 1090, 798, and 474 cm^{-1} can be ascribed to the unsymmetrical stretching vibration, symmetrical stretching vibration and bending vibration modes of Si-O-Si, respectively. For the curves from top to bottom, the absorbance at 3420, 1710, and 1420 cm^{-1} is indexed to -OH, C=O, C-O-H of carboxylic acids, peaks at 3420, 1650, 1380 and 947 cm^{-1} are corresponding to -OH, C=O, C-O of esters, bands at 3350, 3270, and 1620 cm^{-1} can be derived from the stretch vibration and bending vibration of amines. The results indicate the successful functionalization of magnetic nanoparticles with thiol-ene clicked triethoxysilanes.

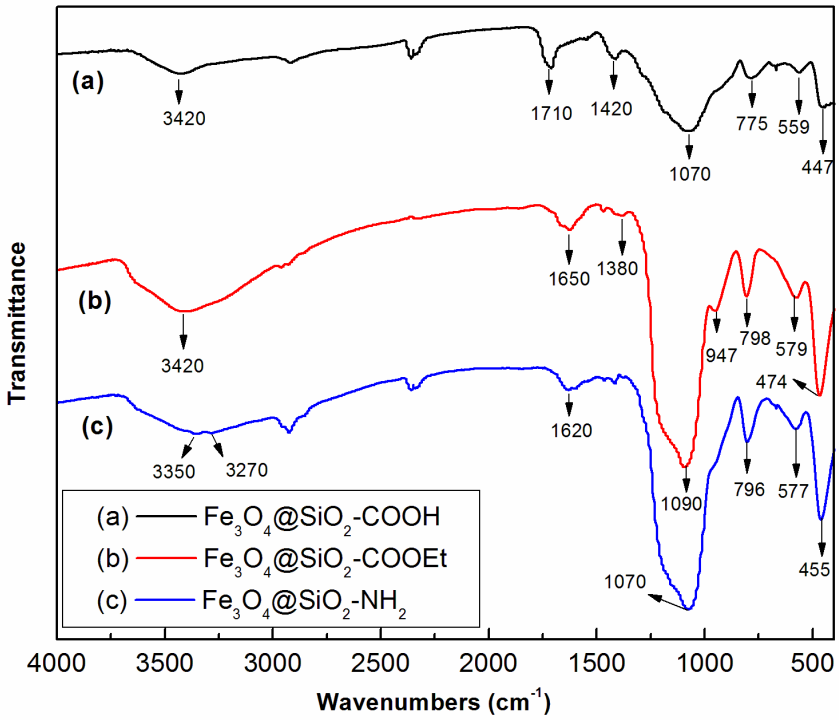

Figure 3.7. FTIR spectra of core-shell functionalized IONPs with thiol-ene clicked triethoxysilanes.

The energy dispersive X-ray spectra (EDX) also show strong evidence of successful surface modification. Peaks referring to sulfur were found in EDX spectra for sample Fe_3O_4@SiO_2–COOH, Fe_3O_4@SiO_2–COOEt, and Fe_3O_4@SiO_2–NH_2. The number of functional groups grafted on the particle were estimated by S/Si ratio on the EDX spectra, as shown in Figure 3.8. For the addition of 20 mol% of triethoxysilanes to TEOS, the S/Si ratio were 2.8 mol%, 2.5 mol% and 5.3 mol% for Fe_3O_4@SiO_2–COOH, Fe_3O_4@SiO_2–COOEt, and Fe_3O_4@SiO_2–NH_2, respectively. Those numbers are corresponding to 1.1, 0.9, 1.3 ligands/nm^2 of -COOH, -COOEt, and -NH_2 groups on the nanoparticles. Compared to the theoretical S/Si ratio of 16.7 mol%, these measured values were much lower. One reason is that the packing surfaces of sample must be very flat for standard quantification using EDX method, but our particles are so small that the X-ray emitted from the nanoparticles may not be collected by the detector because of random diffraction.

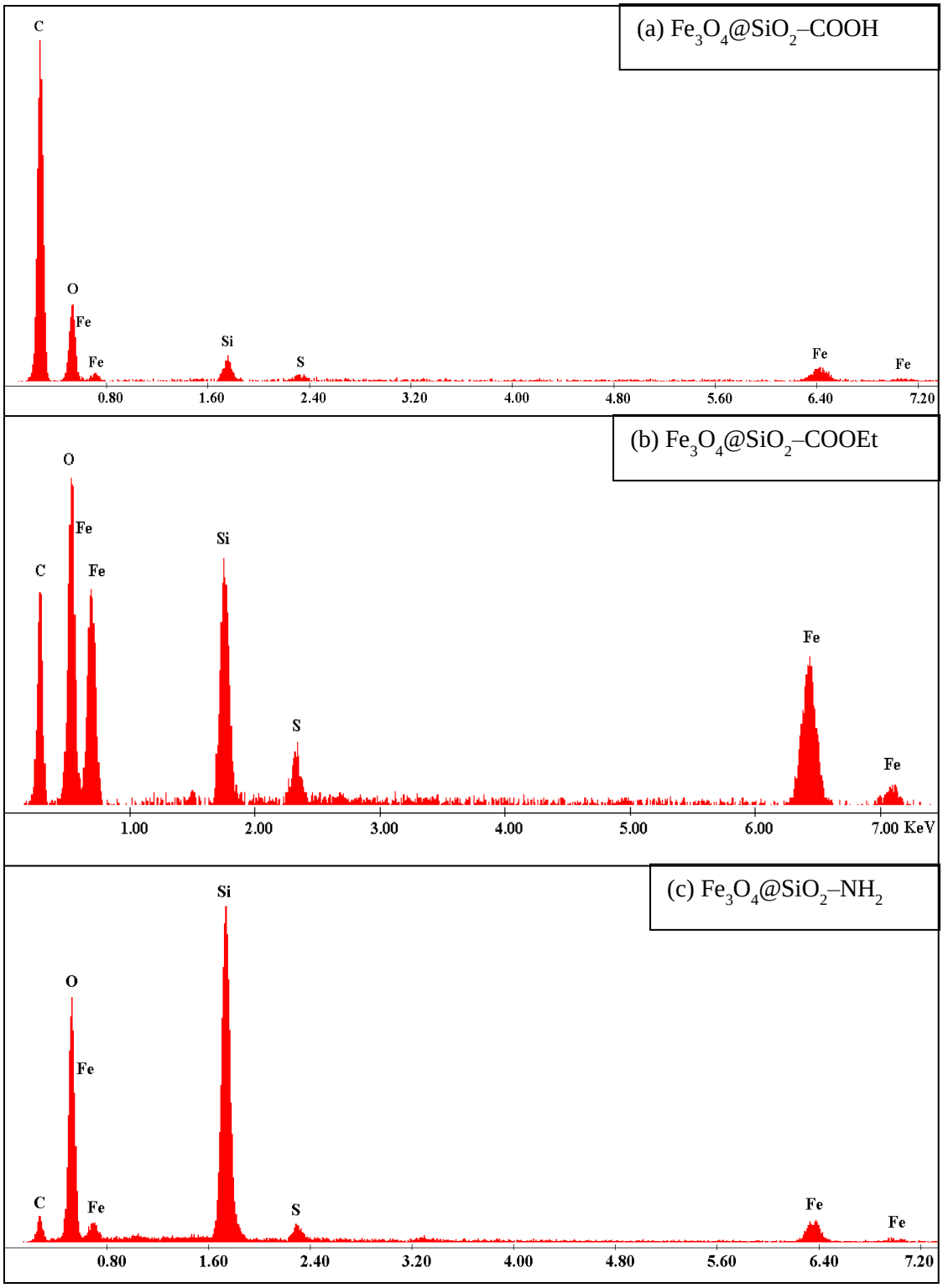

Figure 3.8. EDX spectra of core-shell functionalized IONPs with thiol-ene clicked triethoxysilanes: a) Fe_3O_4@SiO_2–COOH, b) Fe_3O_4@SiO_2–COOEt, c) Fe_3O_4@SiO_2–NH_2.

3. 3. 3 Adsorption ability of surface functionalized IONPs using dye molecules.

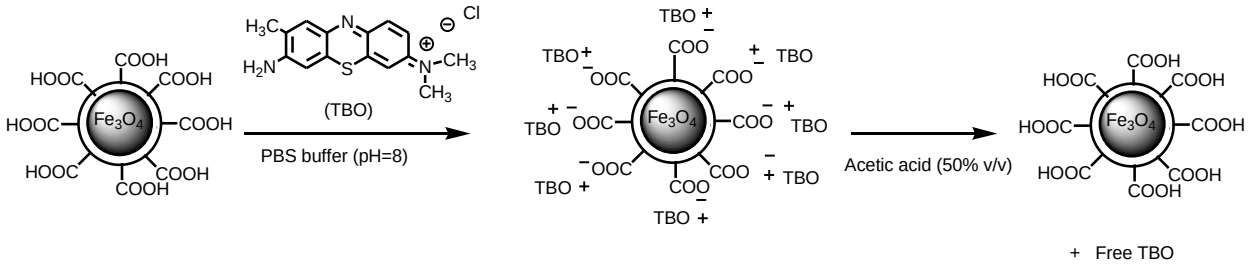

Scheme 3.4. Capture of TBO with Fe_3O_4@SiO_2-COOH IONPs at high pH and release of TBO at low pH.

For the proof of principle, TBO was used to demonstrate the reversible interaction of targets with carboxyl functionalized nanoparticles by changing the surface charges. As shown in Scheme 3.4, the nanoparticles are first incubated in base solution, which will deprotonate the surface and result in a negatively charged surface. When TBO is added, it will immediately bind onto the particle surface via electrostatic binding, leading the residual solution to become clear. Lowering the pH value of the solution allows for the release of bound TBO molecules from the surface and the regeneration of nanoparticles, presenting a blue solution. When the pH of the solution is raised, it became clear again. As shown in Figure 3.9, the capture and release of target molecules are simply realized by adjusting the pH of solution. In addition, the regenerated nanoparticles can be used for repeated cycles of capture and release. These features are ideal for running separation in microfluidic devices.

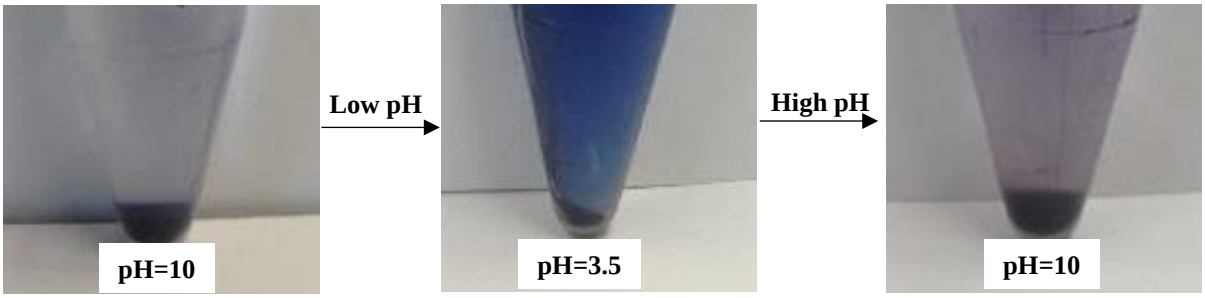

Figure 3.3. Reverse association and dissociation between Fe_3O_4@SiO_2-COOH and TBO by changing pH of solution.

In our study, Fe_3O_4@SiO_2-COOH nanoparticles and TBO molecules were chosen to examine the interaction between resulting functionalized IONPs and target compounds. The adsorption equilibrium experiment was carried by adding increased concentration of TBO solutions into same amount of nanoparticles. As shown in Figure 3.10, the adsorption of nanoparticle for TBO reached its maximum when the concentration of TBO increased to 2.0 x 10^{-6} mol. The maximum loading of TBO molecules onto IONPs at this point calculates as 1.9 x10^4 TBO per nanoparticle, referring to 0.5 TBO/nm^2. Compared the TBO loading with the density of -COOH functional groups 1.1 ligands/nm^2 from the EDX spectra, half of the -COOH groups were not accessible because they were imbedded in the silica matrix. Therefore, only the functional groups on the outer layer are available for the adsorption of target molecules.

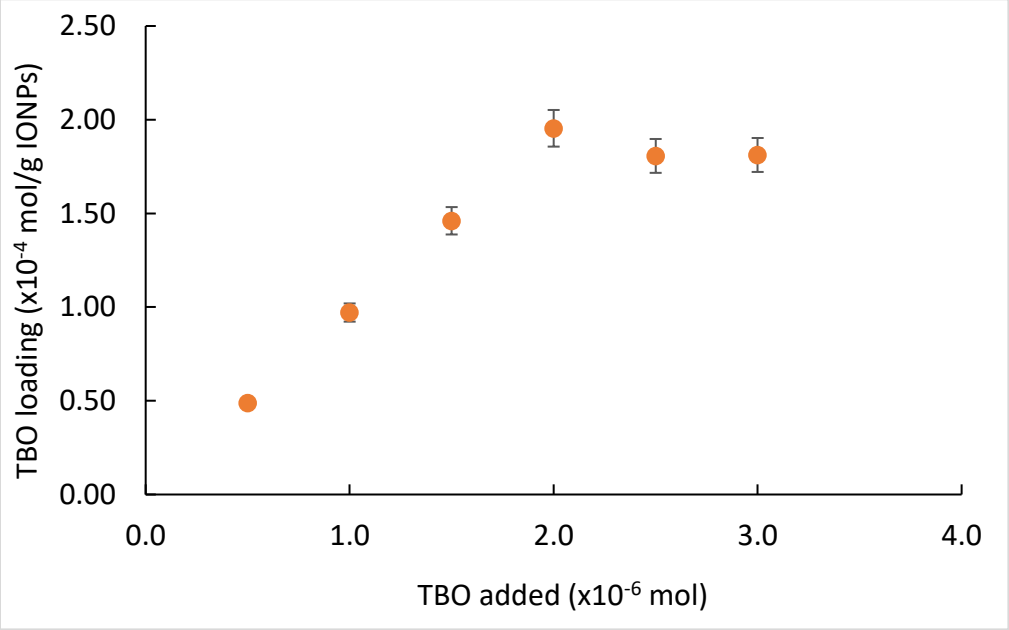

Figure 3.4. The effect of TBO concentration on loading ratio of TBO on Fe_3O_4@SiO_2-COOH IONPs (error bars: stdev of 3 replicates).

The reusability of resulting nanoparticles was examined spectroscopically through cycling experiments. The capture and release procedures were described in the Experimental section 3.2.6. After the nanoparticles and TBO molecules were incubated in PBS buffer for 1 hr, the optical

absorbance of residual solution was measured, from which the TBO concentration of the residual solution could be calculated using a calibration curve, along with equation 3.1:

$$\%\ \text{loading} = \left(1 - \frac{c_{residual}}{c_{initial}}\right) \times 100 \tag{3.1}$$

Second, the nanoparticle precipitates were rinsed with PBS buffer to remove unbound TBO molecules, and acetic acid (50% v/v) was added to release TBO from nanoparticles. The UV absorbance of the solution was measured to calculate the TBO recovery according to calibration curve again (Eq. 3.2).

$$\%\ \text{recovery} = \left(\frac{N_{released}}{N_{loaded}}\right) \times 100 \tag{3.2}$$

where $N_{released}$ is the number of TBO molecules released from the IONPs, N_{loaded} is the number of TBO molecules loaded on the IONPs. After such capture-release process, the nanoparticles were dried, and the same procedure was repeated for 5 cycles. As shown in Figure 3.11, both the TBO loading and recovery were decreased gradually during the 5 cycles. One reason is that each cycle of capture-release experiment involves several wash steps, in which large mass loss of nanoparticles was observed. In addition, samples before and after the cycling experiments were examined by TEM to study the effect of solution on structural deformation. As shown in Figure 3.12, slight decomposition of silica shell was observed after 5 cycles of adsorption-release experiments, due to the exposure of nanoparticles in high pH solutions over time. According to Figure 3.11, a gap between the percentage loading and recovery was found. On the one hand, there is possibly unbound TBO residuals on the particle surface that increased the percentage loading. On the other hand, the mass loss of nanoparticle during the wash steps, as well as incomplete dissociation of TBO from nanoparticles due to equilibrium, might cause the low percentage recovery. Repeated release procedures using fresh acetic acid might improve the percentage

recovery. But there must be a balance between washing and repeated releasing procedures, considering the mass loss of nanoparticles caused by wash steps.

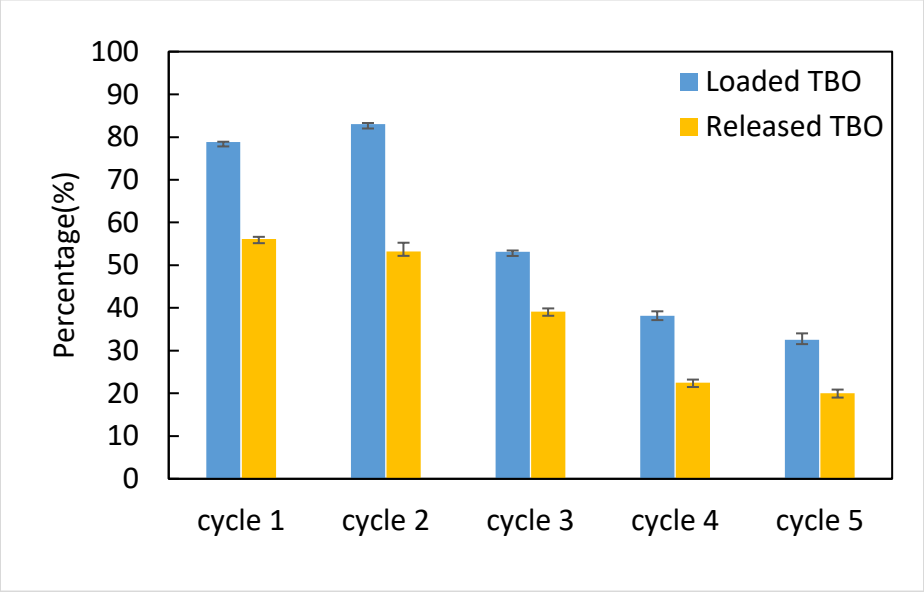

Figure 3.5. Percentage loading and recovery of TBO of 5 cycles[a]. (a: The percentage numbers of each column were obtained from the average value of two parallel samples. And the measurement for each sample was repeated 3 times.)

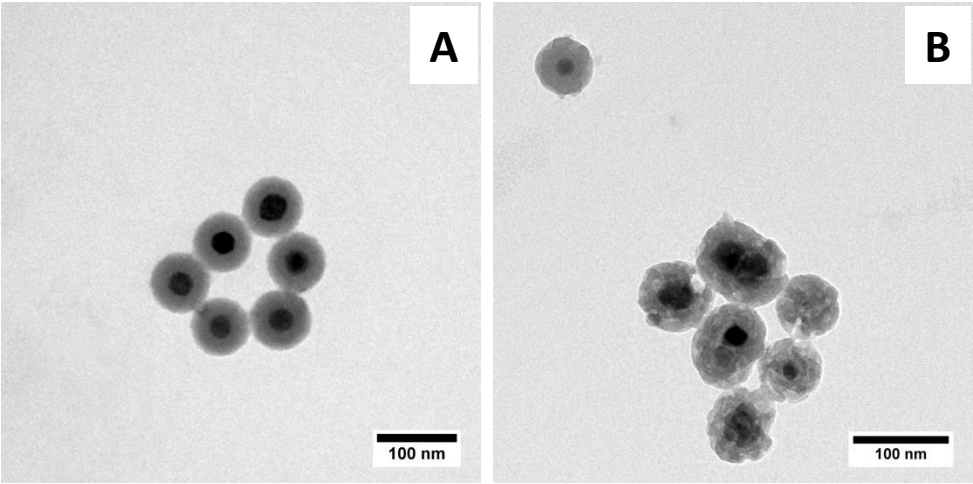

Figure 3.6. TEM images of Fe_3O_4@SiO_2-COOH IONPs before (A) and after (B) 5 cycles.

3. 3. 4 Binding capacity of Fe_3O_4@SiO_2-COOH to natural product

The carboxyl terminated IONPs we synthesized has not only shown good affinity to cationic dye molecules, but also promising to natural products. Ephedrine hydrochloride is a drug

used to prevent low blood pressure and asthma. Here we used it as another model compound to test the binding capacity of Fe_3O_4@SiO_2-COOH for potential drug molecules. The release of ephedrine from nanoparticles was repeated 3 times by adding fresh acid solution, in order to increase the percentage recovery. As shown in Figure 3.13, the result shows that 94.0% of ephedrine hydrochloride molecules were bound to nanoparticles and 76.9% were recovered from the solution after 3 repeated release procedures. This demonstrated the potential of using our functionalized nanoparticles for separation in a microfluidic synthesis system.

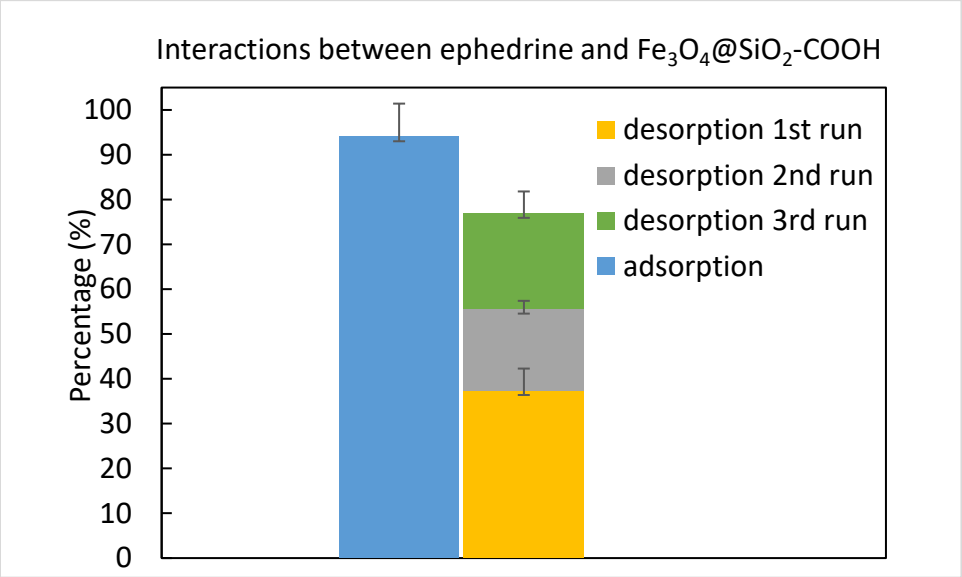

Figure 3.7. Percentage loading and recovery of ephedrine hydrochloride (error bars: stdev of 3 replicates).

3.3.5 Specific binding vs. non-specific binding.

In Chapter 2, we synthesized amine functionalized nanoparticles, and they have shown highly selectivity for fluorescein molecules. The surface was positively charged after incubation in acid solution. The non-functionalized silica coated IONPs Fe_3O_4@SiO_2 showed zero affinity to fluorescein molecules, as shown in Table 2.2. However, because the surface of Fe_3O_4@SiO_2 present negative charges, non-specific adsorption of target cationic compounds due to silica has to

be considered for the carboxyl functionalized nanoparticles, in addition to the adsorption mechanism of Fe_3O_4@SiO_2-COOH via deprotonation of the surface. The adsorption of target cationic compounds using Fe_3O_4@SiO_2-COOH comes from two parts: specific binding though -COOH groups on particle surface and non-specific binding due to negative charges of silica. In Figure 3.14, the percentage of each binding was investigated by using Fe_3O_4@SiO_2 as control groups. The result shows that the loading ratio of Fe_3O_4@SiO_2-COOH for TBO molecules was 98.9%, while the loading ratio of Fe_3O_4@SiO_2 for TBO molecules was 64.0%, indicating that 34.9% TBO molecules were selectively bound onto the nanoparticle due to the surface functionalities. However, the recovery of TBO improved after functionalization. Therefore, the release of TBO molecules from selective binding is easier than the non-specific binding.

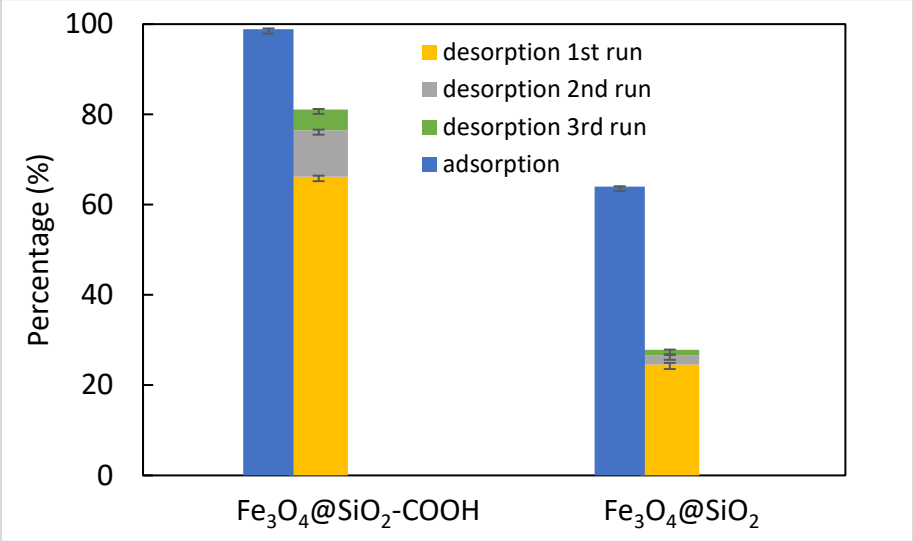

Figure 3.8. Comparison of specific binding and non-specific binding on Fe_3O_4@SiO_2-COOH nanoparticle (error bars: stdev of 3 replicates).

3. 4 Conclusion

Click chemistry was successfully applied for making functionalized precursors for core-shell magnetic nanoparticles in a facile synthesis strategy. By synthesizing organotrialkoxysilanes

precursors via thiol-ene click reaction, a variety of commercially unavailable organotrialkoxysilanes are easy to access with high yield and purity. Also, the steps of making functionalized magnetic nanoparticles were largely reduced using these organotrialkoxysilanes. Tedious wash steps and grafting stage were avoided without undergoing the morphology changes. The resulting uniform single-loaded core-shell magnetic nanoparticles terminated with a variety of functionality are promising to be applied for a wide range of applications in microfluidic separations.

CHAPTER 4. MICROFLUIDIC CONTINUOUS SEPARATION USING FUNCTIONALIZED MAGNETIC NANOPARTICLES

4.1 Introduction

Purification and separation of target molecules using microfluidic devices have received growing interest in recent years due to its potential applications in biological and chemical industries.[32,111,112] Traditional separation techniques, such membrane-based filtering, chromatography, electrophoresis, and precipitation,[113] usually involve problems like clogging, vast solvent consumption, pH gradient formation, low throughput, and contamination. External-fields-based separation on microfluidic platforms, including magnetic magnetophoresis,[111] optical tweezers,[114,115] dielectrophoresis,[116,117] acoustophoresis,[118] have become great alternatives in terms of selectivity and recovery. Particularly, magnetic manipulation of continuous microfluidic separation using functionalized magnetic nanoparticles is attractive because of multiple advantages, such as free of pH gradients, less contaminations, reduced clogging, mild reaction conditions, and enhanced surface area-to-volume ratio to allow for high throughput.[3] For example, separations using electric fields is usually dependent greatly on solution conditions such as ionic strength and pH, and can cause problems such as bubble generations.[119-121] But for magnetic separation, those problems are left behind, and the separation efficiency is highly dependent on the microfabricated channels and the control of the magnetic field strength. Also, continuous magnetic separation in flow overcomes some limitations of magnetic separation in batch systems, including prolonged duration of operation, complicated fluidic handling, and nonspecific trapping of impurities. [122]

Microfluidic magnetic separation involves the interaction between magnetism and fluid flow on a microscale. There are several key forces that need to be considered for magnetic

microfluidic separation: magnetic force, gravitational force, drag force, lift force, and Brownian force The magnetic force and drag forces are more dominant than other forces when considering applications in a microfluidic environment.[123] At a microscopic level fluid exhibit laminar flow, and the inertial and gravitational effects are negligible because of the small particle volume.[32] Therefore, the main challenge of continuous-flow separation lies in the fabrication of microfluidic device so as to guide nanoparticles to desired outlet to achieve both high efficiency and throughput. In addition, high magnetization and superparamagnetic behavior of nanoparticles are prerequisites, considering the fact that high magnetization gives strong magnetic force for high capture efficiencies, and that superparamagnetic particles have zero magnetization in the absence of an external magnetic field so that separation can be fast and efficient without aggregation.

To ensure high magnetization and superparamagnetic behavior, researchers has been directed towards different types of magnetic particles, such as micron-sized magnetic beads and magnetic nanoclusters.[119] It is reported that nano-sized magnetic clusters can not only maintain the same level of magnetization as micron-sized beads, but also have a much higher loading capacity than micron-sized magnetic particles.[124] On the other hand, nanoclusters might cause clogging in the micro channel, and the colloidal stability of nanoclusters might be affected by some pH-sensitive separation process.[125] Therefore, uniform sized and single cored nano-sized magnetic particles with reasonable magnetization are ideal for separation of small molecules. They offer high surface-to-volume ratios for loading capacity and high colloidal stability without causing aggregation of nanoparticles or diminishing of magnetic moments. By taking advantage of a well-developed surface chemistry and a tailor-made functionalization, ready-to-use functionalized magnetic particles are increasingly available with well-controlled surface chemistry providing a high specific binding capacity and low non-specific adsorption.[29] However, the price of those

commercialized magnetic nanoparticles are very expensive. In our previous work, we have successfully synthesized a number of uncommercialized core-shell magnetic IONPs with selected surface functional groups. And they have shown their potential applicability for use in reversible and quantitative affinity-based microfluidic separation.[108]

To our best knowledge, continuous separation of small molecules using single-cored magnetic nanoparticles on a microfluidic device has not yet been reported. For the purpose of proof of principle, blue (Toluidine blue O) and yellow (fluorescein) dye molecules were used as model targets to demonstrate a continuous microfluidic molecular separation process. Our functionalized magnetic nanoparticles are able to selectively interact with TBO in the dye mixture, resulting in the formation of TBO-nanoparticle complex via electrostatic binding, then collected online by magnetophoresis. The microfluidic separation system is shown in Scheme 4.1. It consists of two microfluidic chips: mixing and separation. The mixture coming out from the mixing chip enters the separation microchannel in laminar co-flow with a cushion buffer and extraction buffer. When an external magnetic field is applied on the side of extraction buffer, the nanoparticle-TBO complex would travel across the microchannel and enter into the extraction buffer streamline, where TBO molecules are released from nanoparticles caused by the change of surface charges at lower pH. The released TBO molecules are collected at the desired outlet, leaving fluorescein molecules in the original fluid stream to exit through another outlet. In order to improve the separation efficiency, the middle stream between the extraction buffer stream and the original mixture stream work as cushion buffer to prevent the diffusion of fluorescein into the extraction buffer streamline. Therefore, a continuous “flowing separation” is achieved since the separation occurs through selective adsorption on nanoparticles that are moving along with the fluids. And

our method can be potentially applied to affinity-based separations for a wide range of small ionic molecules and biomolecules by using well established functionalized magnetic nanoparticles.

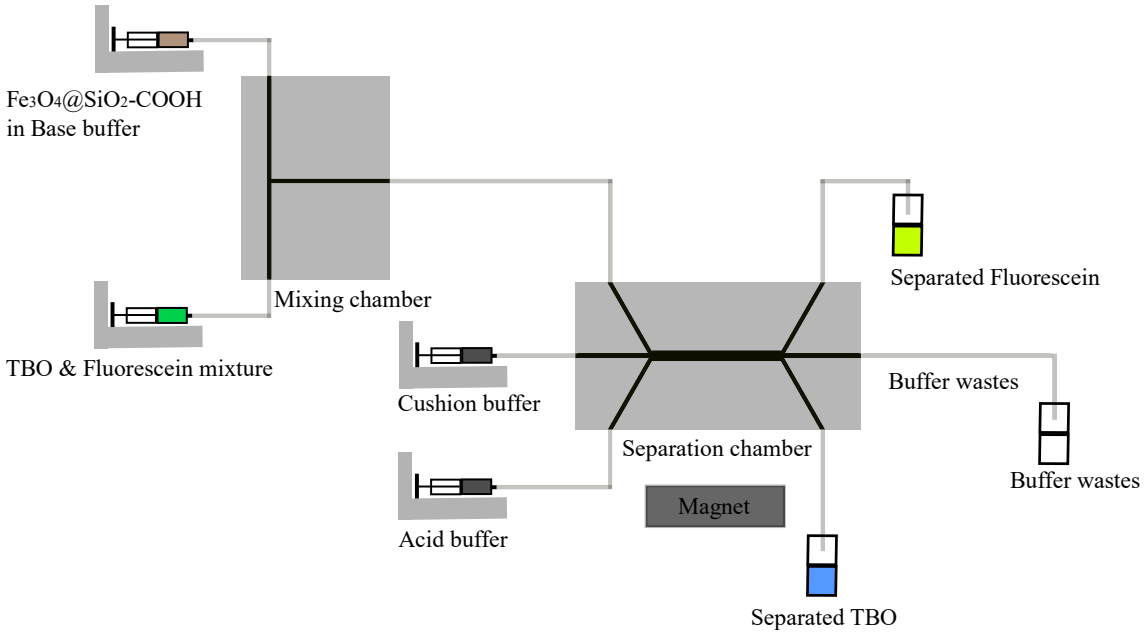

Scheme 4.1. A continuous microfluidic magnetic separation system.

4. 2 Experimental

4. 2. 1 Synthesis of carboxyl functionalized IONPs

All chemicals were purchased from Sigma-Aldrich and used as received. Functionalized IONPs were synthesized using the functionalized precursors we synthesized previously.[109] First, Fe_3O_4 magnetic cores were synthesized by heating a mixture of 5 mmol of $Fe(oleate)_3$, 2.5 mmol of oleic acid, and 32 mL of 1-octadecene up to 320 °C, and refluxed at this temperature for 30 min. The resulting black precipitates were alternatively washed with cyclohexane and ethanol for several times, and dried under vacuum, then stored under Ar as a suspension in cyclohexane with adding of a few drops of oleic acid to stabilize the colloid. Second, carboxyl functionalized triethoxysilane was synthesized via a radical mediated photochemical click reaction by exposing the mixture of triethoxyvinylsilane (5.22 mL, 25 mmol), 3-mercaptopropionic acid (2.18 mL, 25

mmol), and photoinitiator DMPA (128.15 mg, 2 mol%) under UV lamp for 24 hrs at 0 ºC. The reaction was running neat in the absence of any solvent and yielded 95% product. Thirdly, the surface coating of magnetic cores with the thiol-ene synthesized triethoxysilane was conducted in a reverse microemulsion system containing 0.25 mL surfactant Igepal CO-520, 10 mL cyclohexane and 100 μL NH_4OH. By adding 3.0 mg Fe_3O_4 (2.5 mg/mL in cyclohexane) into the reverse microemulsion under controlled conditions, followed by adding TEOS and carboxyl functionalized triethoxysilane, a silica layer was able to grow on the surface of each single magnetic core, and form single cored core-shell structures with carboxyl groups on the outer layer.

4. 2. 2 Fabrication of microfluidic devices

The microfluidic devices were fabricated from PDMS elastomer using a 3D printing technique. [39,126] First, a negative micro-mold of micro-channels was printed out using a Polyjet printer (Stratasys Objet260 Connex3) with resolution of 16 μm. Then PDMS casting procedure is performed by mixing a PDMS base with a curing reagent in a 10:1 ratio (Sylgard 184, Dow Corning, Midland, MI) followed by pouring the degassed mixture onto the micro-mold and curing at 70 ºC for at least 3 h. After curing, the PDMS replica was then carefully peeled off from the micro-mold and bonded onto a glass slide (75(L) x 25 (W) x 0.15 (H) mm^3) by oxygen plasma treatment to form an O–Si–O covalent bond at the PDMS interface.

4. 2. 3 Microfluidic mixing and separation

The mixing and separation efficiency of the chips were examined separately. First, magnetic nanoparticles (2mg/mL) in PBS buffer (2 mM, pH=8) and TBO solution (0.05 mM) were loaded in different syringe pumps, injected into a T-shape mixing chip (250μm (W) x 250μm (D) x 2cm (L)) at the same flow rate. The outlet of the mixing chip was connected to a 0.5 m long tubbing (Scientific Products & Equipment, 200 μm ID) to allow sufficient target molecules to be

adsorbed onto the particles before entering the separation microchannel. The loading efficiency was studied by changing flow rate and dye solution concentrations. Also, all control experiments were done under the same condition except in batch. TBO concentration was determined by measuring the UV-vis absorbance of TBO supernatant (590 nm) collected from the outlet, and compared to standard calibration curve. Then loading efficiency was calculated by comparing the collected TBO concentration and the original TBO concentration.

By connecting the mixing chip with the separation chip, the target-nanoparticle complex generated from the mixing chip entered the separation microchannel, at the same time with another two additional streams, water and acetate buffer. These two streams worked as a cushion streams to prevent diffusion of separated dye molecules, and an extraction stream to release the captured target molecules from nanoparticles, respectively. In the straight separation channel, laminar co-flow of the three streams is dominated. Therefore, when an external magnetic field is applied on the side of acetate buffer, the nanoparticle-TBO complex travel across the microchannel and enter the acetate buffer stream, where TBO molecules are released from nanoparticles and come out from the bottom outlet, while the fluorescein molecules remain in the original fluid stream and exit through the top outlet (shown in Figure 4.1). Effects on separation efficiency were studied by varying flow rate, magnetic forces, and dimension of microfluidic chips.

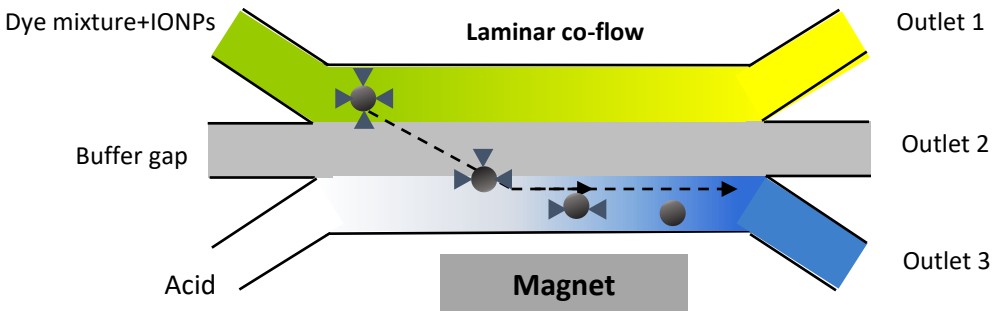

Figure 4.1. Particle trajectory in a laminar co-flow on the separation chip.

4. 3 Results and Discussion

4. 3. 1 Laminar co-flow profile in the separation microchannel

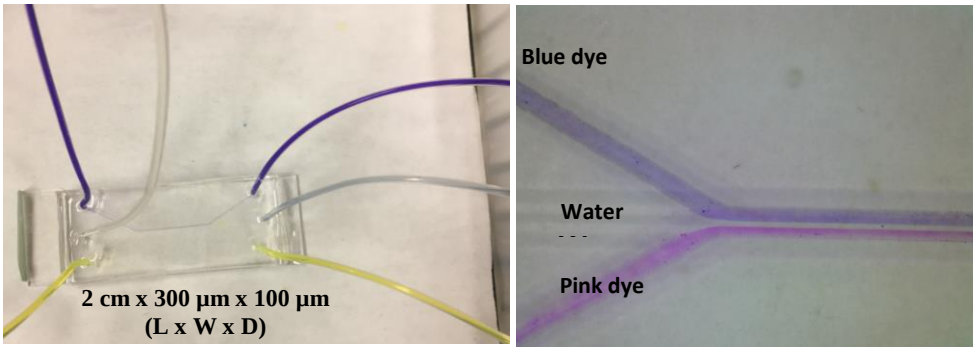

Figure 4.2. Laminar co-flows using colored dye solutions.

Laminar co-flow profile without disturbance between two streams was proved by running different colored dye solutions. As shown in Figure 4.2, the three streamlines enter into the micro-separation channel with little diffusion with each other (<5 % diffusion by measuring UV absorbance of solution collected from each outlet). Also, it is necessary to add a buffer gap in the middle of the other two streamlines to further prevent diffusion of the separated target molecules and original mixture. So when we run real reaction using magnetic nanoparticles, we will be sure that the target molecules we collect are due to separation by microfluidic magnetophoresis instead of diffusion.

4. 3. 2 Experimental results for microfluidic magnetically separation of target molecules

For the proof of principle, a dye mixture of TBO and fluorescein (0.1:1 mM) was picked as model target and nontarget molecules for selective extraction of TBO using our single-cored carboxyl functionalized magnetic nanoparticles in flow. At pH 8, the carboxyl groups were deprotonated and give negative surface charges on the nanoparticles, which allows for fast electrostatic interaction between positively charged TBO at the particle surfaces. It is reported that

at such low Reynolds number, fluid is running in laminar flow, but laminar flow decreases by increasing the angle between two fluids at joint.[127] Therefore we chose 180° for our design to make a T-shape mixing chip, in order to minimize the laminar flow and allow efficient mixing and high capture. As shown in Figure 4.3, the mixing efficiency using our T-shape chip was not affected so much by varying flow rate. The sharp corner of at the T-junction allows for intense collision between the two coming fluids. The efficient mixing may also be attributed to the long travel distance (0.5 m) in the connecting tubing, which gives target molecules and nanoparticles enough time to interact with each other.

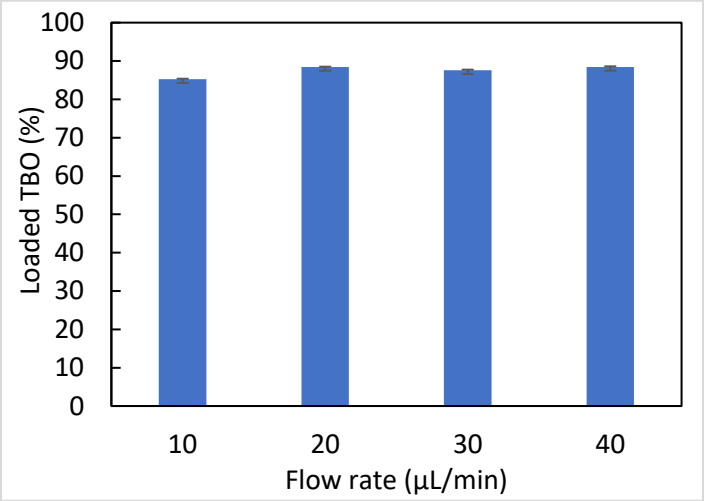

Figure 4.3. Mixing efficiency at different flow rate (error bars: stdev of 3 replicates).

For comparison, the mixing experiments were conducted both in batch and in flow, with increased TBO concentration. In batch, 0.5 mL TBO solutions were mixed with 0.5 mL nanoparticle suspension (2 mg/mL) in a vial and subjected to sonication for 15 min. In flow, TBO solutions and nanoparticle suspension were continuously mixed at the T-mixer at flow rate of 20 µL/min, resulting in mixing at 1:1 volume ratio. UV absorbance of residual solutions were measured in order to determine the amount of TBO molecules loaded on the particle surface at

different TBO concentration. All the residual concentrations were calculated from a calibration curve and the mixing efficiency calculated by equation 3.1. According to Figure 4.4, the percentage loading of TBO in flow was very close to that in batch. In the experiment, laminar flow was observed at outlet of the T-shape mixer, but a maximum of 91.4% TBO loading was achieved. This could due to the long extended tubing, allowing enough diffusion of two fluids while traveling through.

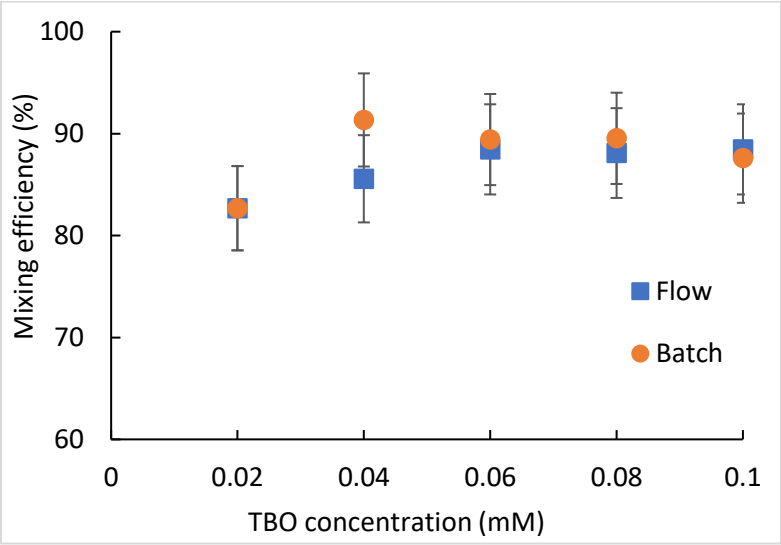

Figure 4.4. Comparison of mixing efficiency between batch and flow (error bars: stdev of 3 replicates).

After demonstrating the mixing efficiency of the mixer, a continuous separation system was set up by combining the mixer and separator together. To examine the separation efficiency of the magnetic microfluidic separator, dye mixture of TBO and fluorescein were used. As shown in Figure 4.5, with decreasing flow rate, more nanoparticles captured with TBO molecules successfully traveled across the micro channel. When they were entering in to the acid stream, TBO molecules were released from the IONPs and continuously collected from the desired outlet 3. With further decrease of flow rate to 1 μL/min, aggregates were observed in the micro channel

and trapped on the side wall of the microchannel by the magnet. At flow rate 10 μL/min, the separation efficiency in continuous flow was close to that in batch. As control experiment, only less 5% percent of TBO molecules was detected from outlet 3 when no magnet was placed beside the microchannel, indicating that the release of TBO molecules happened in the acid stream while they were deflected by external magnetic field.

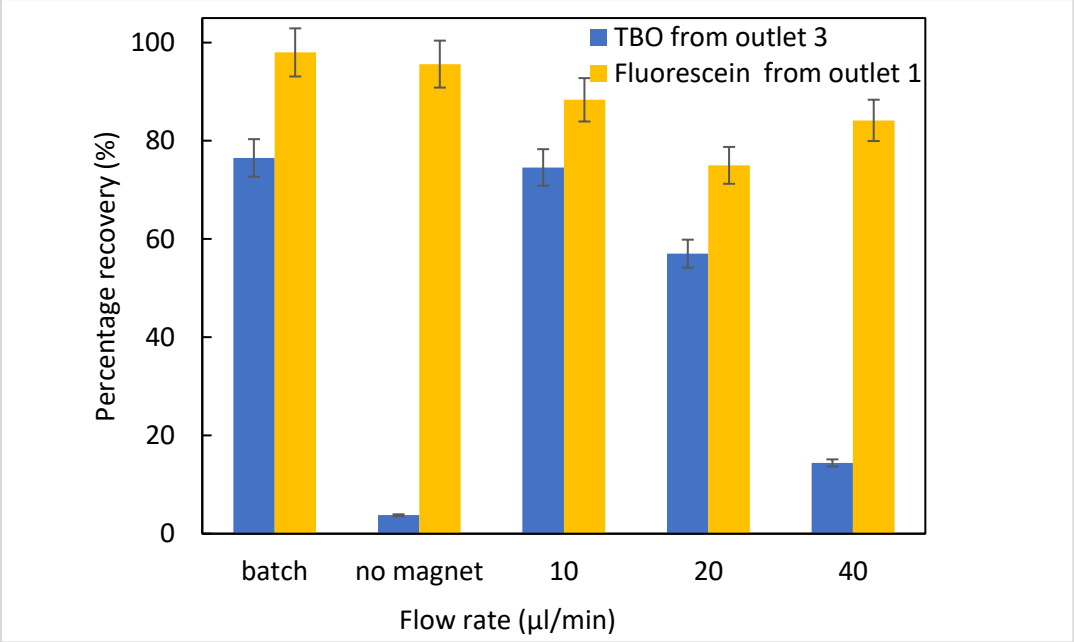

Figure 4.5. Separation efficiency of dye mixture (error bars: stdev of 3 replicates).

The color of collected solutions from each outlet also further proved the successful separation (Figure 4.6). Solution from outlet 1 was the yellow color of fluorescein, while solution from outlet 3 was blue, (the original color of acetate buffer was clear) which was the color of TBO, indicating the successful releasing of TBO molecules from INOPs while they are flowing through the acid stream. Also, separation efficiency could be estimated by the observed amount of INOPs at the bottom of the vials. After centrifugation, IOPNs were observed in acid solution collected from outlet 3, with no INOPs observed in original mixture stream collected from outlet 1, and only

a few IONPs from outlet 2, meaning IONPs traveled across the streams and entered the side close to the magnet.

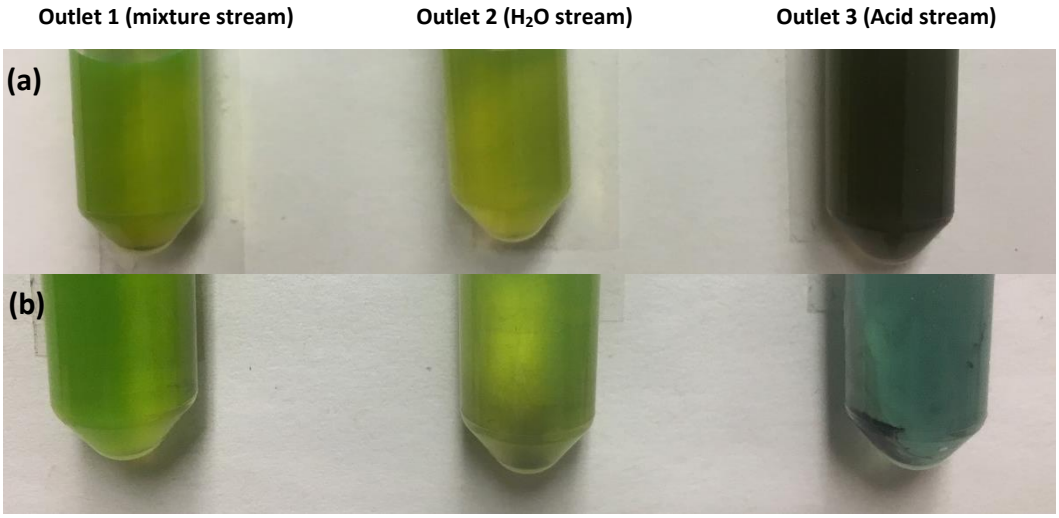

Figure 4.6. Fluids collected from each outlet (a) solutions before centrifugation, b) solutions after centrifugation.

As we discussed in the Introduction chapter, the trajectory of each single magnetic nanoparticle in a microchannel is the result of the balance of the hydrodynamic drag force and magnetic force acting on this nanoparticle. Therefore, the magnetic strength plays a crucial role for successful separation. In a microchannel, we want the magnetic strength strong enough for directing magnetic nanoparticles to come out from the desired outlet, yet not too strong for nanoparticles being trapped in the microchannel and causing clogging. Fortunately, this can be realized by choosing right magnetic source and adjusting the distance between the microchannel and magnet.

We used high-pull neodymium permanent magnets (bought from McMaster-Carr) with different strength to study the effect of magnetic strength on separation efficiency. The magnet was kept a 2 mm distance from the microchannel. A previously described TBO method was used to quantify the amount of nanoparticles collected from each outlet. The magnetic strength closed

to the microchannel was measured using a digital guassmeter (Weite Magnetic Technology Co., Ltd, WT10A) As shown in Figure 4.7, with the increment of magnetic strength, shifts of IONPs occurred among these three outlets. In absence of a magnet, 85.7% IONPs came out from outlet 1, representing the original stream. This result was reversed while increasing the magnetic strength. When the magnetic strength increased to 220 mT, 85.2% of nanoparticles successfully entered the desired outlet 3, representing the extraction stream.

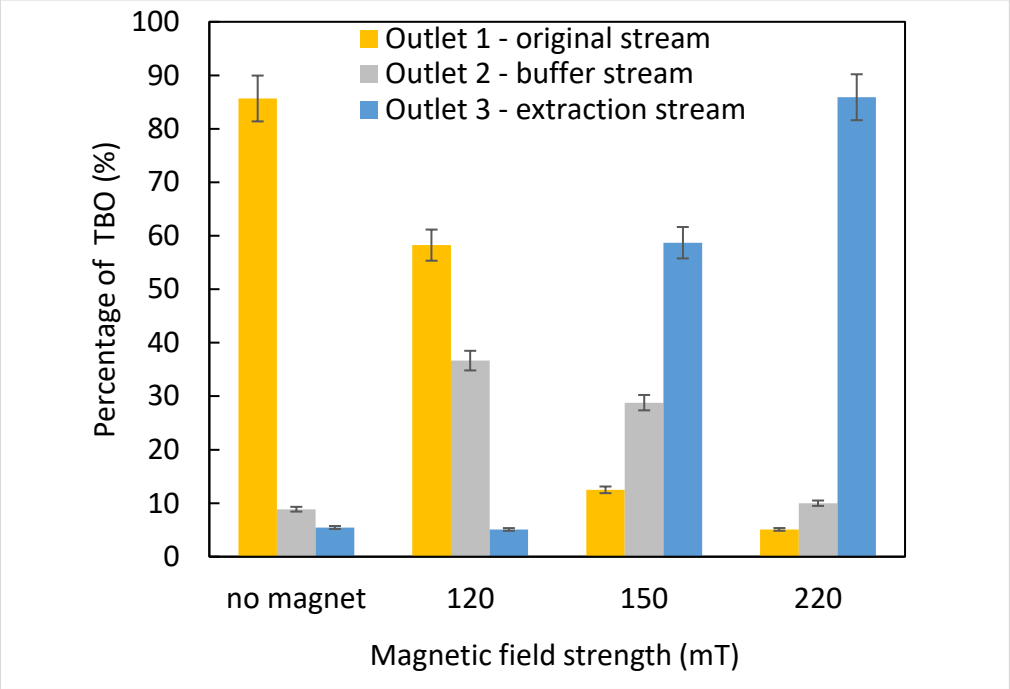

Figure 4.7. Effect of magnetic strength on the separation efficiency (error bars: stdev of 3 replicates).

4.4 Conclusion

A proof of principle continuous microfluidic magnetic separation system was developed. We have demonstrated the magnetophoretic process for continuous separation of small molecules in which carboxyl functionalized IONPs selectively interact with TBO molecules in a mixture with fluorescein via electrostatic binding, and the resulting TBO-IONP complex are recovered online

using magnetophoresis. The high magnetization of magnetic nanoparticles, coupled with dynamic aggregation phenomena after molecule-particle association, allows for the fast deflection of molecules for separation. This microfluidic separation system has shown comparable mixing and separation efficiency with that in batch. Our results reveal the importance of designing and fabricating the microfluidic device, as well as controlling the magnetic strength across the separation channel to achieve efficient separation. We envision this method to eventually enable separation of a wide range of desired target molecules by using the silica-coated IONPs with different affinity ligands, and integration with continuous microfluidic synthesis. Our ongoing efforts include modification of the surface of IONPs with broader scope of functionalities using existing methods to extend the applicability of our separation phase to non-electrostatic based separation. In addition, a multi-stage version of this separation process by connecting single separation units in serial could possibly further increase the separation efficiency.

CHAPTER 5. LIMITATIONS, CONCLUSIONS, AND FUTURE WORK

5.1 Limitations

Separation based on electrostatic binding allows for fast association and dissociation between target compounds and nanoparticles. The most significant limitation for existing magnetophoresis technology is that it is best suited for molecules with large difference in pKa values. The affinity-based separation can be carried out by connecting multiple separators flowing with solutions at different pH. But for organic species with close pKa values, they will have same charge and may not be completely separated by one single separation technique. So purification of such species may be optimal using a different separation technique, and most likely discontinuous.

With respect to the integration of the magnetophoresis with continuous flow synthesis, limitations associated with magnetophoresis are uncertain because it has just recently been hypothesized as a complement for continuous flow synthesis. In this dissertation, we have demonstrated the potential of using magnetophoresis for non-interrupted continuous flow purification, which is the most important factor to realize an automated continuous flow synthesis process. However, several issues need to be addressed to eventually apply those functional nanoparticles for an integrated continuous-flow synthesis system. First, pre-treatment of crude products by acid/base quenching might be needed to transfer the products into ionic species. This could be solved by implementing a work-up stage before the magnetophoresis, so any protonable/deprotonable organic species will be transferred into aqueous solution and captured by magnetic nanoparticles. Second, there is limitation of using silica-coated magnetic nanoparticles in continuous flow purification, because the base solution could decompose the silica layer and result in losing the functional groups for selective binding eventually. Polymers are not ideal solid

scavengers for continuous flow synthesis, because most of them either swell in organic solvent or are not acid/base tolerant. Alternative solid supports such as carbon nanotubes and graphene decorated with magnetic nanoparticles might be good candidates for continuous flow purification. Third, precise control of the magnetic field strength across the whole separation region is crucial for efficient purification. This is difficult to realize by simply placing one or two permanent magnets beside the microchannel. Placing multiple small magnets at different spots or using hybrid magnets might improve the separation efficiency. Also, simulating the magnetic field across the separation region would help us predict the particle trajectories. Furthermore, the device geometries have been optimized to enhance the separation efficiency by adding a cushion buffer between the original fluid stream and the extraction stream. But there is still diffusion observed from the middle stream which is the cushion buffer. This could be solved by increasing the flow rate of the cushion buffer. New design should be optimized to control pressure at each outlet so that the proportion of solution coming out from each outlet could be precisely predicted. Scaling-up is another issue for all the existing continuously flow purification techniques. For the magnetophoresis technique, scaling-up can be achieved by continuously running the flow purification for a long period of time, because theoretically magnetophoresis does not interrupt the flow.

5.2 Conclusions

Integrated multistep continuous-flow synthesis and purification is pursued in current pharmaceutical industry. However, the lack of efficient separation technology limits the development of such integrated system. A continuous microfluidic magnetic separation technology which utilizes surface-functionalized magnetic particles to selectively capture target molecules is promising to realize this goal. In the microchannel, the migration of magnetic particles is manipulated through an external magnetic force. We developed a facile method to make high quality of core-shell magnetic nanoparticles with versatile surface functionalities for potential application in continuous-flow synthesis, including catalyst loading and product purification.

First, triethoxysilanes with a variety of functionalities have been successfully synthesized using work-up-free thiol-ene click reactions. Then core-shell functionalized IONPs composed of a single-core structure were made by a reverse microemulsion sol-gel process. The morphology, size, and colloidal stability of resulting nanoparticles are well controlled. Furthermore, we have successfully demonstrated the separation efficiency of resulting nanoparticles by using two dye molecules: toluidine blue O (TBO) and sodium fluorescein. More importantly, our model can be potentially used for other types of magnetic-based separation by introducing different functionalities on the particle surface.

Second, we fabricated a microfluidic device using PDMS to realize continuous separation of target compounds. The combination of a mixer with a separator allows for the automated continuous isolation. On-line capture and release of TBO molecules from a mixture of toluidine blue O (TBO) and fluorescein has been successfully realized in this separation device through magnetic-field-directed migration of nanoparticles. The laminar co-flow profile allows for the continuous dissociation of TBO molecules from nanoparticle surface by entering an undisturbed

acid stream with the assistance of an external magnetic force. The device has shown high separation selectivity and efficiency, along with excellent reliability and flexibility to be modified using an 3D printing technique.

5.3 Future Work

Up until now, proof-of-principle studies of functional magnetic nanoparticles for continuous separation in microfluidic device have been conducted and demonstrated. The separation using magnetophoresis technology is based on the migration of nanoparticles, which is determined by hydrodynamic viscous drag force and magnetic force acting on a magnetic nanoparticle. The particle trajectory inside a microchannel relies on the balance of these two vectors. So an in-depth understanding of the theory will help us predict the particle movement in the microchannel as well as improve separation efficiency by adjusting parameters such as nanoparticle size, dimensions and design of microfluidic device, and flow rate. Therefore, the next step will be focused on finding the optimized parameters for continuous separation in microfluidic device by mathematical modeling, or using existed software such as COMSOL Multiphysics, to simulate the particle trajectories.

In our lab, an automated synthetic system has been created by implementing an in-line gas chromatography mass spectrometry (GC/MS) analytical instrument with a microwave assisted continuous organic synthesis (MACOS) flow reactor system. This system is aimed to run, analyze and optimize a synthetic transformation in a fully automated and continuous mode. The development of a continuous flow purification device would fill the vacancy of in-line purification for our existing MACOS system. Therefore, we are interested in exploring the separation efficiency of our functionalized IONPs for a broader scope of compounds from organic synthesis. The proof of principle studies using dye molecules in this work have shown the potential of the functionalized IONPs for separation in microfluidic devices. The amine and carboxylic acid functional groups on the IONPs allows for the separation of a variety of drug candidates containing deprotonable/protonable species, such as carboxylic acid, hydroxide, amine, via ionic interactions.

We will investigate the continuous flow separation by running some classic organic reactions. Our previous colleagues have demonstrated the capabilities of the MACOS system by running a scope of organic synthesis, including Suzuki-Miyaura cross-coupling, Heck cross-coupling, Nucleophilic aromatic substitution, Claisen rearrangement, Diels-Alder cycloaddition, and Hydrosilylation.[128] We can use those chemical transformations to investigate the continuous magnetically steered flow purification. For example, we can apply the Claisen rearrangement of allyl phenyl ether to 2-allyl phenol to explore the capabilities of the magnetically-steered continuous flow separation device and then implement it with the MACOS system. The work-up process of this reaction involves the deprotonation of the 2-allylphenol in base and transferring it into aqueous layer. At this point, connecting the magnetic separator with the work-up would allow for the adsorption of 2-allyl phenol by the carboxyl functionalized IONPs.

With the versatile strategies for surface modification, we also want to exploit other types affinity-based separations. Additionally, the interactions between nanoparticles and target molecules are 1:1 binding ratio using current thiol-ene strategy for surface modification. In the future, we want to explore selective binding of one ligand for multiple molecules.

Also, we want to focus on developing a closed-cycled continuous microfluidic magnetic separation system for integrated multi operation units for separation, including selective binding, separation, and regeneration of nanoparticles. As shown in the figure below, it consists of three microfluidic chips: mixing, separation, and recycle. The chips are connected using plastic tubing. On the mixing chip, pre-activated nanoparticle suspension and crude solution are injected into a T-shape mixing chamber. Target molecules are able to be captured by the magnetic nanoparticles from crude mixture. On the separation chip, the nanoparticle-target complexes are separated from the original stream by traveling across the microchannel in the presence of an external magnetic

field. By removing the magnet, the nanoparticles and buffer wastes enter into the third chamber, where buffer wastes are collected, and the nanoparticles are regenerated by washing with neutral buffer. After regeneration, the nanoparticles can be activated, and the next cycle of separation can be started. Therefore, a closed cycled continuous-flow separation is achieved since the separation occurs through selective adsorption on nanoparticles that are moving along with the fluids.

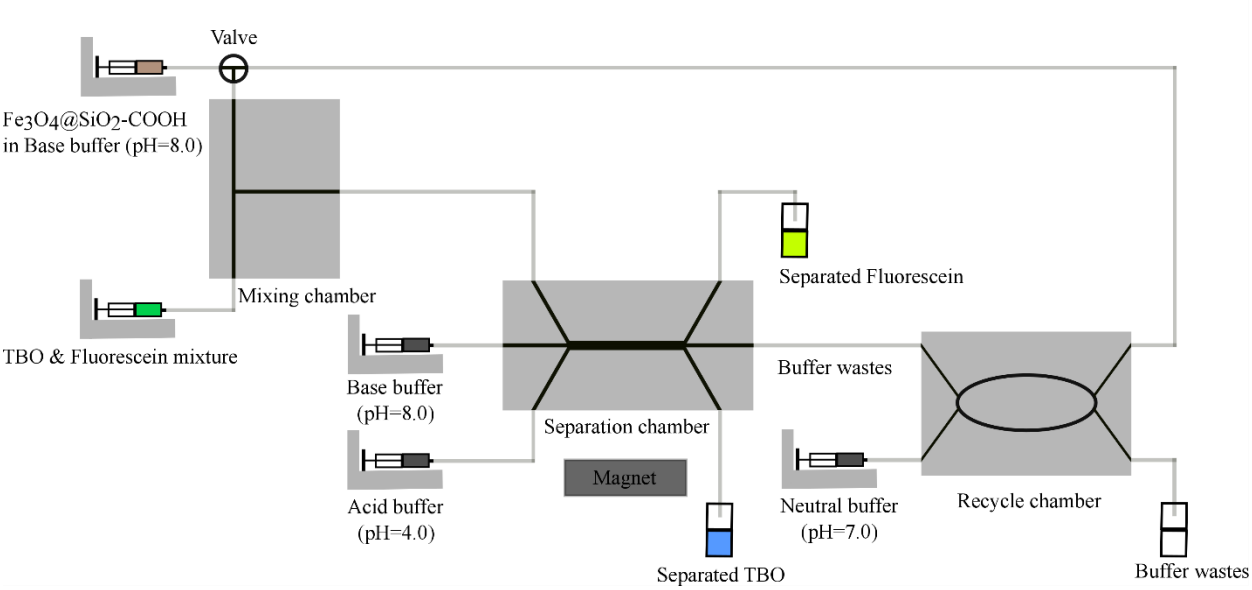

Scheme 5.1. A closed-cycled magnetically steered continuous microfluidic separation system.

CHAPTER 6. REFERENCES

(1) Gutmann, B.; Cantillo, D.; Kappe, C. O. *Angew.Chem. Int. Ed.* **2015**, *54*, 6688.

(2) Price, G. A.; Mallik, D.; Organ, M. G. *J. Flow Chem.* **2017**, *7*, 82.

(3) Khashan, S. A.; Dagher, S.; Alazzam, A.; Mathew, B.; Hilal-Alnaqbi, A. *J. Micromech. Microeng.* **2017**, *27*, 055016.

(4) Loren, B. P.; Wleklinski, M.; Koswara, A.; Yammine, K.; Hu, Y.; Nagy, Z. K.; Thompson, D. H.; Cooks, R. G. *Chem. Sci.* **2017**, *8*, 4363.

(5) Hartman, R. L.; Jensen, K. F. *Lab. Chip* **2009**, *9*, 2495.

(6) Heider, P. L.; Born, S. C.; Basak, S.; Benyahia, B.; Lakerveld, R.; Zhang, H.; Hogan, R.; Buchbinder, L.; Wolfe, A.; Mascia, S.; Evans, J. M. B.; Jamison, T. F.; Jensen, K. F. *Org. Process Res. Dev.t* **2014**, *18*, 402.

(7) Bogdan, A. R.; Poe, S. L.; Kubis, D. C.; Broadwater, S. J.; McQuade, D. T. *Angew. Chem. Int. Ed.* **2009**, *48*, 8547.

(8) Snead, D. R.; Jamison, T. F. *Angew. Chem. Int. Ed.* **2015**, *54*, 983.

(9) Borukhova, S.; Noel, T.; Metten, B.; de Vos, E.; Hessel, V. *ChemSusChem* **2013**, *6*, 2220.

(10) Mascia, S.; Heider, P. L.; Zhang, H.; Lakerveld, R.; Benyahia, B.; Barton, P. I.; Braatz, R. D.; Cooney, C. L.; Evans, J. M.; Jamison, T. F.; Jensen, K. F.; Myerson, A. S.; Trout, B. L. *Angew. Chem. Int. Ed.* **2013**, *52*, 12359.

(11) Adamo, A.; Beingessner, R. L.; Behnam, M.; Chen, J.; Jamison, T. F.; Jensen, K. F.; J-C.M., M.; Myerson, A. S.; Revalor, E. M.; Snead, D. R.; Stelzer, T.; Weeranoppanant, N.; Wong, S. Y.; Zhang, P. *Science* **2016**, *352*, 61.

(12) Agostino, F. J.; Krylov, S. N. *Trends Analyt. Chem.* **2015**, *72*, 68.

(13) Kralj, J. G.; Sahoo, H. R.; Jensen, K. F. *Lab. Chip.* **2007**, *7*, 256.

(14) Imbrogno, J.; Rogers, L.; Thomas, D. A.; Jensen, K. F. *Chem. Commun.* **2017**, *54*, 70.

(15) Rajendran, A.; Paredes, G.; Mazzotti, M. *J. Chromatogr. A* **2009**, *1216*, 709.

(16) Lee, J. W.; Horváth, Z.; O'Brien, A. G.; Seeberger, P. H.; Seidel-Morgenstern, A. *Chem. Eng. J.* **2014**, *251*, 355.

(17) O'Brien, A. G.; Horvath, Z.; Levesque, F.; Lee, J. W.; Seidel-Morgenstern, A.; Seeberger, P. H. *Angew. Chem. Int. Ed.* **2012**, *51*, 7028.

(18) Horváth, Z.; Horosanskaia, E.; Lee, J. W.; Lorenz, H.; Gilmore, K.; Seeberger, P. H.; Seidel-Morgenstern, A. *Org. Process Res. Dev.* **2015**, *19*, 624.

(19) Benz, C.; Boomhoff, M.; Appun, J.; Schneider, C.; Belder, D. *Angew. Chem. Int. Ed.* **2015**, *54*, 2766.

(20) Pamme, N. *Lab Chip* **2007**, *7*, 1644.

(21) Degen, I. L.; Kutsenok, B. S.; Zhuravleva, E. A.; Eglit, E. *Ortop. Travmatol. Protez.* **1977**, 67.

(22) Gómez-Pastora, J.; Xue, X.; Karampelas, I. H.; Bringas, E.; Furlani, E. P.; Ortiz, I. *Sep. Purif. Technol.* **2017**, *172*, 16.

(23) Liang, L.; Xuan, X. *Biomicrofluidics* **2012**, *6*, 44106.

(24) Xia, H. M.; Wan, S. Y.; Shu, C.; Chew, Y. T. *Lab Chip* **2005**, *5*, 748.

(25) Hejazian, M.; Li, W.; Nguyen, N. T. *Lab Chip* **2015**, *15*, 959.

(26) Furlani, E. P. *J. Appl. Phys.* **2006**, *99*, 024912.

(27) Zhu, T.; Marrero, F.; Mao, L. *NSTI-Nanotech* **2010**, *2*, 436.

(28) Zhang, K.; Liang, Q.; Ma, S.; Mu, X.; Hu, P.; Wang, Y.; Luo, G. *Lab Chip* **2009**, *9*, 2992.

(29) Gassner, A. L.; Abonnenc, M.; Chen, H. X.; Morandini, J.; Josserand, J.; Rossier, J. S.; Busnel, J. M.; Girault, H. H. *Lab Chip* **2009**, *9*, 2356.

(30) Son, O.-T.; Roh, J. W.; Song, S.-H.; Park, J.-S.; Lee, W.; Jung, H. *Biochip J.* **2008**, *2*, 186.

(31) Leong, S. S.; Yeap, S. P.; Lim, J. K. *Interface Focus* **2016**, *6*, 0048.

(32) Ramadan, Q.; Gijs, M. A. *Analyst* **2011**, *136*, 1157.

(33) Shevkoplyas, S. S.; Siegel, A. C.; Westervelt, R. M.; Prentiss, M. G.; Whitesides, G. M. *Lab Chip* **2007**, *7*, 1294.

(34) Gómez-Pastora, J.; Karampelas, I. H.; Xue, X.; Bringas, E.; Furlani, E. P.; Ortiz, I. *J. Phys. Chem. C* **2017**, *121*, 7466.

(35) Lee, C. S.; Lee, H.; Westervelt, R. M. *Appl. Phys. Lett.* **2001**, *79*, 3308.

(36) Xia, N.; Hunt, T. P.; Mayers, B. T.; Alsberg, E.; Whitesides, G. M.; Westervelt, R. M.; Ingber, D. E. *Biomed. microdevices* **2006**, *8*, 299.

(37) Han, K. H.; Frazier, A. B. *Lab Chip* **2006**, *6*, 265.

(38) Manz, A.; Graber, N.; Widmer, H. M. *Sensors and Actuators* **1990**, *B1*, 244.

(39) Tsao, C.-W. *Micromachines* **2016**, *7*, 225.

(40) Yang, H.; Zhuang, Y.; Hu, H.; Du, X.; Zhang, C.; Shi, X.; Wu, H.; Yang, S. *Adv. Funct. Mater.* **2010**, *20*, 1733.

(41) Huber, D. L. *Small* **2005**, *1*, 482.

(42) Pfaff, A.; Schallon, A.; Ruhland, T. M.; Majewski, A. P.; Schmalz, H.; Freitag, R.; Muller, A. H. E. *Biomacromolecules* **2011**, *12*, 3805.

(43) Lu, A. H.; Salabas, E. L.; Schuth, F. *Angew. Chem. Int. Ed.* **2007**, *46*, 1222.

(44) Feng, Z.; Zhu, S.; Martins de Godoi, D. R.; Samia, A. C.; Scherson, D. *Anal. Chem.* **2012**, *84*, 3764.

(45) Turcheniuk, K.; Tarasevych, A. V.; Kukhar, V. P.; Boukherroub, R.; Szunerits, S. *Nanoscale* **2013**, *5*, 10729.

(46) A. Bee, R. M., S. Neveu. *J. Magn. Magn. Mater.* **1995**, *149*, 6.

(47) Sun, S.; Zeng, H.; Robinson, D. B.; Raoux, S.; Rice, P. M.; Wang, S. X.; Li, G. *J. Am. Chem. Soc.* **2004**, *126*, 273.

(48) Park, J.; An, K.; Hwang, Y.; Park, J. G.; Noh, H. J.; Kim, J. Y.; Park, J. H.; Hwang, N. M.; Hyeon, T. *Nat. Mater.* **2004**, *3*, 891.

(49) S. Solinas, G. P., M. P. Morales, C. J. Serna *Acta mater.* **2001**, 2805.

(50) Deng, H.; Li, X.; Peng, Q.; Wang, X.; Chen, J.; Li, Y. *Angew. Chem. Int.Ed.* **2005**, *44*, 2782.

(51) Wu, W.; Wu, Z.; Yu, T.; Jiang, C.; Kim, W.-S. *Sci. Technol. Adv. Mater.* **2016**, *16*, 023501.

(52) Kwon, S. G.; Piao, Y.; J., P.; Angappane, S.; Jo, Y.; Hwang, N.-M.; Park, J.-G.; T., H. *J. Am. Chem. Soc.* **2007**, *129*, 12571.

(53) Jamshaid, T.; Neto, E. T. T.; Eissa, M. M.; Zine, N.; Kunita, M. H.; El-Salhi, A. E.; Elaissari, A. TRAC-*Trend. Anal. Chem.* **2016**, *79*, 344.

(54) Willis, A. L.; Nicholas J. Turro, N. J.; O'Brien, S. *Chem. Mater.* **2005**, *17*, 5970.

(55) Lee, J.; Isobe, T.; Senna, M. *Colloids Surf. A.* **1996**, *109*, 121.

(56) Park, J.; Lee, E.; Hwang, N.-M.; Kang, M.; Kim, S. C.; Hwang, Y.; Park, J.-G.; Noh, H.-J.; Kim, J.-Y.; Park, J.-H.; Hyeon, T. *Angew. Chem. Int. Ed.* **2005**, *117*, 2932.

(57) Li, Z.; Sun, Q.; Gao, M. *Angew. Chem. Int. Ed.* **2004**, *44*, 123.

(58) Hu, F. Q.; Wei, L.; Zhou, Z.; Ran, Y. L.; Li, Z.; Gao, M. Y. *Adv. Mater.* **2006**, *18*, 2553.

(59) Cao, J.; Chen, J.; Yi, L.; Li, P.; Qi, L. W. *Electrophoresis* **2008**, *29*, 2310.

(60) Ganguli, A. K.; Ahmad, T. *J. Nanosci. Nanotechnol.* **2007**, *7*, 2029.

(61) Reddy, L. H.; Arias, J. L.; Nicolas, J.; Couvreur, P. *Chem. Rev.* **2012**, *112*, 5818.

(62) Ho, K. M.; Li, P. *Langmuir.* **2008**, *24*, 1801.

(63) Chen, W.; Lu, F.; Chen, C. C.; Mo, K. C.; Hung, Y.; Guo, Z. X.; Lin, C. H.; Lin, M. H.; Lin, Y. H.; Chang, C.; Mou, C. Y. *NMR Biomed.* **2013**, *26*, 1176.

(64) Boni, A.; Albertazzi, L.; Innocenti, C.; Gemmi, M.; Bifone, A. *Langmuir*. **2013**, *29*, 10973.

(65) Budgin, A. M.; Kabachii, Y. A.; Shifrina, Z. B.; Valetsky, P. M.; Kochev, S. S.; Stein, B. D.; Malyutin, A.; Bronstein, L. M. *Langmuir*. **2012**, *28*, 4142.

(66) Xu, S.; Song, X.; Guo, J.; Wang, C. *ACS Appl. Mater. Interfaces.* **2012**, *4*, 4764.

(67) Majewski, A. P.; Stahlschmidt, U.; Jerome, V.; Freitag, R.; Muller, A. H.; Schmalz, H. *Biomacromolecules* **2013**, *14*, 3081.

(68) Ruhland, T. M.; Lang, J. R. V.; Alt, H. G.; Müller, A. H. E. *Eur. J. Inorg. Chem.* **2013**, *2013*, 2146.

(69) Gage, S. H.; Stein, B. D.; Nikoshvili, L.; Matveeva, V. G.; Sulman, M. G.; Sulman, E. M.; Morgan, D. G.; Yuzik-Klimova, E. Y.; Mahmoud, W. E.; Bronstein, L. M. *Langmuir*. **2013**, *29*, 466.

(70) Zimny, K.; Mascaro, B.; Brunet, T.; Poncelet, O.; Aristégui, C.; Leng, J.; Sandre, O.; Mondain-Monval, O. *J. Mater. Chem. B* **2014**, *2*, 1285.

(71) Duong, B.; Khurshid, H.; Gangopadhyay, P.; Devkota, J.; Stojak, K.; Srikanth, H.; Tetard, L.; Norwood, R. A.; Peyghambarian, N.; Phan, M. H.; Thomas, J. *Small* **2014**, *10*, 2840.

(72) Chang, Y.; Yang, C.; Zheng, X. Y.; Wang, D. Y.; Yang, Z. G. *ACS Appl. Mater. Interfaces*. **2014**, *6*, 768.

(73) Jiang, S.; Win, K. Y.; Liu, S.; Teng, C. P.; Zheng, Y.; Han, M. Y. *Nanoscale* **2013**, *5*, 3127.

(74) Dong, A.; Ye, X.; Chen, J.; Kang, Y.; Gordon, T.; Kikkawa, J. M.; Murray, C. B. *J. Am. Chem. Soc.* **2011**, *133*, 998.

(75) Hao, R.; Xing, R.; Xu, Z.; Hou, Y.; Gao, S.; Sun, S. *Adv. Mater.* **2010**, *22*, 2729.

(76) Treuel, L.; Malissek, M.; Grass, S.; Diendorf, J.; Mahl, D.; Meyer-Zaika, W.; Epple, M. *J. Nanopart. Res.* **2012**, *14*.

(77) Moros, M.; Pelaz, B.; Lopez-Larrubia, P.; Garcia-Martin, M. L.; Grazu, V.; de la Fuente, J. M. *Nanoscale*. **2010**, *2*, 1746.

(78) Henry, A.-I.; Bingham, J. M.; Ringe, E.; Marks, L. D.; Schatz, G. C.; Van Duyne, R. P. *J. Phys. Chem. C.* **2011**, *115*, 9291.

(79) Li, L.; Wang, T.; Zhang, L.; Su, Z.; Wang, C.; Wang, R. *Chemistry*. **2012**, *18*, 11417.

(80) Ivanchikhina, A. V.; Tovstun, S. A.; Razumov, V. F. *J. Colloid Interface Sci.* **2013**, *395*, 127.

(81) Ding, H. L.; Zhang, Y. X.; Wang, S.; Xu, J. M.; Xu, S. C.; Li, G. H. *Chem. Mater.* **2012**, *24*, 4572.

(82) Chen, F.; Bu, W.; Chen, Y.; Fan, Y.; He, Q.; Zhu, M.; Liu, X.; Zhou, L.; Zhang, S.; Peng, W.; Shi, J. *Chem. Asian. J.* **2009**, *4*, 1809.

(83) Jiang, F.; Fu, Y.; Zhu, Y.; Tang, Z.; Sheng, P. *J. Alloy. Compd.* **2012**, *543*, 43.

(84) Vogt, C.; Toprak, M. S.; Muhammed, M.; Laurent, S.; Bridot, J.-L.; Müller, R. N. *J. Nanopart. Res.* **2009**, *12*, 1137.

(85) Katagiri, K.; Narahara, M.; Sako, K.; Inumaru, K. *J. Sogel Sci. Technol.* **2017**, *84*, 110.

(86) Lemyre, J. L.; Lamarre, S.; Beaupre, A.; Ritcey, A. M. *Langmuir*. **2010**, *26*, 10524.

(87) Yu, K.; Zhang, X.; Tong, H.; Yan, X.; Liu, S. *Mater. Lett.* **2013**, *106*, 151.

(88) Liu, Y.; Chen, T.; Wu, C.; Qiu, L.; Hu, R.; Li, J.; Cansiz, S.; Zhang, L.; Cui, C.; Zhu, G.; You, M.; Zhang, T.; Tan, W. *J. Am. Chem. Soc.* **2014**, *136*, 12552.

(89) Rolf Koole, M. M. v. S., Jan Hilhorst, Celso de Mello Donegá, Dannis C. 't Hart, Alfons van Blaaderen, Daniel Vanmaekelbergh, Andries Meijerink *Chem. Mater.* **2008**, *20*, 2503.

(90) Wang, J.; Shah, Z. H.; Zhang, S.; Lu, R. *Nanoscale* **2014**, *6*, 4418.

(91) Yathindranath, V.; Sun, Z.; Worden, M.; Donald, L. J.; Thliveris, J. A.; Miller, D. W.; Hegmann, T. *Langmuir.* **2013**, *29*, 10850.

(92) Chen, Y.; Zhang, Y. *Anal Bioanal Chem*.**2011**, 399,2503.

(93) Yoon, T. J.; Yu, K. N.; Kim, E.; Kim, J. S.; Kim, B. G.; Yun, S. H.; Sohn, B. H.; Cho, M. H.; Lee, J. K.; Park, S. B. *Small* **2006**, *2*, 209.

(94) Ryan D. Rutledge, C. L. W., Jonathan W. Pittman, R. Shane Addleman,; Mark Engelhard, W. C., and Marvin G. Warner *Langmuir.* **2010**, *26*, 12285.

(95) Bloemen, M.; Sutens, B.; Brullot, W.; Gils, A.; Geukens, N.; Verbiest, T. *ChemPlusChem* **2015**, *80*, 50.

(96) Nicosia, C.; Krabbenborg, S. O.; Chen, P.; Huskens, J. *J. Mater. Chem. B* **2013**, *1*, 5417.

(97) Hudson, R.; Li, C.-J.; Moores, A. *Green Chem.* **2012**, *14*, 622.

(98) Toulemon, D.; Pichon, B. P.; Leuvrey, C.; Zafeiratos, S.; Papaefthimiou, V.; Cattoën, X.; Bégin-Colin, S. *Chem. Mater.* **2013**, *25*, 2849.

(99) Burglova, K.; Moitra, N.; Hodacova, J.; Cattoen, X.; Man, M. W. *J. Org. Chem.* **2011**, *76*, 7326.

(100) McDonald, A. R.; Dijkstra, H. P.; Suijkerbuijk, B. M. J. M.; van Klink, G. P. M.; van Koten, G. *Organometallics* **2009**, *28*, 4689.

(101) Escorihuela, J.; Marcelis, A. T. M.; Zuilhof, H. *Adv. Mater. Interfaces* **2015**, *2*, n/a.

(102) Bhairamadgi, N. S.; Gangarapu, S.; Caipa Campos, M. A.; Paulusse, J. M.; van Rijn, C. J.; Zuilhof, H. *Langmuir.* **2013**, *29*, 4535.

(103) Hoyle, C. E.; Bowman, C. N. *Angew. Chem. Int. Ed.* **2010**, *49*, 1540.

(104) Denes, F.; Pichowicz, M.; Povie, G.; Renaud, P. *Chem. Rev.* **2014**, *114*, 2587.

(105) Tucker-Schwartz, A. K.; Farrell, R. A.; Garrell, R. L. *J. Am. Chem. Soc.* **2011**, *133*, 11026.

(106) Jian, G. Q.; Liu, Y. X.; He, X. W.; Chen, L. X.; Zhang, Y. K. *Nanoscale* **2012**, *4*, 6336.

(107) Lu, X.; Sun, F.; Wang, J.; Zhong, J.; Dong, Q. *Macromol. Rapid Commun.* **2009**, *30*, 2116.

(108) Chen, X.; Organ, M. G.; Pietro, W. J. *J. Nanosci. Adv. Tech.* **2016**, *1*, 25.

(109) Chen, X.; Pietro, W. J.; Organ, M. G. *J. Nanosci. Adv. Tech.* **2017**, *2*, 5.

(110) Garcia-Fernandez, M. J.; Martinez-Calvo, L.; Ruiz, J.-C.; Wertheimer, M. R.; Concheiro, A.; Alvarez-Lorenzo, C. *Plasma Process. Polym.* **2012**, *9*, 540.

(111) Lenshof, A.; Laurell, T. *Chem. Soc. Rev.* **2010**, *39*, 1203.

(112) van Reenen, A.; de Jong, A. M.; den Toonder, J. M.; Prins, M. W. *Lab Chip* **2014**, *14*, 1966.

(113) Safarik, I.; Safarikova, M. *Biomagn. Res. Technol.* **2004**, *2*, 7.

(114) Dufresne, E. R.; Grier, D. G. *Rev. Sci. Instrum.* **1998**, *69*, 1974.

(115) Nguyen, N.-T. *Microfluid. Nanofluid.* **2011**, *12*, 1.

(116) Latham, A. H.; Williams, M. E. *Acc. Chem. Res.* **2008**, *41*, 411.

(117) Doh, I.; Cho, Y.-H. *Sensor Actuat. A-Phys.* **2005**, *121*, 59.

(118) Petersson, F.; Aberg, L.; Sward-Nilsson, A.-M.; Laurell, T. *Anal. Chem* **2007**, *79*, 5117.

(119) Lee, S. H. S.; Hatton, T. A.; Khan, S. A. *Microfluid. Nanofluid.* **2011**, *11*, 429.

(120) Agostino, F. J.; Cherney, L. T.; Kanoatov, M.; Krylov, S. N. *Anal. Chem.* **2014**, *86*, 5656.

(121) Agostino, F. J.; Cherney, L. T.; Galievsky, V.; Krylov, S. N. *Angew. Chem. Int. Ed*. **2013**, *52*, 7256.

(122) Cardoso, S.; Leitao, D. C.; Dias, T. M.; Valadeiro, J.; Silva, M. D.; Chicharo, A.; Silverio, V.; Gaspar, J.; Freitas, P. P. *J. Phys. D-Appl. Phys.* **2017**, *50*, 213001.

(123) Kim, M. J.; Lee, D. J.; Youn, J. R.; Song, Y. S. *RSC Adv.* **2016**, *6*, 32090.

(124) Ditsch, A.; Laibinis, P. E.; Wang, D. I. C.; Hatton, T. A. *Langmuir.* **2005**, *21*, 6006.

(125) Lai, J. J.; Nelson, K. E.; Nash, M. A.; Hoffman, A. S.; Yager, P.; Stayton, P. S. *Lab Chip* **2009**, *9*, 1997.

(126) Gross, B.; Lockwood, S. Y.; Spence, D. M. *Anal. Chem.* **2017**, *89*, 57.

(127) Deng, B.; Tian, Y.; Yu, X.; Song, J.; Guo, F.; Xiao, Y.; Zhang, Z. *Anal. Chim. Acta.* **2014**, *820*, 104.

(128) Organ, M. G.; Comer, E. *Chem. Eur. J.*, **2005**, 11, 7223.

LIST OF PUBLICATIONS

(1) **Xia Chen**, William J. Pietro, Michael G. Organ. A Facile and Controlled Preparation Method of Multifunctional Core-Shell Magnetic Nanoparticles by Thiol-ene Click Reaction for Microfluidic Separation. *J. Nanosci. Adv. Tech.* **2017**, 2(1): 5-14.

(2) **Xia Chen**, Michael G. Organ, William J. Pietro. One-pot Synthesis of Size Controllable Amine-Functionalized Core-Shell Magnetic Nanoparticles for Use in Microfluidic Flow Separators. *J. Nanosci. Adv. Tech.* **2016**, 1: 25-31.

APPENDIX - NMR SPECTRA OF MOLECULES SYNTHESIZED IN CHAPTER 3

^{1}H-NMR spectrum of (3-azidopropyl)triethoxysilane (Compound 1)

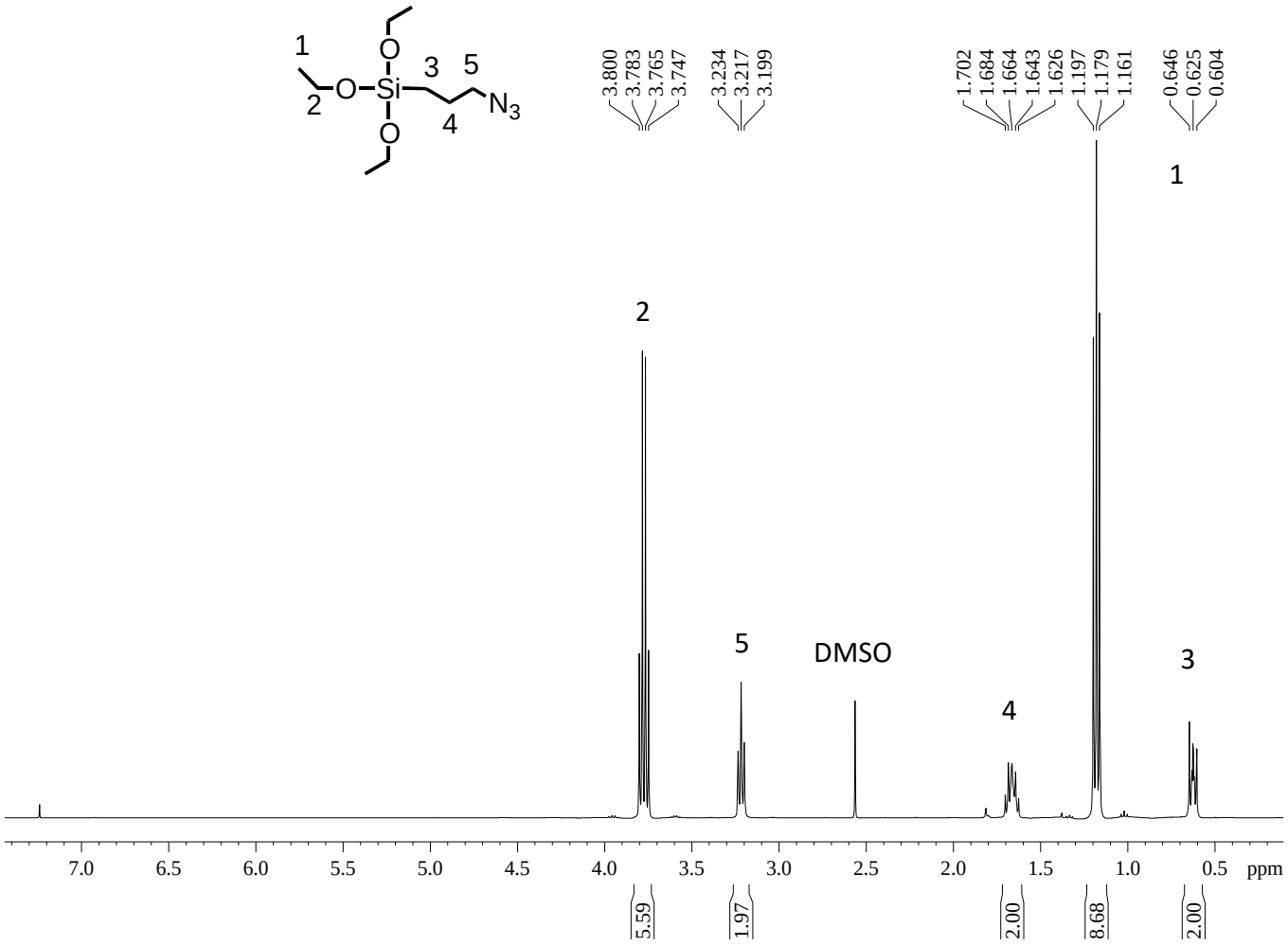

^{1}H-NMR spectrum of [(2-Propynylcarbamate)propyl] Triethoxysilane (PPTEOS) (Compound 2)

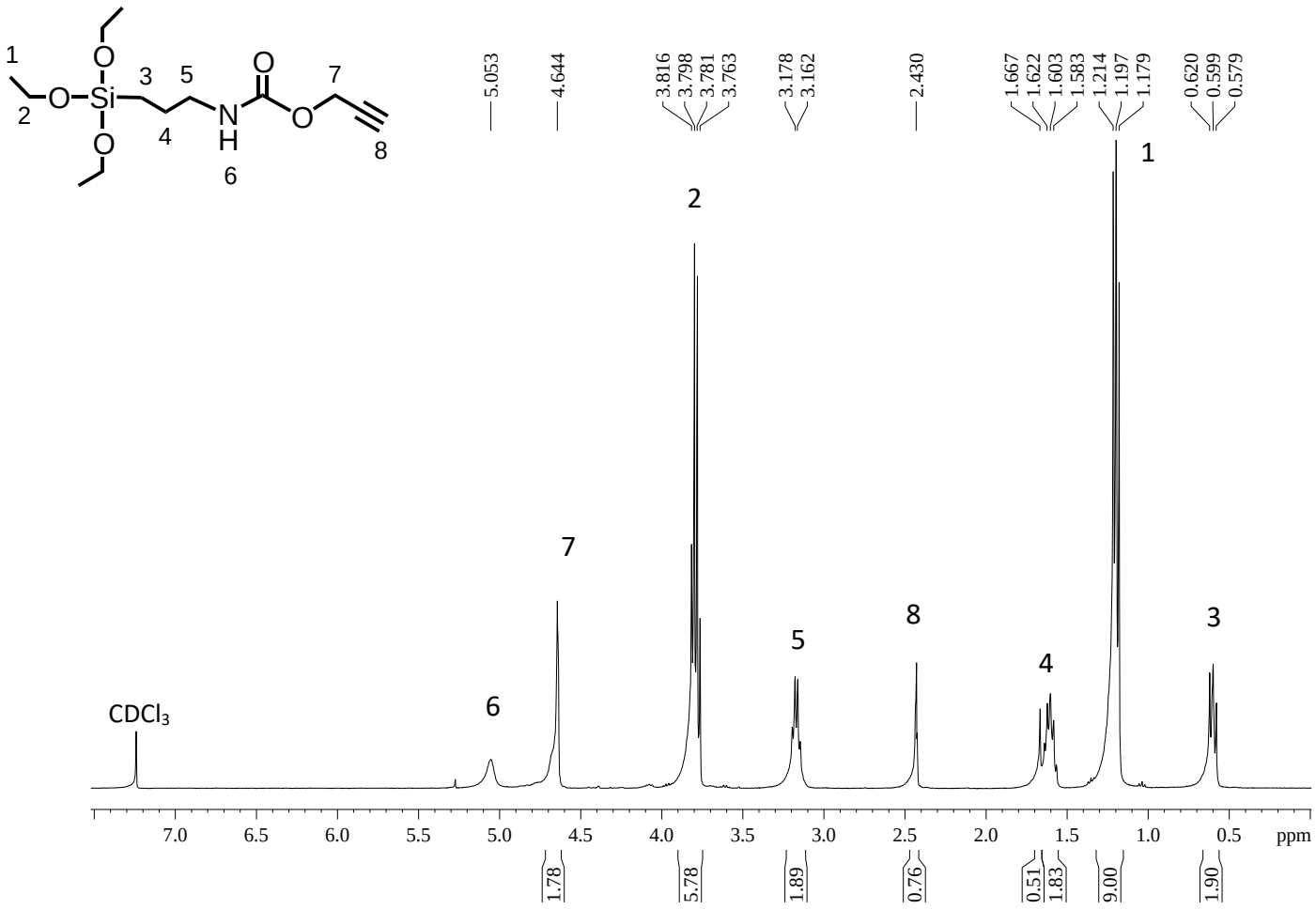

^{1}H-NMR spectrum of 3-(2-(triethoxysilyl)ethylthio)propanoic acid (Compound 3)

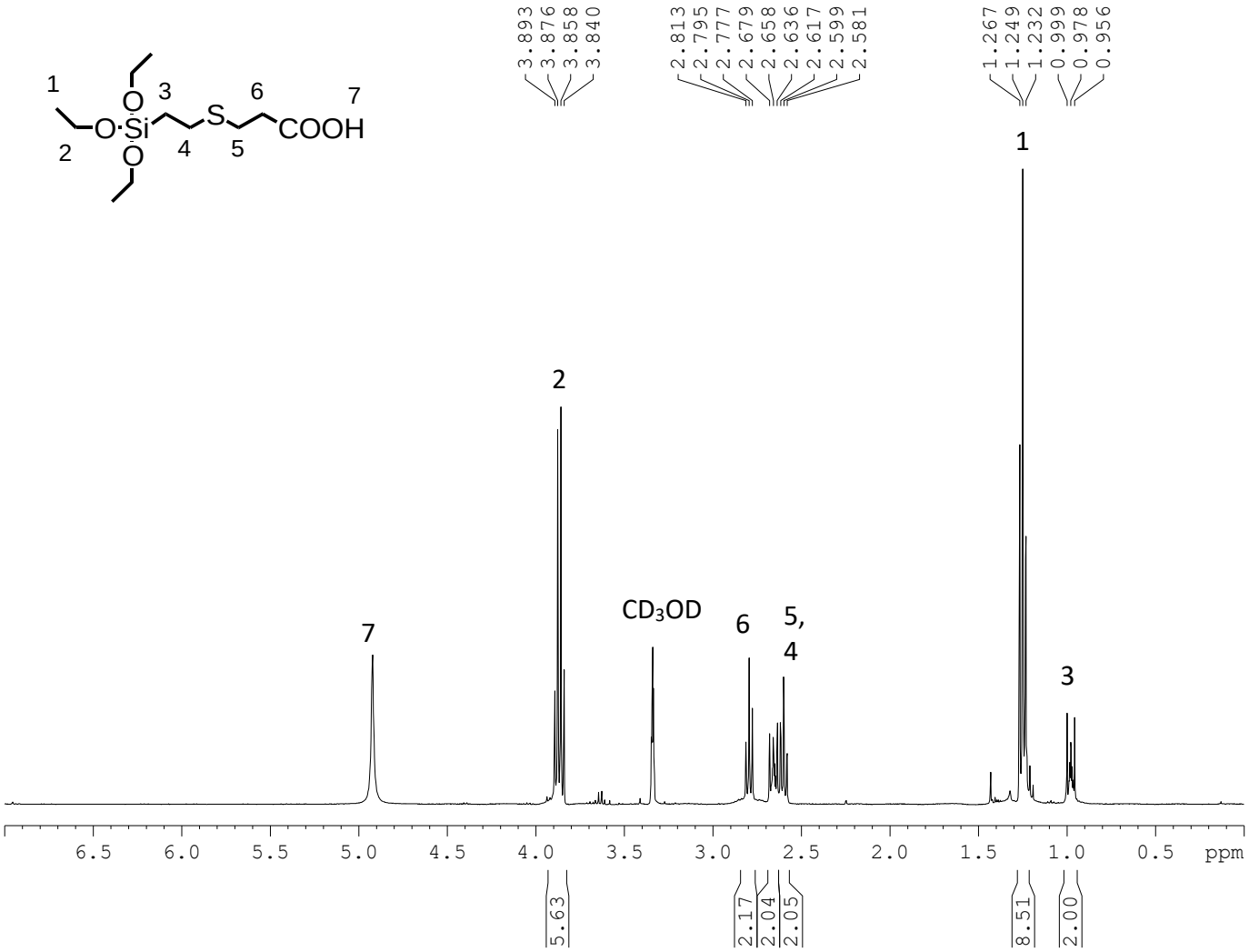

^{13}C-NMR spectrum of 3-(2-(triethoxysilyl)ethylthio)propanoic acid (Compound 3)

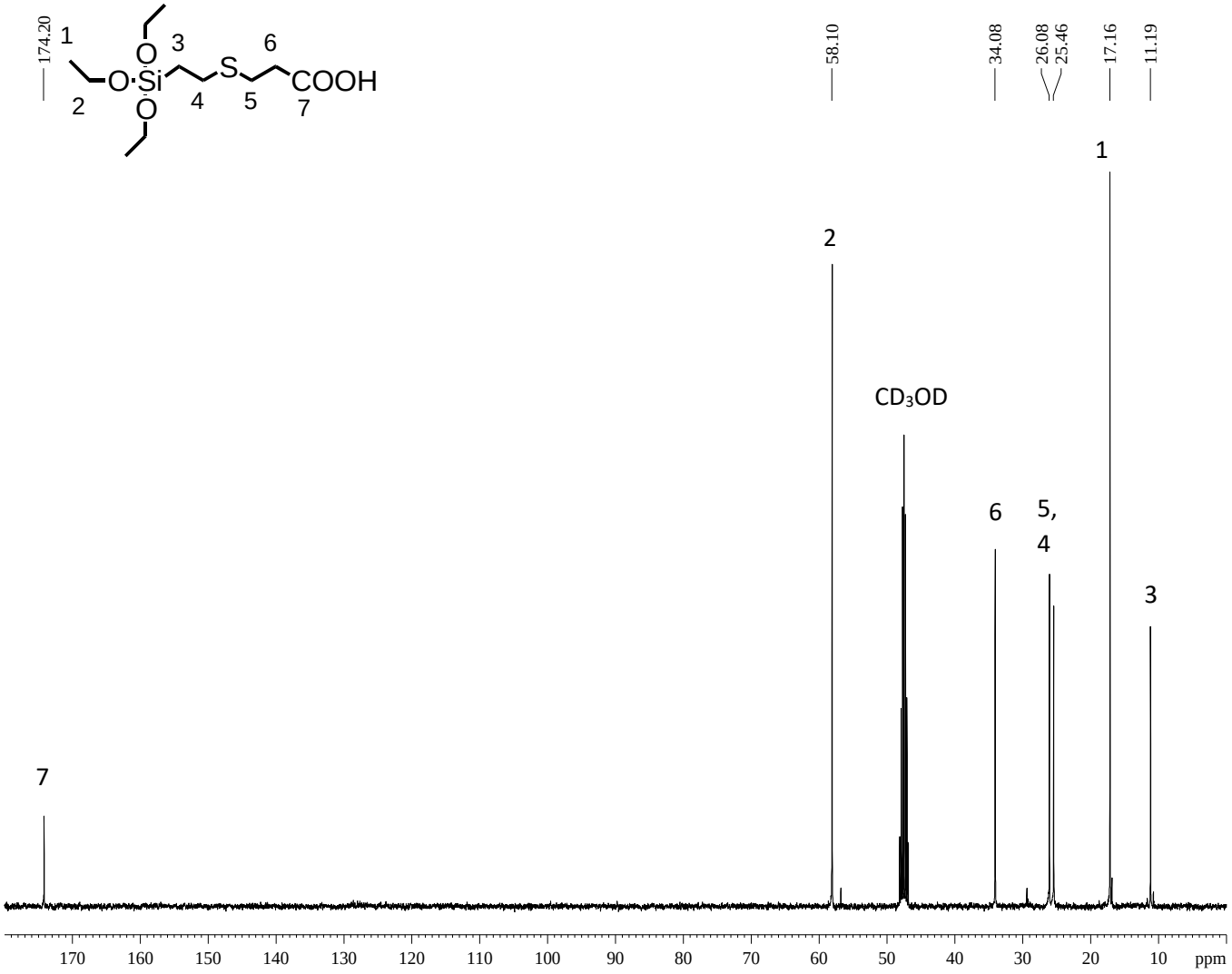

[1]H-NMR spectrum of 2-(2-(triethoxysilyl)ethylthio) ethanamine. (Compound 4)

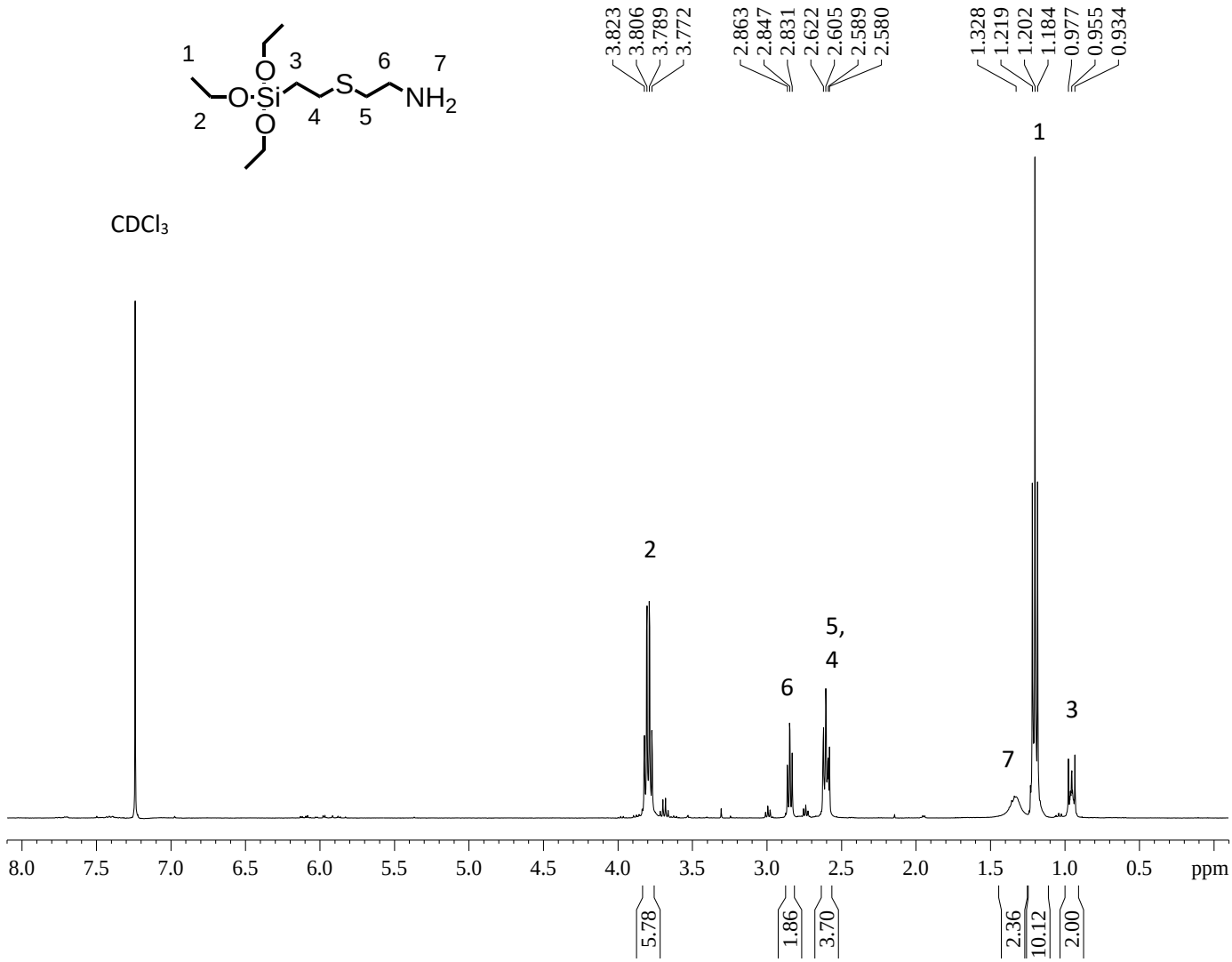

^{13}C-NMR spectrum of 2-(2-(triethoxysilyl)ethylthio) ethanamine (Compound 4)

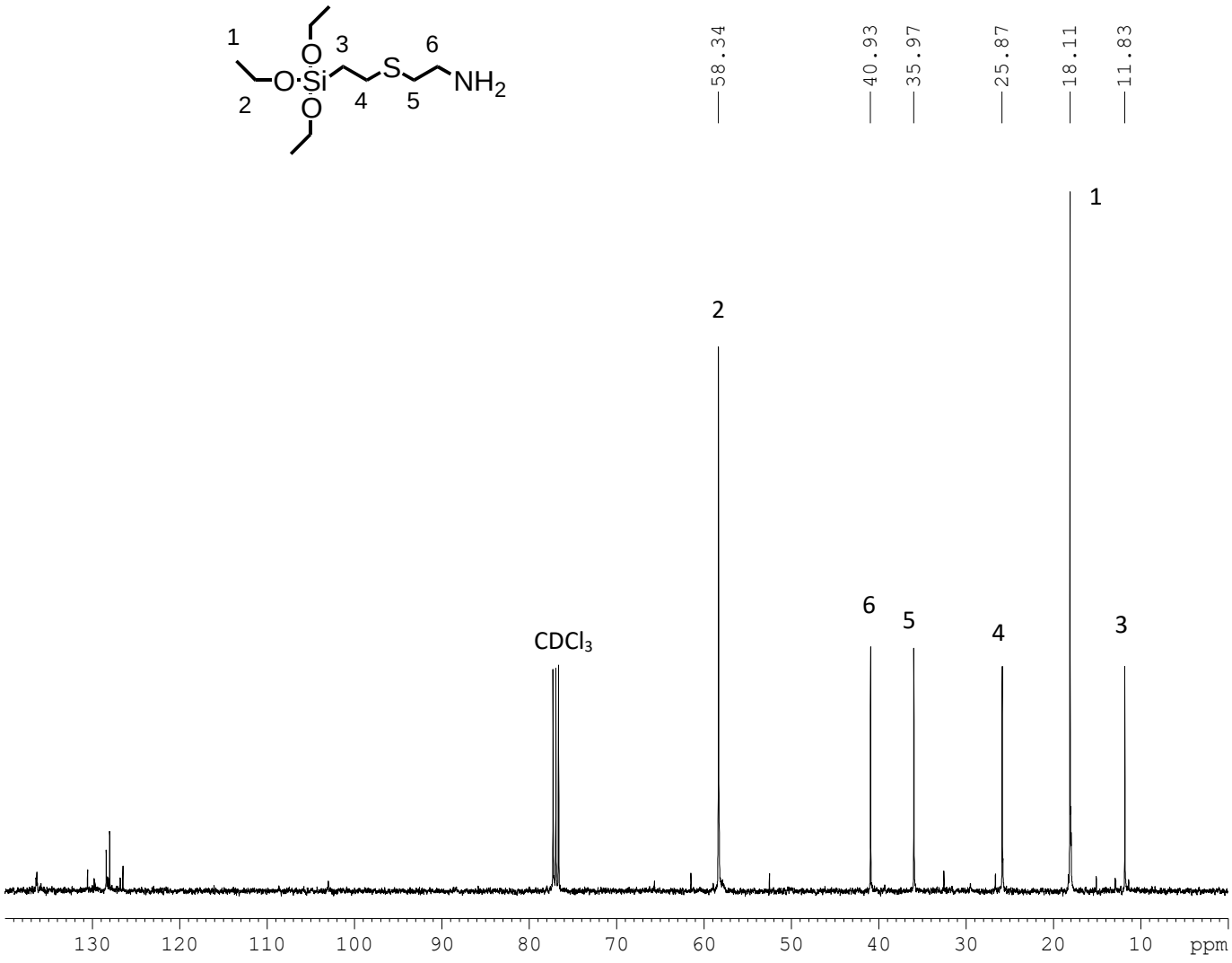

^{1}H-NMR spectrum of ethyl 2-(2-(triethoxysilyl)ethylthio)acetate (Compound 5)

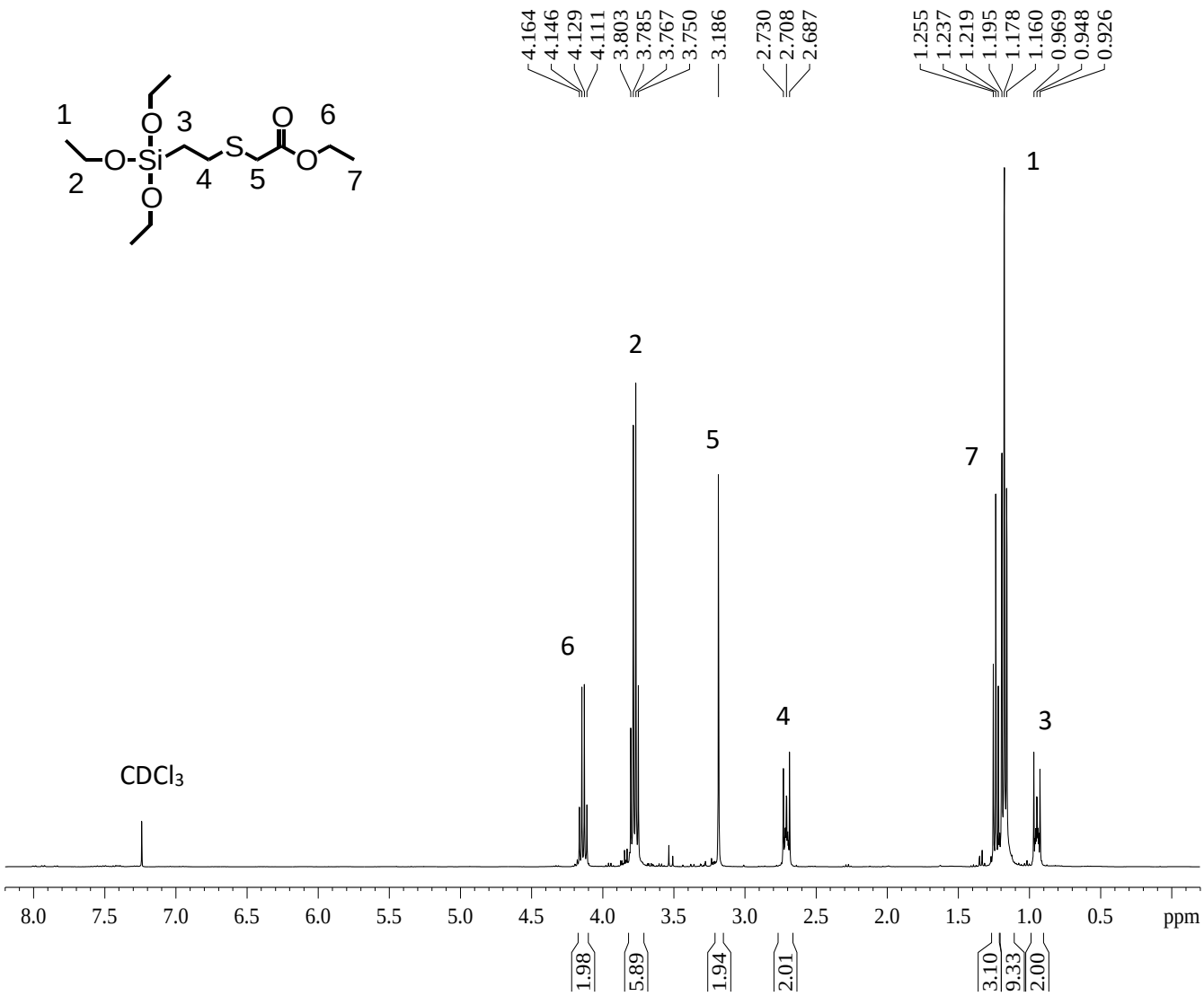

^{13}C-NMR spectrum of ethyl 2-(2-(triethoxysilyl)ethylthio)acetate (Compound 5)